



**Calhoun: The NPS Institutional Archive**  
**DSpace Repository**

---

Theses and Dissertations

1. Thesis and Dissertation Collection, all items

---

2011-12

# Aerodynamic analysis of M33 projectile using the CFX code

Wong, Chee Heng

Monterey, California. Naval Postgraduate School

---

<http://hdl.handle.net/10945/10711>

---

This publication is a work of the U.S. Government as defined in Title 17, United States Code, Section 101. Copyright protection is not available for this work in the United States.

*Downloaded from NPS Archive: Calhoun*



Calhoun is the Naval Postgraduate School's public access digital repository for research materials and institutional publications created by the NPS community. Calhoun is named for Professor of Mathematics Guy K. Calhoun, NPS's first appointed -- and published -- scholarly author.

**Dudley Knox Library / Naval Postgraduate School**  
**411 Dyer Road / 1 University Circle**  
**Monterey, California USA 93943**

<http://www.nps.edu/library>



**NAVAL  
POSTGRADUATE  
SCHOOL**

**MONTEREY, CALIFORNIA**

**THESIS**

**AERODYNAMIC ANALYSIS OF THE M33 PROJECTILE  
USING THE CFX CODE**

by

Wong, Chee Heng

December 2011

Thesis Advisor:  
Second Reader:

Max F. Platzer  
Anthony Gannon

**Approved for public release: distribution is unlimited**

THIS PAGE INTENTIONALLY LEFT BLANK

REPORT DOCUMENTATION PAGE			Form Approved OMB No. 0704-0188
Public reporting burden for this collection of information is estimated to average 1 hour per response, including the time for reviewing instruction, searching existing data sources, gathering and maintaining the data needed, and completing and reviewing the collection of information. Send comments regarding this burden estimate or any other aspect of this collection of information, including suggestions for reducing this burden, to Washington headquarters Services, Directorate for Information Operations and Reports, 1215 Jefferson Davis Highway, Suite 1204, Arlington, VA 22202-4302, and to the Office of Management and Budget, Paperwork Reduction Project (0704-0188) Washington DC 20503.			
1. AGENCY USE ONLY (Leave blank)	2. REPORT DATE December 2011	3. REPORT TYPE AND DATES COVERED Master's Thesis	
4. TITLE AND SUBTITLE Aerodynamic Analysis of the M33 Projectile Using the CFX Code		5. FUNDING NUMBERS	
6. AUTHOR(S) Wong Chee Heng		8. PERFORMING ORGANIZATION REPORT NUMBER	
7. PERFORMING ORGANIZATION NAME(S) AND ADDRESS(ES) Naval Postgraduate School Monterey, CA 93943-5000		10. SPONSORING/MONITORING AGENCY REPORT NUMBER	
9. SPONSORING /MONITORING AGENCY NAME(S) AND ADDRESS(ES) N/A		11. SUPPLEMENTARY NOTES The views expressed in this thesis are those of the author and do not reflect the official policy or position of the Department of Defense or the U.S. Government. IRB Protocol number _____ N/A _____.	
12a. DISTRIBUTION / AVAILABILITY STATEMENT Approved for public release: distribution is unlimited		12b. DISTRIBUTION CODE <u>A</u>	
13. ABSTRACT (maximum 200 words)  The M33 projectile has been analyzed using the ANSYS CFX code that is based on the numerical solution of the full Navier-Stokes equations. Simulation data were obtained against various Mach numbers ranging from M= 0.5 to M2.6 at 0° and 2° angles of attack. Simulation data were also obtained against various angles of attack from 0° to 85° for M= 0.5. For Mach numbers between M= 0.5 to 2.6, the results obtained using the combined k-epsilon and Shear Stress Transport model show good agreement with the experimental range data for the normal force and pitching moment coefficient. The drag coefficient at zero angle of attack tended to be over predicted by an average error of 11.6% with the highest error occurring at M= 1.5. For varying angle of attack up to 85° at M= 0.5, the results obtained from CFX code were compared with simulation results obtained from AP09. The data showed good agreement only up to 20° angles of attack.			
14. SUBJECT TERMS Aerodynamic, M33, Projectiles, CFX, Normal Force, Pitching Moment, Drag, Coefficient		15. NUMBER OF PAGES 97	
		16. PRICE CODE	
17. SECURITY CLASSIFICATION OF REPORT Unclassified	18. SECURITY CLASSIFICATION OF THIS PAGE Unclassified	19. SECURITY CLASSIFICATION OF ABSTRACT Unclassified	20. LIMITATION OF ABSTRACT UU

NSN 7540-01-280-5500

Standard Form 298 (Rev. 2-89)  
Prescribed by ANSI Std. Z39-18

THIS PAGE INTENTIONALLY LEFT BLANK

**Approved for public release: distribution is unlimited**

**AERODYNAMIC ANALYSIS OF M33 PROJECTILE USING THE CFX CODE**

Wong Chee Heng  
Major, Singapore Armed Forces  
Mechanical and Manufacturing Engineering  
Nanyang Technological University of Singapore, 2005

Submitted in partial fulfillment of the  
requirements for the degree of

**MASTER OF SCIENCE IN MECHANICAL ENGINEERING**

from the

**NAVAL POSTGRADUATE SCHOOL  
December 2011**

Author: Wong Chee Heng

Approved by: Maximilian F. Platzer  
Thesis Advisor

Anthony Gannon  
Second Reader

Knox T. Millsaps  
Chair, Department of Mechanical and Aeronautical Engineering

THIS PAGE INTENTIONALLY LEFT BLANK

## **ABSTRACT**

The M33 projectile has been analyzed using the ANSYS CFX code that is based on the numerical solution of the full Navier-Stokes equations. Simulation data were obtained against various Mach numbers ranging from  $M= 0.5$  to  $M= 2.6$  at  $0^\circ$  and  $2^\circ$  angles of attack. Simulation data were also obtained against various angles of attack from  $0^\circ$  to  $85^\circ$  for  $M= 0.5$ .

For Mach numbers between  $M= 0.5$  to  $2.6$ , the results obtained using the combined k-epsilon and Shear Stress Transport model show good agreement with the experimental range data for the normal force and pitching moment coefficient. The drag coefficient at zero angle of attack tended to be over predicted by an average error of 11.6% with the highest error occurring at  $M= 1.5$ .

For varying angle of attack up to  $85^\circ$  at  $M= 0.5$ , the results obtained from CFX code were compared with simulation results obtained from AP09. The data showed good agreement only up to  $20^\circ$  angles of attack.

THIS PAGE INTENTIONALLY LEFT BLANK

## TABLE OF CONTENTS

<b>I.</b>	<b>INTRODUCTION.....</b>	<b>1</b>
<b>II.</b>	<b>LITERATURE REVIEW .....</b>	<b>3</b>
<b>III.</b>	<b>SOLUTION TECHNIQUES.....</b>	<b>5</b>
	<b>A. THEORETICAL APPROACH .....</b>	<b>5</b>
	<b>1. General.....</b>	<b>5</b>
	<b>2. Governing Equations.....</b>	<b>5</b>
	<b>3. Conical Shock Wave .....</b>	<b>5</b>
	<b>B. COMPUTATIONAL APPROACH .....</b>	<b>5</b>
	<b>1. General.....</b>	<b>5</b>
	<b>2. Governing Equations.....</b>	<b>6</b>
	<b>3. Boundary Conditions.....</b>	<b>7</b>
	<b>4. Turbulence Model.....</b>	<b>7</b>
	<b>5. Free-stream Flow .....</b>	<b>8</b>
	<b>6. Results .....</b>	<b>8</b>
<b>IV.</b>	<b>PROCESS AND PROCEDURES.....</b>	<b>11</b>
	<b>A. SOLIDWORKS 2010.....</b>	<b>11</b>
	<b>1. Introduction.....</b>	<b>11</b>
	<b>2. Two Dimensional Model.....</b>	<b>11</b>
	<b>3. Three Dimensional Model .....</b>	<b>12</b>
	<b>B. CFX .....</b>	<b>13</b>
	<b>1. Introduction.....</b>	<b>13</b>
	<b>2. Mesh .....</b>	<b>13</b>
	<b>3. Pre-processor.....</b>	<b>15</b>
	<b>4. Post-processor .....</b>	<b>16</b>
	<b>C. AP09 .....</b>	<b>17</b>
	<b>1. Introduction.....</b>	<b>17</b>
	<b>2. M33 Projectile Configuration and Input Parameters .....</b>	<b>17</b>
	<b>3. Results .....</b>	<b>18</b>
<b>V.</b>	<b>RESULTS AND ANALYSIS .....</b>	<b>21</b>
	<b>A. LINEARITY AT LOW ANGLES OF ATTACK .....</b>	<b>21</b>
	<b>B. EFFECTS OF MACH NUMBERS .....</b>	<b>23</b>
	<b>1. k- epsilon Model .....</b>	<b>23</b>
	<b>2. Shear Stress Transport Model.....</b>	<b>25</b>
	<b>3. Combined k- <math>\epsilon</math> and SST Model .....</b>	<b>27</b>
	<b>C. EFFECTS OF ANGLES OF ATTACK.....</b>	<b>29</b>
	<b>D. SENSITIVITY STUDIES FOR CFX.....</b>	<b>31</b>
	<b>1. Flow vs Orientation Adjustment Approach .....</b>	<b>31</b>
	<b>2. Control Volume.....</b>	<b>32</b>
<b>VI.</b>	<b>CONCLUSION AND RECOMMENDATIONS.....</b>	<b>35</b>
	<b>LIST OF REFERENCES.....</b>	<b>37</b>

<b>APPENDIX A.</b>	<b>SOLIDWORKS PROCESSES AND PROCEDURES .....</b>	<b>39</b>
<b>A.</b>	<b>INTRODUCTION.....</b>	<b>39</b>
<b>B.</b>	<b>2D MODEL.....</b>	<b>39</b>
<b>C.</b>	<b>3D MODEL.....</b>	<b>41</b>
<b>APPENDIX B.</b>	<b>CFX PROCESSES AND PROCEDURES.....</b>	<b>43</b>
<b>A.</b>	<b>INTRODUCTION.....</b>	<b>43</b>
<b>B.</b>	<b>GEOMETRY.....</b>	<b>43</b>
<b>C.</b>	<b>MESH.....</b>	<b>43</b>
<b>1.</b>	<b>Named Selections .....</b>	<b>43</b>
<b>2.</b>	<b>Mesh Sizing.....</b>	<b>44</b>
<b>3.</b>	<b>Face Sizing .....</b>	<b>44</b>
<b>D.</b>	<b>PRE-PROCESSOR.....</b>	<b>45</b>
<b>1.</b>	<b>Domain Conditions .....</b>	<b>45</b>
<b>2.</b>	<b>Boundary Conditions.....</b>	<b>45</b>
<b>3.</b>	<b>Solver.....</b>	<b>47</b>
<b>E.</b>	<b>POST-PROCESSOR .....</b>	<b>47</b>
<b>1.</b>	<b>Flow Field .....</b>	<b>47</b>
<b>2.</b>	<b>Forces .....</b>	<b>47</b>
<b>APPENDIX C.</b>	<b>AP09 PROCESSES AND PROCEDURES.....</b>	<b>49</b>
<b>A.</b>	<b>M33 PROJECTILE CONFIGURATION AND INPUT PARAMETERS.....</b>	<b>49</b>
<b>B.</b>	<b>GEOMETRY INPUTS.....</b>	<b>50</b>
<b>C.</b>	<b>AERODYNAMIC INPUTS .....</b>	<b>53</b>
<b>D.</b>	<b>RESULTS .....</b>	<b>55</b>
<b>APPENDIX D.</b>	<b>DETAILED RESULTS .....</b>	<b>59</b>
<b>A.</b>	<b>CFX .....</b>	<b>59</b>
<b>1.</b>	<b>Simulation Data.....</b>	<b>59</b>
<b>2.</b>	<b>Flow Diagrams at Various Mach Numbers .....</b>	<b>65</b>
<b>3.</b>	<b>Flow Diagrams at Various Angles of Attack .....</b>	<b>71</b>
<b>4.</b>	<b>Cross-Sectional Flow .....</b>	<b>76</b>
<b>B.</b>	<b>AP09 .....</b>	<b>78</b>
	<b>INITIAL DISTRIBUTION LIST .....</b>	<b>79</b>

## LIST OF FIGURES

Figure 1.	Free-Stream Flow Diagram (CFX).....	8
Figure 2.	Force Diagram (CFX).....	9
Figure 3.	Schematic of the M33 Projectile.....	11
Figure 4.	Solid 3D Model of M33 Projectile (SolidWorks).....	12
Figure 5.	Cavity of M33 Projectile (SolidWorks).....	12
Figure 6.	Mesh of M33 Projectile (CFX).....	13
Figure 7.	Inflation Layers (CFX).....	14
Figure 8.	Face Sizing at Base (CFX).....	15
Figure 9.	Face Sizing at Nose Tip (CFX).....	15
Figure 10.	Velocity Vector (CFX).....	16
Figure 11.	Local Mach Number Contour (CFX).....	16
Figure 12.	Local Pressure Contour (CFX).....	17
Figure 13.	$C_{D0}$ vs Mach (AP09).....	19
Figure 14.	$C_{N\alpha}$ vs Mach (AP09).....	19
Figure 15.	$C_L$ vs $\alpha$ (AP09).....	20
Figure 16.	$C_D$ vs $\alpha$ (AP09).....	20
Figure 17.	$C_N$ vs $\alpha$ _Subsonic (CFX).....	21
Figure 18.	$C_N$ vs $\alpha$ _Transonic (CFX).....	22
Figure 19.	$C_N$ vs $\alpha$ _Supersonic (CFX).....	22
Figure 20.	$C_{N\alpha}$ vs Mach Numbers_k- $\epsilon$ Model (CFX).....	23
Figure 21.	$C_{M\alpha}$ vs Mach Number_k- $\epsilon$ Model (CFX).....	24
Figure 22.	$C_{D0}$ vs Mach Number_k- $\epsilon$ Model (CFX).....	24
Figure 23.	$C_{N\alpha}$ vs Mach Numbers_SST Model (CFX).....	25
Figure 24.	$C_{M\alpha}$ vs Mach Numbers_SST Model (CFX).....	26
Figure 25.	$C_{D0}$ vs Mach Numbers_SST Model (CFX).....	26
Figure 26.	$C_{N\alpha}$ vs Mach Numbers_Combined k- $\epsilon$ / SST Model (CFX).....	27
Figure 27.	$C_{M\alpha}$ vs Mach Numbers_Combined k- $\epsilon$ / SST Model (CFX).....	28
Figure 28.	$C_{D0}$ vs Mach Numbers_Combined k- $\epsilon$ / SST Model (CFX).....	28
Figure 29.	$C_L$ vs $\alpha$ (CFX & AP09).....	29
Figure 30.	$C_D$ vs $\alpha$ (CFX & AP09).....	30
Figure 31.	Cross Sectional Flow (CFX).....	31
Figure 32.	Sensitivity Study on Geometry Adjustment for Angle of Attack (CFX).....	32
Figure 33.	Sensitivity Study on Control Volume for $C_{N\alpha}$ (CFX).....	33
Figure 34.	Sensitivity Study on Control Volume for $C_{D0}$ (CFX).....	33
Figure 35.	Plotting Individual Points (SolidWorks).....	39
Figure 36.	Straight Lines for Afterbody (SolidWorks).....	40
Figure 37.	Tangent Arcs for nose (SolidWorks).....	40
Figure 38.	2D Control Volume (SolidWorks).....	41
Figure 39.	3D Control Volume (SolidWorks).....	41
Figure 40.	Revolved Cut for 2D Projectile Sketch (SolidWorks).....	42
Figure 41.	Geometry Interface (CFX).....	43
Figure 42.	Named Selections (CFX).....	44

Figure 43.	Face Sizing (CFX).	45
Figure 44.	Boundary Conditions at 0° (CFX).	47
Figure 45.	Configuration-New-Body-Alone (AP09).	49
Figure 46.	Inputs-Geometry-Geometry (AP09).	49
Figure 47.	Geometry Data Entry Interface (AP09).	50
Figure 48.	Nose Geometry Data Entry Interface (AP09).	51
Figure 49.	Nose Profile Data Entry Interface (AP09).	51
Figure 50.	Afterbody Geometry Data Entry Interface (AP09).	52
Figure 51.	Afterbody Profile Data Entry Interface (AP09).	52
Figure 52.	Boattail/ Flare Data Entry Interface (AP09).	53
Figure 53.	Inputs-Aerodynamics (AP09).	53
Figure 54.	Aerodynamics Data Entry Interface-Free-Stream Conditions (AP09).	54
Figure 55.	Mach Sweep Data Entry Interface (AP09).	54
Figure 56.	Aerodynamics Data Entry Interface-Options (AP09).	55
Figure 57.	Aerodynamic Options Data Entry Interface (AP09).	55
Figure 58.	Generate – Aerodynamic Output File (AP09).	56
Figure 59.	Outputs-Aerodynamics-Plots/ Tables (AP09).	56
Figure 60.	Output Interface (AP09).	57
Figure 61.	Flow Diagrams at Various Mach Numbers for 0° and 2° (CFX).	70
Figure 62.	Flow Diagram at Various Angles of Attack (CFX).	75
Figure 63.	Cross-Sectional Flow across Symmetry Plane (CFX).	77

## LIST OF TABLES

Table 1.	M33 Input Parameters (AP09).....	18
Table 2.	Mesh Sizing Input Parameters (CFX).....	44
Table 3.	Boundary Condition Input Parameters (CFX).....	46
Table 4.	Post-Processor Input Parameters (CFX).....	48
Table 5.	Simulation Results for $C_N$ vs $\alpha$ _Subsonic (CFX).....	59
Table 6.	Simulation Results for $C_N$ vs $\alpha$ _Transonic (CFX).....	60
Table 7.	Simulation Results for $C_N$ vs $\alpha$ _Supersonic (CFX).....	60
Table 8.	Simulation Results for k- $\epsilon$ model (CFX).....	61
Table 9.	Simulation Results for SST Model (CFX).....	62
Table 10.	Simulation Results for $C_L$ and $C_D$ at High AOA (CFX).....	63
Table 11.	Sensitivity Study on Tilted Body vs Tilted Flow (CFX).....	63
Table 12.	Sensitivity Study on 20X Control Volume (CFX).....	64
Table 13.	Simulation Results for $C_{N\alpha}$ and $C_{D0}$ (AP09).....	78
Table 14.	Simulation Results for $C_L$ and $C_D$ at High AOA (AP09).....	78

THIS PAGE INTENTIONALLY LEFT BLANK

## LIST OF ACRONYMS AND ABBREVIATIONS

$C_L$	= lift coefficient
$C_D$	= drag coefficient
$C_{D0}$	= drag coefficient at zero yaw
$C_N$	= normal force coefficient
$C_{N\alpha}$	= normal force coefficient with respect to angle of attack
$C_M$	= pitching moment coefficient
$C_{M\alpha}$	= pitching moment coefficient with respect to angle of attack
$\mu$	= viscosity
$\rho$	= density
$P$	= pressure
$t$	= time
$u$	= speed in x-axis
$v$	= speed in y-axis
$w$	= speed in z-axis
$T$	= temperature
$c_v$	= specific heat at constant volume
$\tau$	= tensile stress
$R$	= gas constant
$e$	= internal energy
$k_e$	= thermal conductivity
$k$	= turbulent kinetic energy
$\varepsilon$	= turbulent dissipation
$\omega$	= specific dissipation
$\alpha$	= angle of attack
$F_y$	= normal force
$F_x$	= axial force
$F_D$	= drag force
$F_L$	= lift force

$T_z$  = torque in z-axis

$V$  = speed

$S_{\text{ref}}$  = reference area

$l_{\text{ref}}$  = reference length

## **ACKNOWLEDGMENTS**

It is my greatest delight to acknowledge the dedicated guidance and support rendered by my thesis advisor, Professor Maximilian F. Platzer. His vast knowledge and experience in the field of aerodynamic studies was undoubtedly, a key factor to the accomplishment of this report. I would also like to extend my gratitude to my second reader, Professor Anthony Gannon, for his unyielding support and recommendations in dealing with the CFX code.

I am also thankful to Professor Garth Hobson and my fellow students, Mr. Sor Wei Lun and Mr. Wee Hong Chuan for their support in deriving the computational approach for the simulation.

Lastly, I would like to thank my wife, Siangwee, and our children for their love and understanding in the completion of this report.

THIS PAGE INTENTIONALLY LEFT BLANK

## I. INTRODUCTION

The employment of artillery to strike strategic targets or simply to provide overwhelming fire power over adversaries has been one of the key tactics employed in the history of combat. In view of this, the design of projectiles achieving longer ranges and better accuracies was viewed as the main thrust of this research and development. To achieve this, we need to understand the effects on the aerodynamic properties of the projectile during its flight with specific interest against the variation of speed and angle of attack.

Conventional approach to predict the aerodynamic properties of a projectile is through wind tunnel and actual range testing. Alternate methods using Computational Fluid Dynamic (CFD) software or other computational codes are also able to predict these properties fairly well. This report aims to validate the aerodynamic properties of the M33 projectile at different Mach numbers as well as at various angles of attack using the CFX code.

The ANSYS-CFX code is a commercial CFD program used to simulate fluid flow in a variety of applications such as gas turbine engines and aircraft aerodynamics. The numerical solution techniques employed are based on the Reynolds-averaged Navier-Stokes equations and the Euler equations. Results obtained through the CFX code will also be compared with previous results obtained by other codes such as the Aeroprediction Code 2009 (AP09) and the Parabolized Navier-Stokes (PNS) viscous flow solver. The results will also be compared with experimental range data to assess the codes accuracy.

In view of the extensiveness of the research requirements, this report will only study the aerodynamic properties of a static M33 in flight. The effects of a rotation in the case of a spin-stabilized projectile will not be studied. Due to the unclassified nature of the study, research will also be limited to only unclassified information or information from open-source documents.

THIS PAGE INTENTIONALLY LEFT BLANK

## II. LITERATURE REVIEW

Conventional approaches of aerodynamic prediction on flight bodies are done using wind tunnel and actual range testing. This approach is both time consuming and cost intensive. With the development of modern CFD methods and software, engineers are able to achieve significant accuracies in the prediction of aerodynamic properties without the hassle of time and cost.

There are numerous unclassified studies and researches done on the aerodynamic prediction of projectiles. The Army Research Laboratory (ARL) provides a wide range of experimental data and simulation results on such studies. Aerodynamic predictions using traditional codes such as MCDRAG and NSWCAP for drag predictions of projectiles at transonic and supersonic speeds have already been done since the 1980s [1]. More advanced computational methods such as PNS and AP09 have also achieved fairly accurate results [2] – [3]. This provides a strong baseline for comparison of the results obtained with the CFX code.

With the development of the ANSYS-CFX code, engineers can also study the flow field and its relation to the aerodynamic properties of the projectile. It is the objective of this report to provide data on the aerodynamic properties of the M33 projectile at various speeds and angles of attack using the CFX code. Solution techniques and procedures for this report are referenced to the previous study done by Mr Tan Wei Chieh [4]. Results from this report will be matched against experimental data available for the M33 projectile found in [5], [6] and [7], as well as the computational data obtained from the AP09 program. The processes and procedures in the development of this report will also be documented in detail for future course works and analytical studies using the CFX code.

THIS PAGE INTENTIONALLY LEFT BLANK

### III. SOLUTION TECHNIQUES

#### A. THEORETICAL APPROACH

##### 1. General

For flow over bodies of revolution, the slender body theory is applicable to yield reasonable estimates of the aerodynamic forces and moments provided that the small perturbation theory is satisfied [8].

##### 2. Governing Equations

$$F_L = \rho_\infty V^2 \pi \alpha [R_{nose}^2 - R_{base}^2] \quad (1)$$

Using the base area as the reference area, Equation (1) leads to

$$C_L = 2\alpha \quad (2)$$

It is understood that no lift will be generated at zero angle of attack. The equations also imply that for a body of constant diameter or a body with a pointed nose and tail, no lift will be generated as well [8]. The slender body theory provides rough estimates for the aerodynamic properties but more accurate analysis are usually required in practice.

##### 3. Conical Shock Wave

Since lift is primarily generated by the nose cone, it is imperative to understand the aerodynamic properties occurring at the nose during flight. The study of the conical shock wave has been done by Jones [9] and Kopal [10] to satisfy the non-linear differential equations between the shock and the body at zero incidences to the free-stream. The solutions were later computed by Sims [11] in 1964.

#### B. COMPUTATIONAL APPROACH

##### 1. General

The CFX simulation was done using a half-bodied symmetry model. This was achieved by cutting out a half-bodied M33 projectile configuration from the control volume. This approach will show the flow field across the projectile as well as save

computational time. Flow is simulated by setting the front of the control volume facing the tip of the projectile as an inlet.

## 2. Governing Equations

The governing equations for the CFX code are the conservation equations for mass, momentum and energy for a compressible medium. Equation (3) is the mass conservation equation (continuity equation) and Equations (4) are the momentum conservation equations (Navier-Stokes equations) for compressible flow. Together with the energy equation in Equation (5) and the equation of state in Equation (6), these six equations constitute a system to solve for the six unknowns that are the velocity component  $u$ ,  $v$ ,  $w$ , the pressure, the density and the temperature.

$$\frac{\partial \rho}{\partial t} + \frac{\partial(\rho u)}{\partial x} + \frac{\partial(\rho v)}{\partial y} + \frac{\partial(\rho w)}{\partial z} = 0 \quad (3)$$

$$\begin{aligned} \rho \frac{\partial u}{\partial t} + \rho u \frac{\partial u}{\partial x} + \rho v \frac{\partial u}{\partial y} + \rho w \frac{\partial u}{\partial z} = & -\frac{\partial P}{\partial x} + \frac{\partial}{\partial x} \left\{ 2\mu \frac{\partial u}{\partial x} - \left(\frac{2}{3}\right) \mu \left( \frac{\partial u}{\partial x} + \frac{\partial v}{\partial y} + \frac{\partial w}{\partial z} \right) \right\} \\ & + \frac{\partial}{\partial y} \left\{ \mu \left( \frac{\partial u}{\partial y} + \frac{\partial v}{\partial x} \right) \right\} + \frac{\partial}{\partial z} \left\{ \mu \left( \frac{\partial w}{\partial x} + \frac{\partial u}{\partial z} \right) \right\} \\ \rho \frac{\partial v}{\partial t} + \rho u \frac{\partial v}{\partial x} + \rho v \frac{\partial v}{\partial y} + \rho w \frac{\partial v}{\partial z} = & -\frac{\partial P}{\partial y} + \frac{\partial}{\partial y} \left\{ 2\mu \frac{\partial v}{\partial y} - \left(\frac{2}{3}\right) \mu \left( \frac{\partial u}{\partial x} + \frac{\partial v}{\partial y} + \frac{\partial w}{\partial z} \right) \right\} \\ & + \frac{\partial}{\partial x} \left\{ \mu \left( \frac{\partial u}{\partial y} + \frac{\partial v}{\partial x} \right) \right\} + \frac{\partial}{\partial z} \left\{ \mu \left( \frac{\partial w}{\partial y} + \frac{\partial v}{\partial z} \right) \right\} \\ \rho \frac{\partial w}{\partial t} + \rho u \frac{\partial w}{\partial x} + \rho v \frac{\partial w}{\partial y} + \rho w \frac{\partial w}{\partial z} = & -\frac{\partial P}{\partial z} + \frac{\partial}{\partial z} \left\{ 2\mu \frac{\partial w}{\partial z} - \left(\frac{2}{3}\right) \mu \left( \frac{\partial u}{\partial x} + \frac{\partial v}{\partial y} + \frac{\partial w}{\partial z} \right) \right\} \\ & + \frac{\partial}{\partial x} \left\{ \mu \left( \frac{\partial w}{\partial x} + \frac{\partial u}{\partial z} \right) \right\} + \frac{\partial}{\partial y} \left\{ \mu \left( \frac{\partial v}{\partial z} + \frac{\partial w}{\partial y} \right) \right\} \end{aligned} \quad (4)$$

$$\begin{aligned} \rho \frac{D}{Dt} \left( e + \frac{V^2}{2} \right) = & \frac{\partial}{\partial x} \left( k_e \frac{\partial T}{\partial x} \right) + \frac{\partial}{\partial y} \left( k_e \frac{\partial T}{\partial y} \right) + \frac{\partial}{\partial z} \left( k_e \frac{\partial T}{\partial z} \right) - \frac{\partial}{\partial x} (Pu) - \frac{\partial}{\partial y} (Pv) - \frac{\partial}{\partial z} (Pw) \\ & + \frac{\partial}{\partial x} \{ u\tau_{xx} \} + \frac{\partial}{\partial y} \{ u\tau_{yx} \} + \frac{\partial}{\partial z} \{ u\tau_{zx} \} + \frac{\partial}{\partial x} \{ v\tau_{xy} \} + \frac{\partial}{\partial y} \{ v\tau_{yy} \} + \frac{\partial}{\partial z} \{ v\tau_{zy} \} \\ & + \frac{\partial}{\partial x} \{ w\tau_{xz} \} + \frac{\partial}{\partial y} \{ w\tau_{yz} \} + \frac{\partial}{\partial z} \{ w\tau_{zz} \} \end{aligned} \quad (5)$$

where:

$$\frac{D}{Dt} = \frac{\partial}{\partial t} + u \frac{\partial}{\partial x} + v \frac{\partial}{\partial y} + w \frac{\partial}{\partial z}$$

$$\begin{aligned}
e &= c_v T \\
\tau_{xy} = \tau_{yx} &= \mu \left( \frac{\partial v}{\partial x} + \frac{\partial u}{\partial y} \right) \\
\tau_{yz} = \tau_{zy} &= \mu \left( \frac{\partial w}{\partial y} + \frac{\partial v}{\partial z} \right) \\
\tau_{zx} = \tau_{xz} &= \mu \left( \frac{\partial u}{\partial z} + \frac{\partial w}{\partial x} \right) \\
\tau_{xx} &= -\frac{2}{3} \mu \left( \frac{\partial u}{\partial x} + \frac{\partial v}{\partial y} + \frac{\partial w}{\partial z} \right) + 2\mu \frac{\partial u}{\partial x} \\
\tau_{yy} &= -\frac{2}{3} \mu \left( \frac{\partial u}{\partial x} + \frac{\partial v}{\partial y} + \frac{\partial w}{\partial z} \right) + 2\mu \frac{\partial v}{\partial y} \\
\tau_{zz} &= -\frac{2}{3} \mu \left( \frac{\partial u}{\partial x} + \frac{\partial v}{\partial y} + \frac{\partial w}{\partial z} \right) + 2\mu \frac{\partial w}{\partial z} \\
P &= R\rho T \tag{6}
\end{aligned}$$

### 3. Boundary Conditions

The surface of the projectile is set as an adiabatic wall under no-slip conditions. The inlet and outlet boundary condition are set as free-stream conditions while a symmetry condition is applied at the centerline axis of the projectile. The rest of the control surfaces are set as opening. The default flow field is set as free-stream conditions.

### 4. Turbulence Model

The k-epsilon (k-  $\epsilon$ ) and Shear Stress Transport (SST) model were explored for the turbulence modeling of the simulation.

The k-  $\epsilon$  model is a two equation model using the turbulent kinetic energy, k and the turbulent dissipation,  $\epsilon$ . It accounts for history effects like convection and diffusion of turbulent energy that makes it a reasonably accurate prediction model although it does not perform well in cases with large adverse pressure gradients and flow separation [12].

The SST model combines the effects of the k-omega (k- $\omega$ ) model which uses specific dissipation,  $\omega$  and the k-  $\epsilon$  model. The k- $\omega$  model is used in the inner parts of the boundary layer while the k-  $\epsilon$  model is used in the free-stream as the prior model is too sensitive to the inlet free-stream turbulence properties. The SST model performs well for

cases of adverse pressure gradients and separated flow but tends to over-predict turbulence level in regions with large normal strain and strong acceleration [12].

## 5. Free-stream Flow

The free-stream velocity is simulated as the u-component of the inlet boundary condition for zero angle of attack. At other angle of attack with reference to the X-Y plane, the inlet flow is divided into the u-component and v-component as shown in Figure 1. This approach will simulate flow at different angles of attack and save computational time.

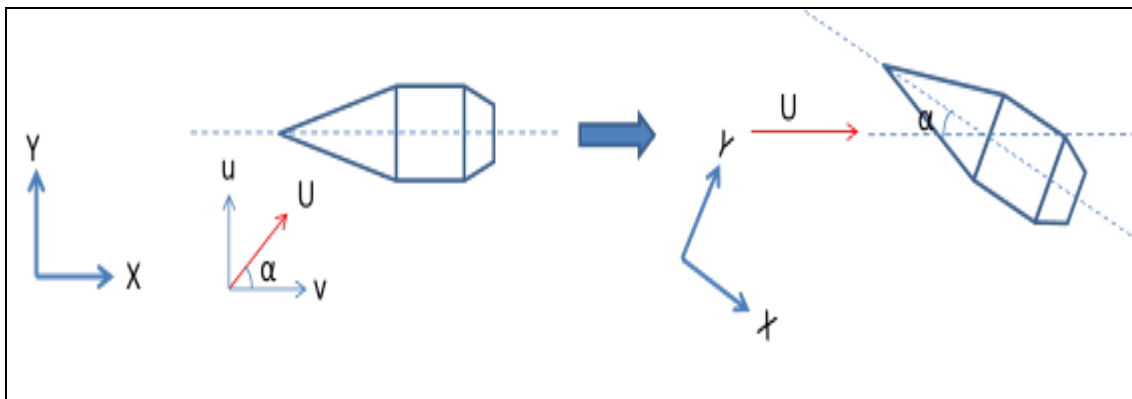


Figure 1. Free-Stream Flow Diagram (CFX).

The u and v component were derive from the free-stream Mach number using Equation (7).

$$\begin{aligned}
 u &= Mach \times 340.3 \times \cos \alpha \\
 v &= Mach \times 340.3 \times \sin \alpha
 \end{aligned}
 \tag{7}$$

## 6. Results

$F_y$  and  $F_x$  obtained from the CFX simulations represents the axial and normal force respectively. At zero angle of attack,  $F_y$  and  $F_x$  are equivalent to the lift ( $F_L$ ) and drag force ( $F_D$ ) respectively. For other angles of attack,  $F_y$  and  $F_x$  are not equal to  $F_L$  and  $F_D$  as shown in Figure 2.  $F_L$  and  $F_D$  will have to be obtained through further calculations as shown in Equation (8).

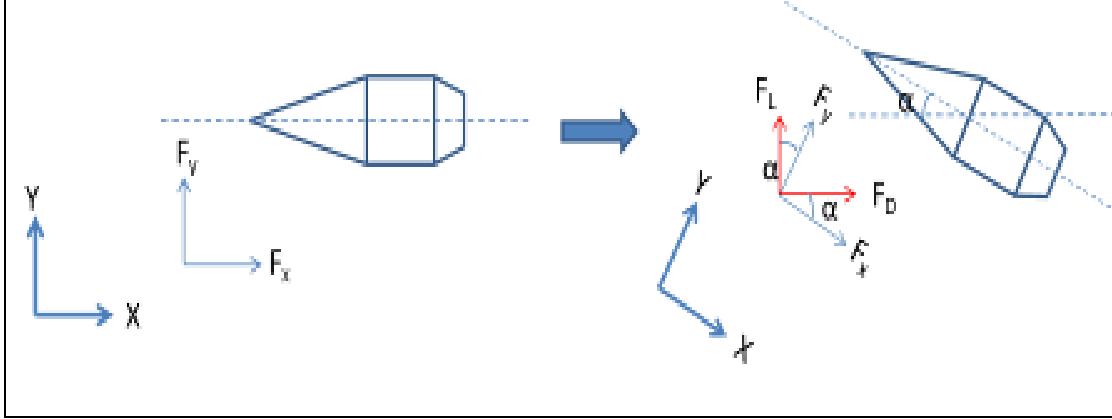


Figure 2. Force Diagram (CFX).

$$\begin{aligned}
 F_D &= F_x \cos \alpha + F_y \sin \alpha \\
 F_L &= F_y \cos \alpha - F_x \sin \alpha
 \end{aligned} \tag{8}$$

After obtaining  $F_y$ ,  $F_x$  and the torque with respect to  $z$ -axis ( $T_z$ ), the results for  $C_L$  and  $C_D$  at various angles of attack were derived using Equation (9) while  $C_{N\alpha}$ ,  $C_{M\alpha}$  at various Mach numbers were derived using Equation (10), (11) and (12).  $C_{D0}$  is simply the drag coefficient at zero angle of attack.  $0^\circ$  and  $2^\circ$  were used for the computation for  $C_{N\alpha}$  and  $C_{M\alpha}$ . Note that all the forces obtained from the simulation need to be multiplied by two as the model only accounts for a half-bodied projectile. The length from the projectile base to the center of gravity (0.023m) was used as the reference length for the computation of  $C_M$ .

$$\begin{aligned}
 C_L &= \frac{2F_L}{\frac{1}{2}\rho V^2 S_{ref}} \\
 C_D &= \frac{2F_D}{\frac{1}{2}\rho V^2 S_{ref}}
 \end{aligned} \tag{9}$$

$$C_N = C_L \cos \alpha + C_D \sin \alpha \tag{10}$$

$$C_M = \frac{2T_z}{\frac{1}{2}\rho V^2 S_{ref} l_{ref}} \quad (11)$$

$$C_{N\alpha} = \frac{C_{N(\alpha_2)} - C_{N(\alpha_1)}}{\alpha_2 - \alpha_1}$$

$$C_{M\alpha} = \frac{C_{M(\alpha_2)} - C_{M(\alpha_1)}}{\alpha_2 - \alpha_1} \quad (12)$$

## IV. PROCESS AND PROCEDURES

### A. SOLIDWORKS 2010

#### 1. Introduction

SolidWorks 2010 is a 3D mechanical CAD software used for design and modeling purposes. It was released in December 2010 and has been upgraded to its latest version of SolidWorks 2012 in September 2011. It uses a parametric featured-based method to create models and assemblies. Details of the processes and input parameters can be found in Appendix A.

#### 2. Two Dimensional Model

The 2D model of the M33 projectile as shown in Figure 3 was drawn with reference to the geometry inputs in [6].

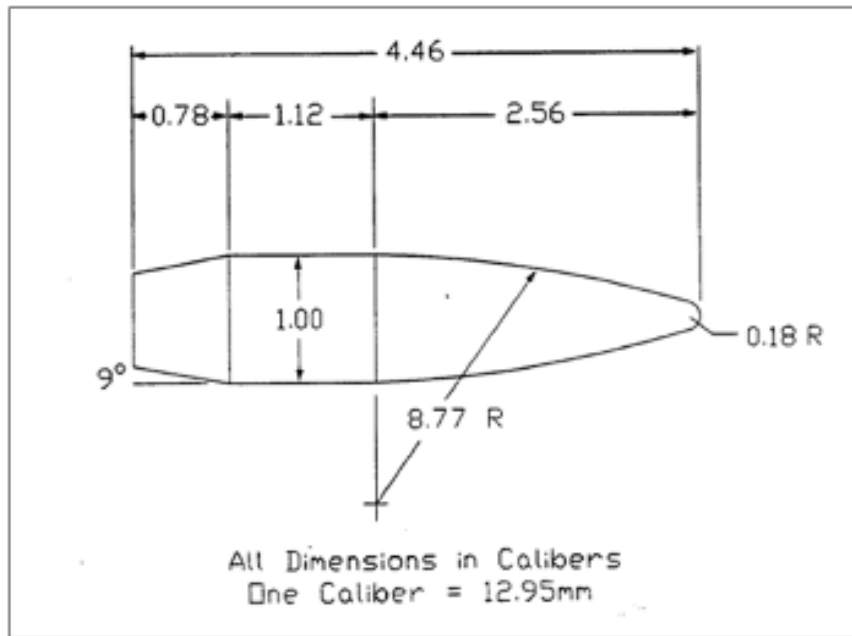


Figure 3. Schematic of the M33 Projectile.

The ogive nose profile of the M33 projectile was drawn using tangent arcs for the nose cone and nose tip. The control volume was set as 10 times the reference length of the projectile to avoid wall interference effects as is often seen in wind tunnel testing.

### 3. Three Dimensional Model

There are two ways to produce the 3D model of the M33 projectile for simulation. One way is to generate the projectile as a full solid 3D model as shown in Figure 4 and the other is to cut out the half-body of the projectile from the control volume as a cavity as shown in Figure 5. The latter method was chosen for simplicity and saving of computational time.

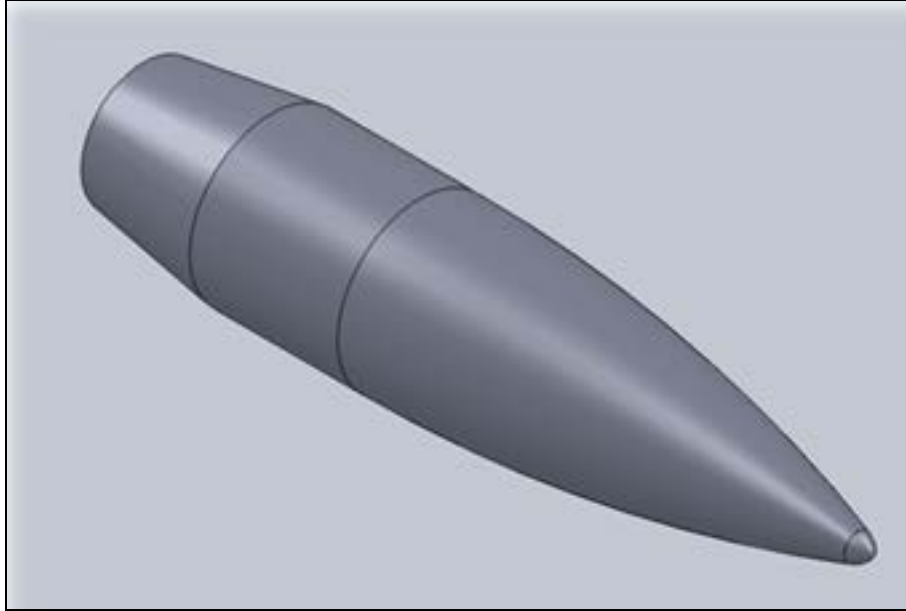


Figure 4. Solid 3D Model of M33 Projectile (SolidWorks).

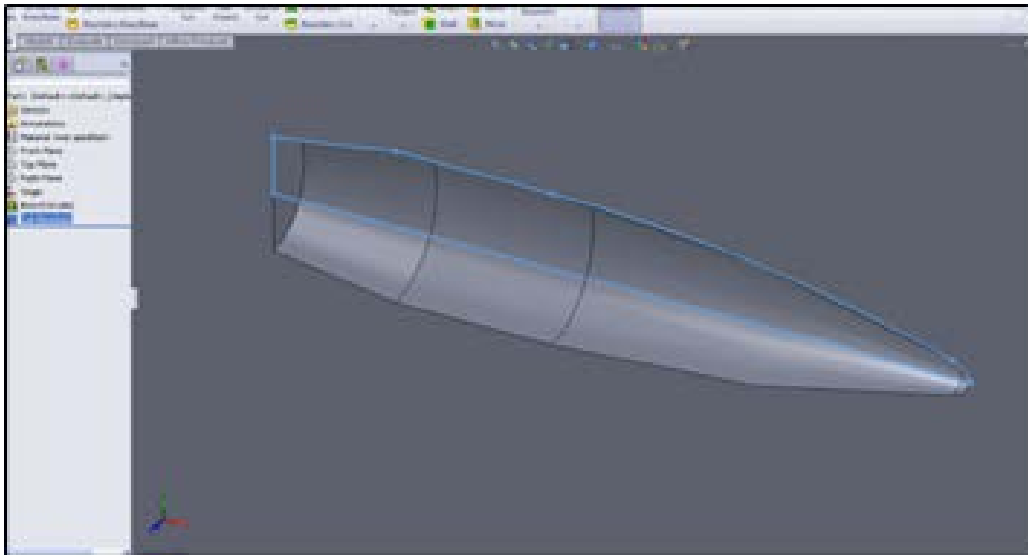


Figure 5. Cavity of M33 Projectile (SolidWorks).

The model was saved as a parasolid file to be imported into the geometry interface of the ANSYS-CFX code.

## B. CFX

### 1. Introduction

The CFX code uses the full Navier-Stokes equations to solve for fluid flows over a region of interest with given specific boundary conditions. It complements traditional empirical methods and wind tunnel testing as an alternate, cost-effective tool with vivid graphic interface for the study of fluid flow. Details for the processes and input parameters can be found in Appendix B.

### 2. Mesh

A portion of the mesh for over 650,000 nodes and 2 million elements is seen in Figure 6.

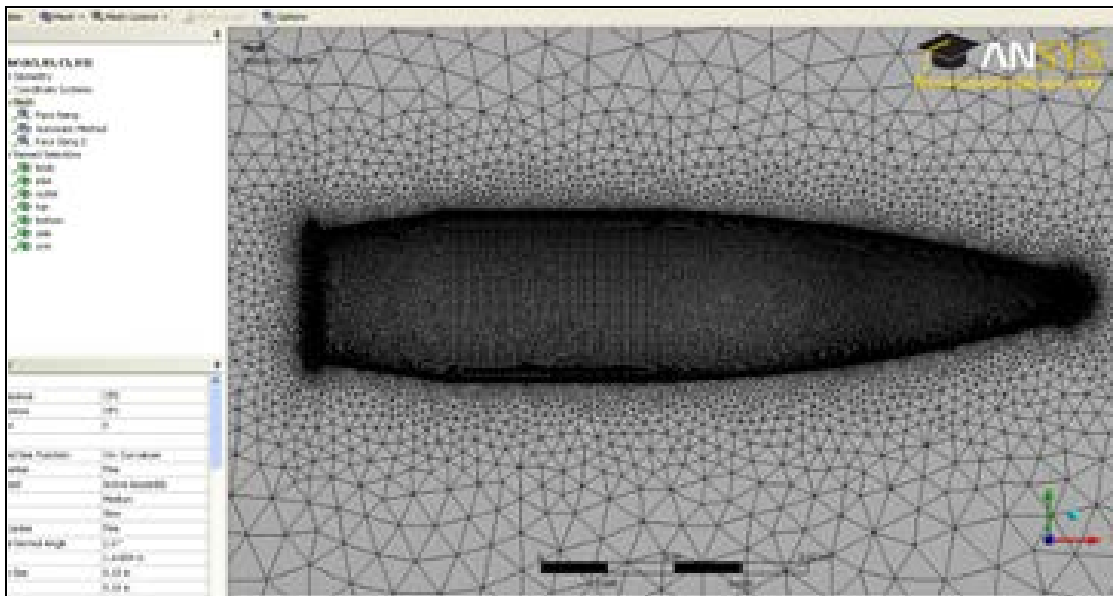


Figure 6. Mesh of M33 Projectile (CFX).

The parameters for the mesh input differ from model to model. Engineers need to discover the optimal input parameters to achieve high fidelity through trials and errors. The fundamentals for better fidelity were to reduce the element size and achieving a small Y-plus value after post-processing. Reducing the element size refines the mesh

especially in areas with protruding angles. This will reduce the computational error. Y-plus is the non-dimensional wall distance for a wall-bounded flow that is commonly used in boundary layer theory and in defining the law of the wall [13].

To reduce element size, engineers can try to reduce the sizing input parameters for minimum and maximum size along with the curvature angle in the mesh module. This will produce a model with higher number of nodes and elements but need not necessarily increase the fidelity of the results significantly. A mesh with large numbers of elements would require longer computational time as well.

To achieve smaller Y-plus values, engineers should refine the mesh parameters at critical area of interest. This will improve the fidelity of the simulation without having to increase the mesh size significantly. For this report, the areas of interest are the surfaces of the projectile especially at the nose tip and base. Inflation layers can be set at the surface of the projectile for refinement as shown in Figure 7. The maximum thickness for the inflation layer will depend on the projectile geometry size and the number of layers that can be inserted will depend on the maximum thickness and growth rate defined. Specific face sizing can be applied at surfaces of the base and nose tip to further refine the mesh as shown in Figure 8 and 9.

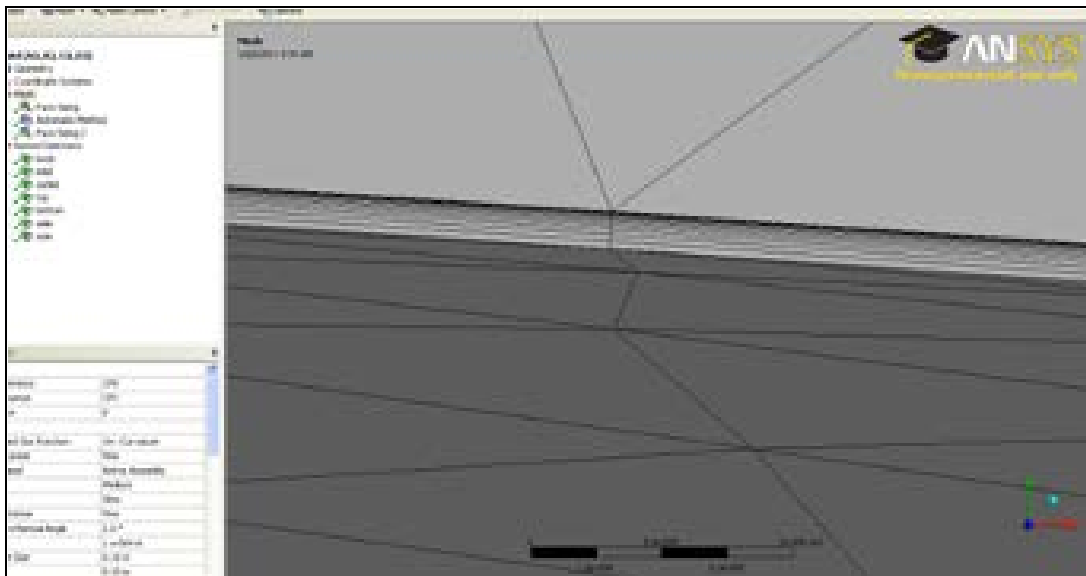


Figure 7. Inflation Layers (CFX).

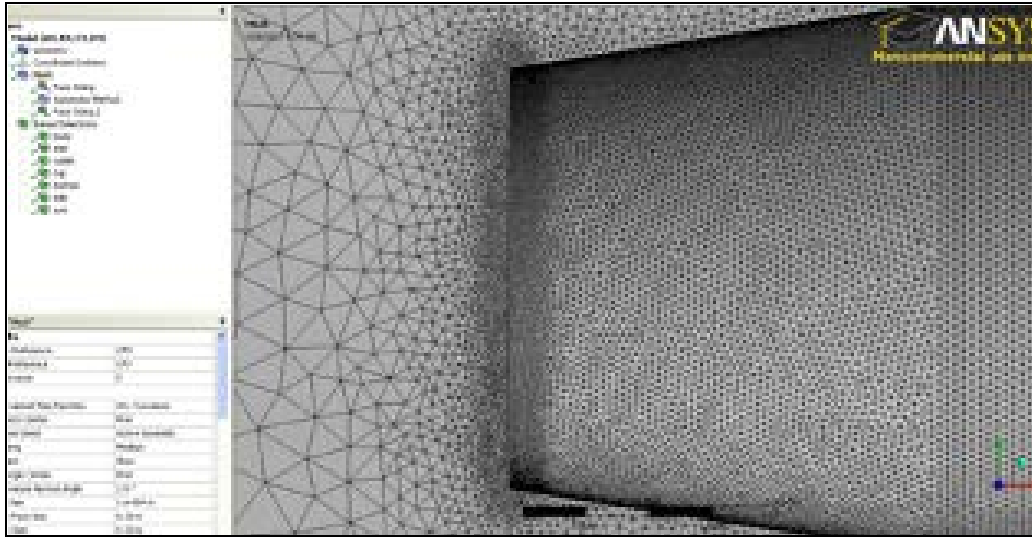


Figure 8. Face Sizing at Base (CFX).

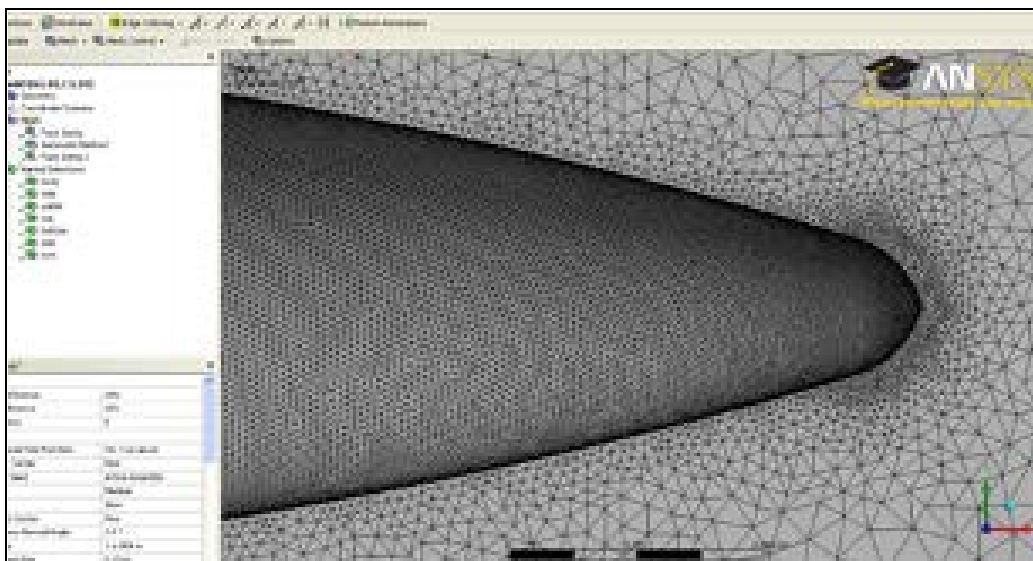


Figure 9. Face Sizing at Nose Tip (CFX).

### 3. Pre-processor

The model was set to analysis the flow at steady-state conditions with the fluid definition set as air-ideal gas. The simulations were run with both the  $k-\epsilon$  and SST model for high speed conditions and compressibility effects. For speed of M0.5 to M1.0 and M1.5 to M2.6, the inlet flow conditions were set as mixed flow and supersonic flow respectively with a static temperature setting of 288.15K. Outlet conditions were set as

subsonic flow throughout with a static pressure of 0 Pa. Openings were set as entrainments with a static pressure of 0 Pa as well.

#### 4. Post-processor

Flow across the projectile was studied by inserting a plane across the X-Y axis on the symmetry plane. Velocity vectors with local Mach number and pressure contours as shown in Figure 10, 11 and 12 can be applied onto the plane to understand the flow field of the projectile in flight.

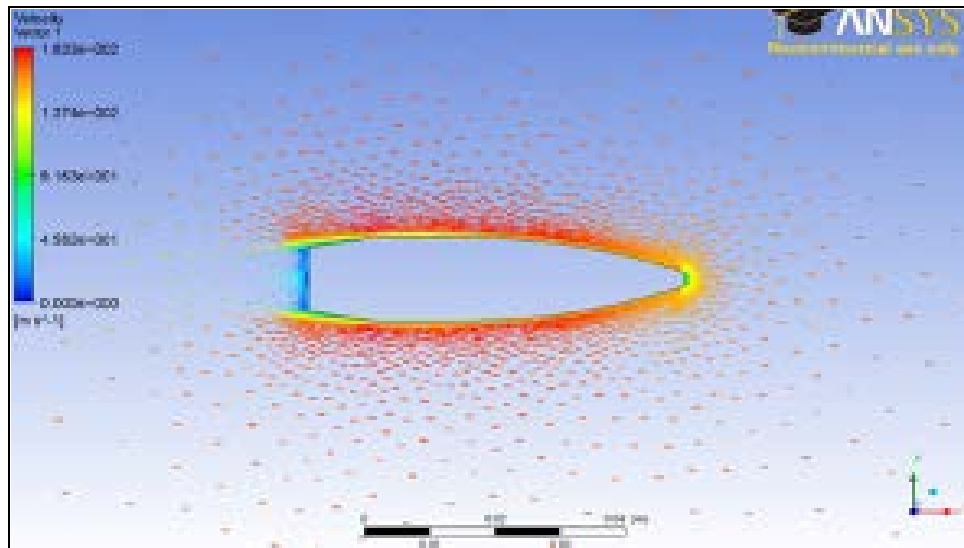


Figure 10. Velocity Vector (CFX).

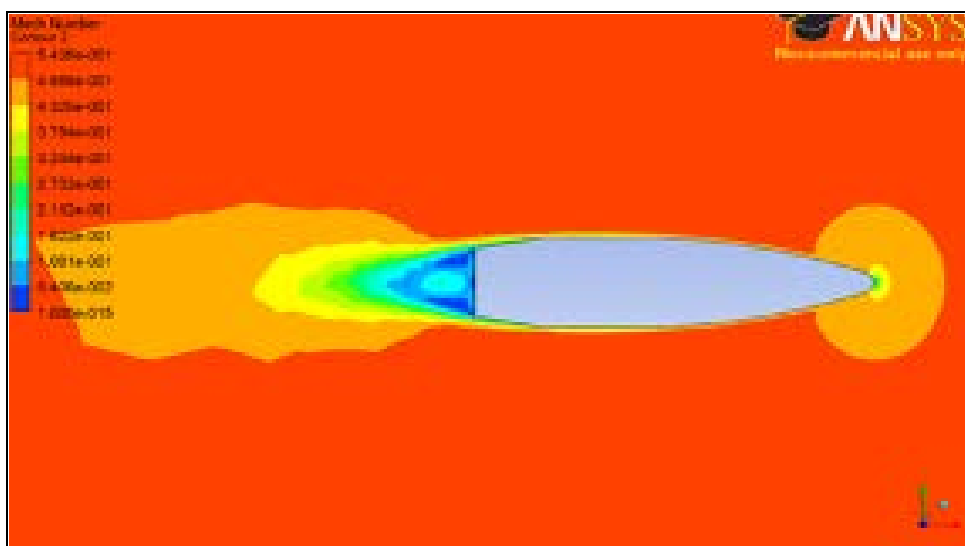


Figure 11. Local Mach Number Contour (CFX).

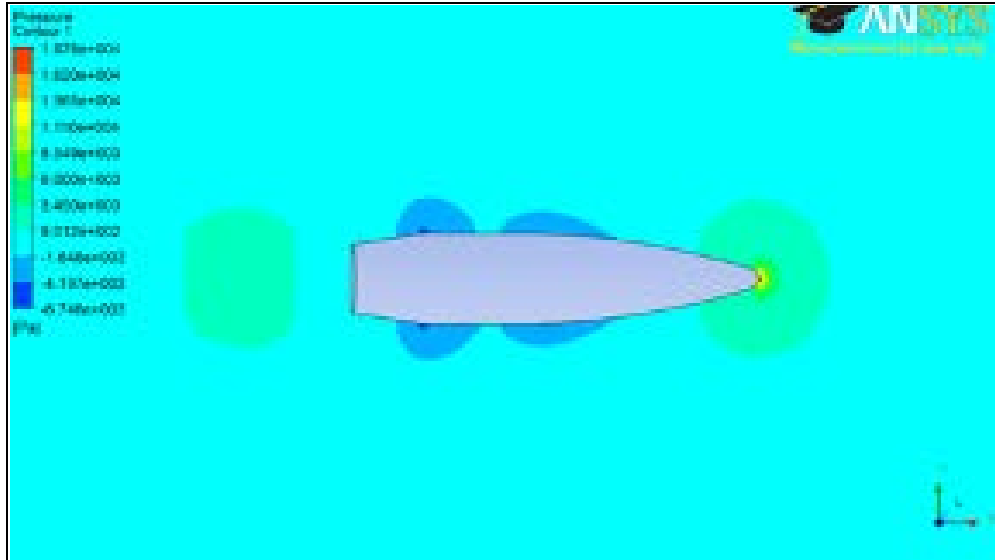


Figure 12. Local Pressure Contour (CFX).

The function calculator was used to extract the respective Y-plus, force and torque results from the simulations as shown in Appendix D.

## C. AP09

### 1. Introduction

AP09 uses a semi-empirical technique for the estimation of aerodynamic properties on spin stabilized projectiles as well as various missile configurations. The program was developed in 1972 and has since evolved with the combination of experimental results with theoretical methodology to produce reasonable aerodynamic prediction for flight bodies.

In this study, the AP09 was used to compute the various aerodynamic properties of the M33 projectile to be compared with the results derived from CFX. Details of the processes and input parameters can be found in Appendix C.

### 2. M33 Projectile Configuration and Input Parameters

Table 1 shows the input parameters for the M33 projectile configuration with reference to [14].

<b>General</b>	
Reference Diameter	12.95mm
Distance of Moment from Nose Tip	33.15mm
<b>Nose Geometry</b>	
Nose Cross Sectional Shape	Circular
Circular Radius at Nose	6.475mm
Nose Profile	Secant Ogive Blunt
Radius of Curvature	113.57mm
Spherical Cap Radius	2.33mm
Length of Nose	33.15mm
<b>Afterbody Geometry</b>	
Longitudinal Afterbody Coordinate from Nose Tip	47.66mm
<b>Boattail/ Flare</b>	
Longitudinal Boattail/ Flare Coordinate from Nose Tip	57.76mm
Corresponding Boattail/ Flare Characteristic Half Width	4.875mm
<b>Options</b>	
Sea level	
Dynamic derivatives	
Spin stabilized	

Table 1. M33 Input Parameters (AP09).

### 3. Results

The program was run for “Mach Sweep” from  $M= 0.5$  to  $3.0$  with an interval size of  $0.15$  at  $0^\circ$  and  $2^\circ$  angle of attack. The results obtained were compared to previous results in the API reference [3] to check for error rate. The results obtained agree fairly well with the API reference as shown in Figure 13 and 14.

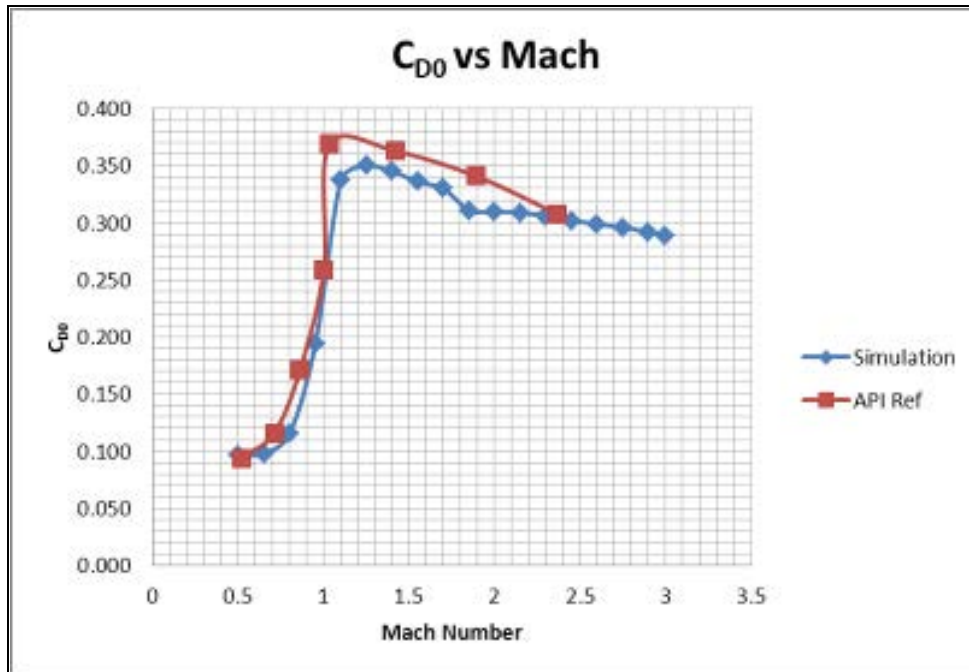


Figure 13. C<sub>D0</sub> vs Mach (AP09).

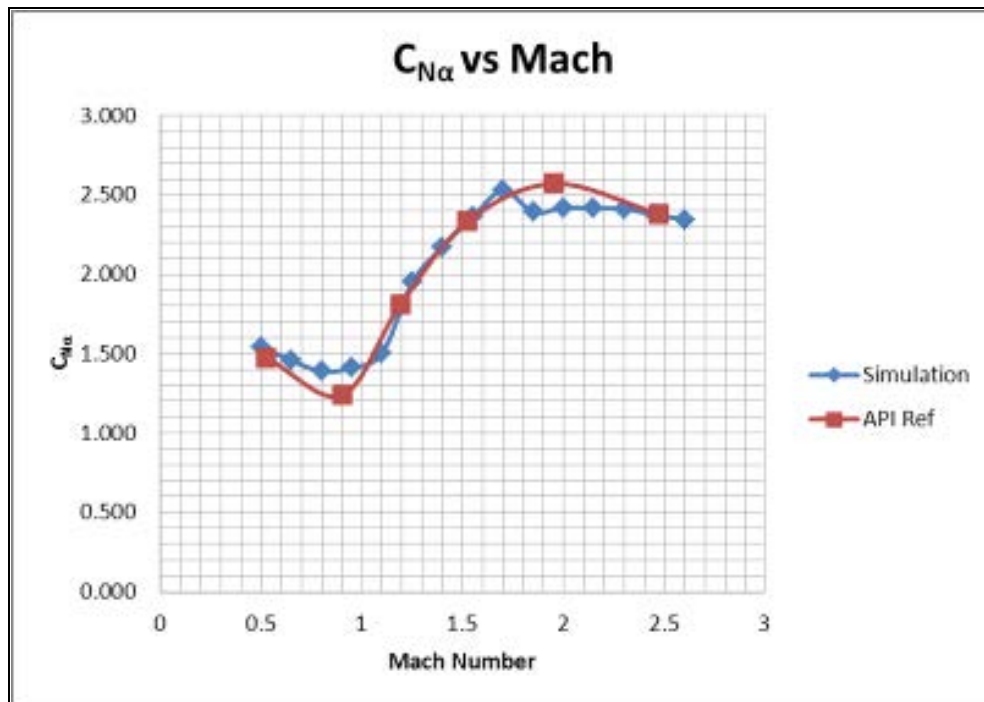


Figure 14. C<sub>Nα</sub> vs Mach (AP09).

From the same configuration and input parameters, the plots for  $C_L$  vs  $\alpha$  and  $C_D$  vs  $\alpha$  at  $M= 0.5$  for  $0^\circ$  to  $85^\circ$  angles of attack as shown in Figure 15 and 16 were generated for comparison with the results from CFX.

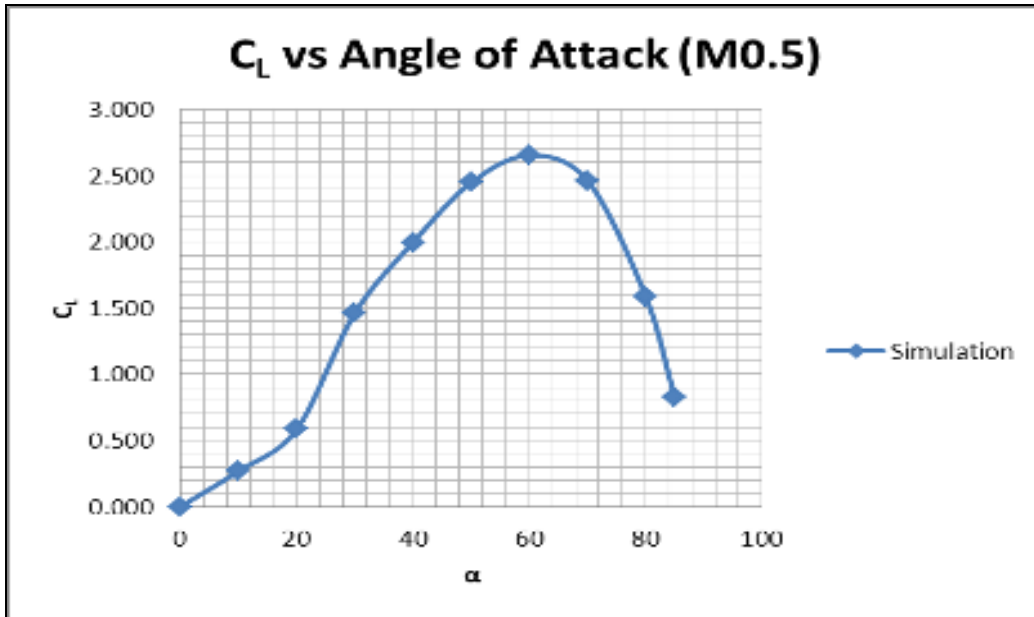


Figure 15.  $C_L$  vs  $\alpha$  (AP09).

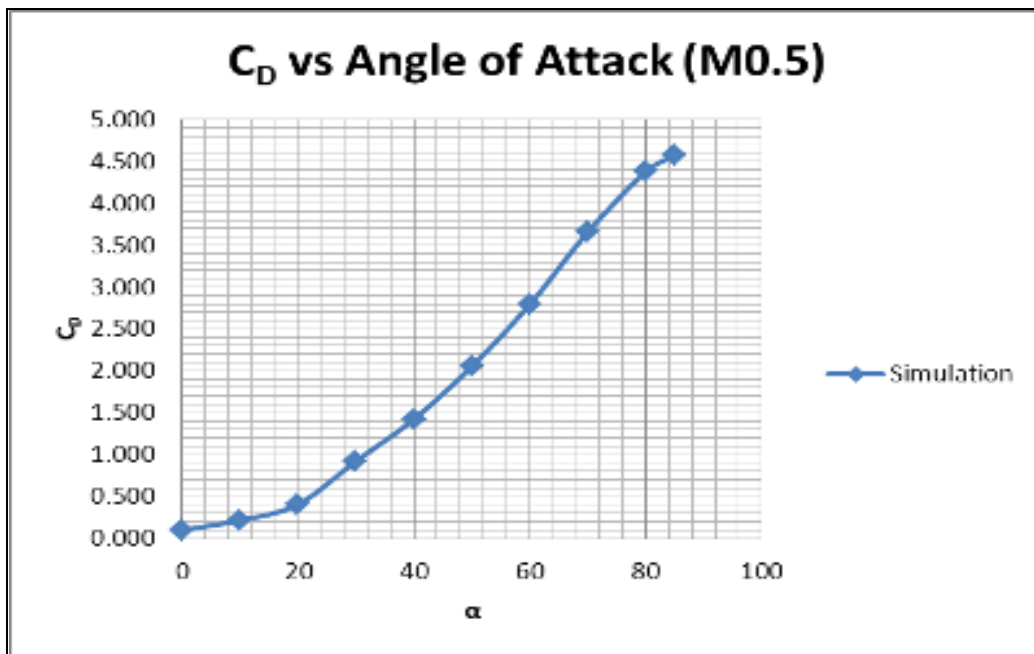


Figure 16.  $C_D$  vs  $\alpha$  (AP09).

## V. RESULTS AND ANALYSIS

### A. LINEARITY AT LOW ANGLES OF ATTACK

To calculate  $C_{N\alpha}$  and  $C_{M\alpha}$ , we must first ensure that the aerodynamic properties are linear at low angles of attack. Figure 18 and 20 shows that the results for  $C_N$  are fairly linear for subsonic and supersonic Mach numbers up to  $6^\circ$  angles of attack. For transonic Mach numbers as shown in Figure 19,  $C_N$  is only linear up to  $4^\circ$  angles of attack.

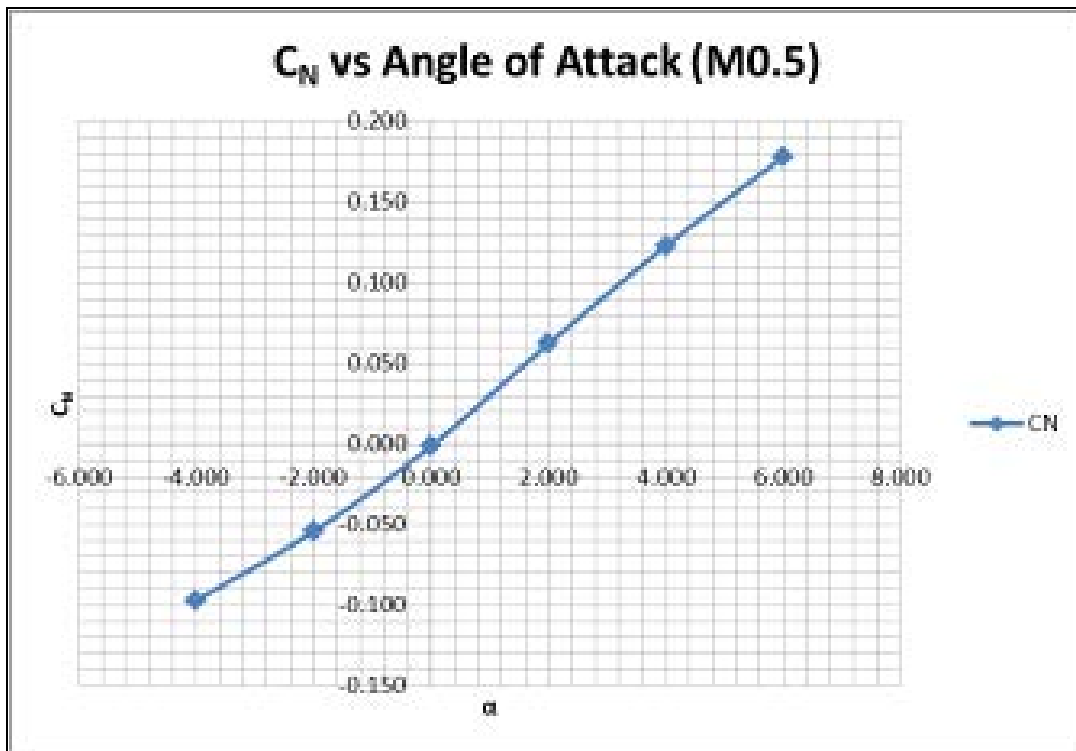


Figure 17.  $C_N$  vs  $\alpha$ \_Subsonic (CFX).

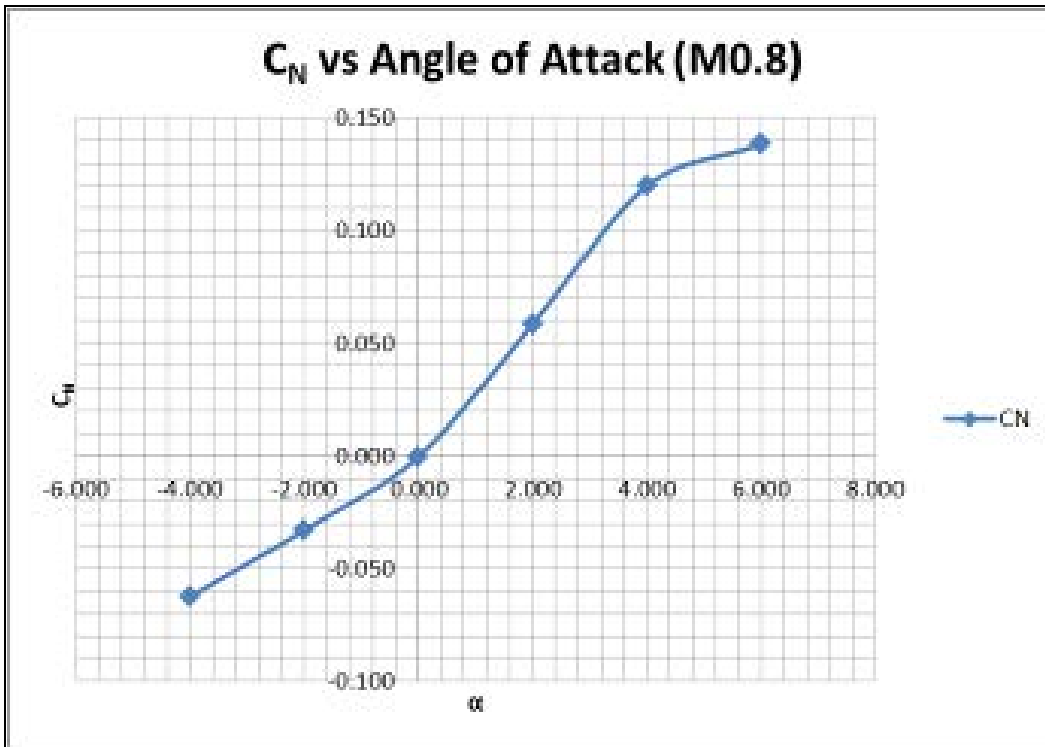


Figure 18.  $C_N$  vs  $\alpha$ \_Transonic (CFX).

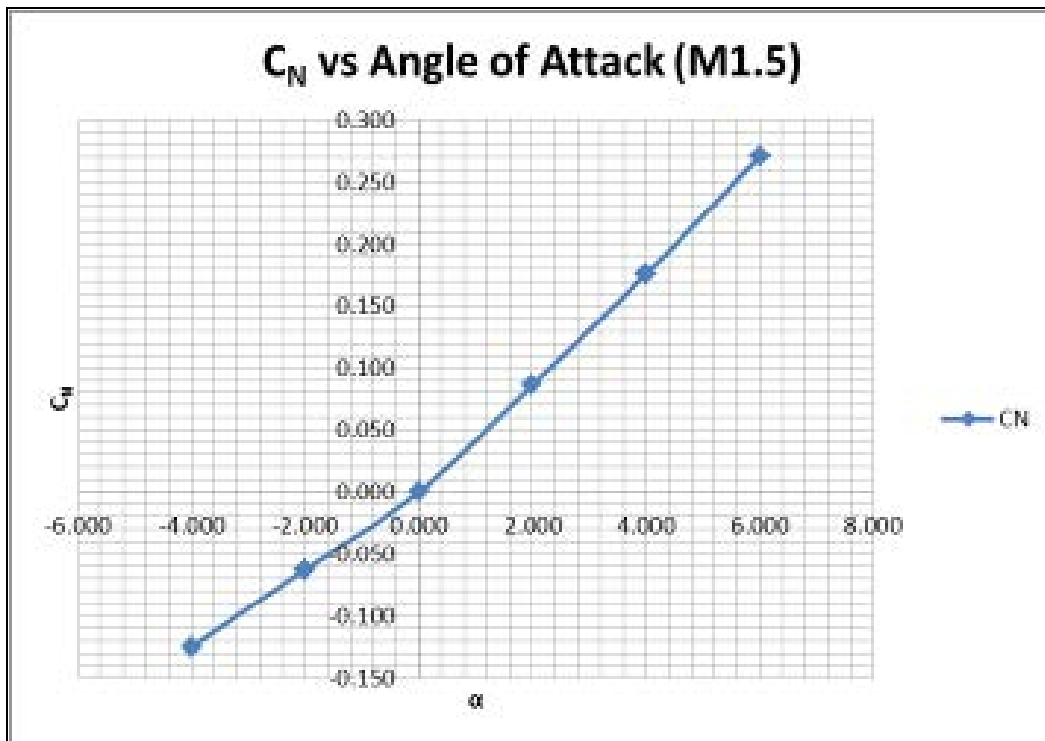


Figure 19.  $C_N$  vs  $\alpha$ \_Supersonic (CFX).

## B. EFFECTS OF MACH NUMBERS

### 1. k- epsilon Model

The results from the k-  $\epsilon$  model show good agreement with experimental data for both  $C_{N\alpha}$  and  $C_{M\alpha}$ , but tend to over predict for  $C_{D0}$  at higher Mach numbers as shown in Figures 21, 22 and 23. This could be due to the models insufficiency in cases with large adverse pressure gradient and separated flow, as stated in [12].

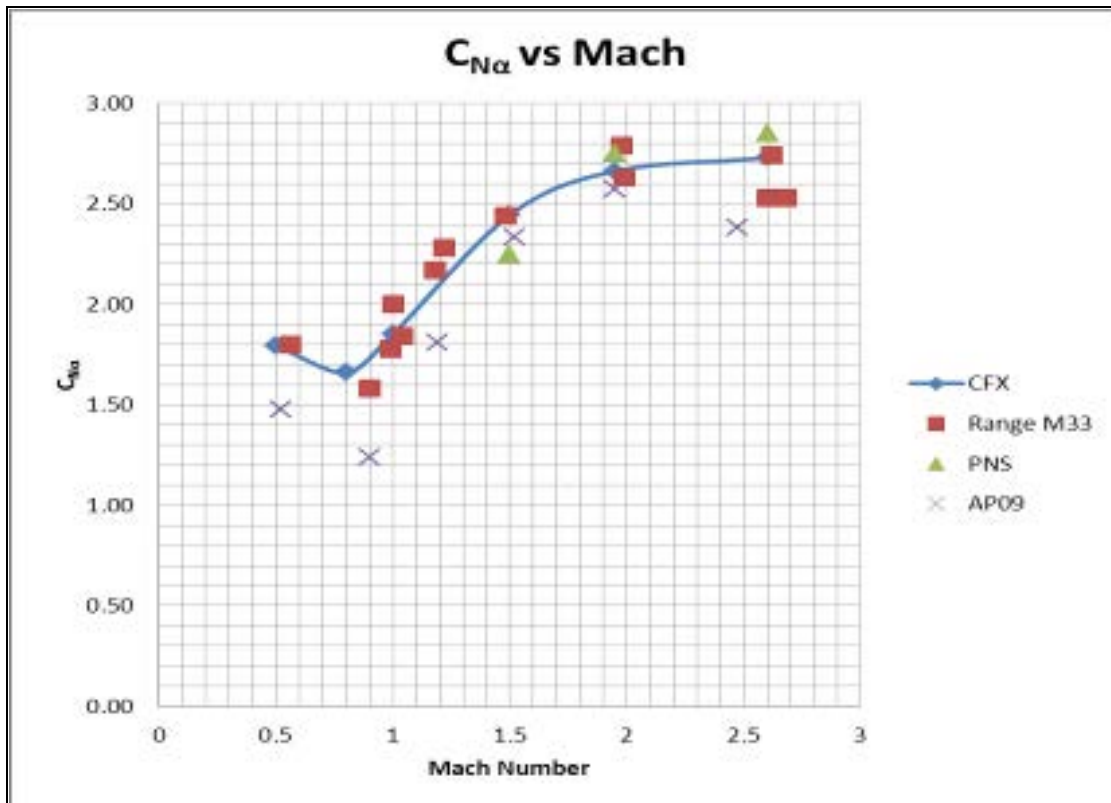


Figure 20.  $C_{N\alpha}$  vs Mach Numbers\_k-  $\epsilon$  Model (CFX).

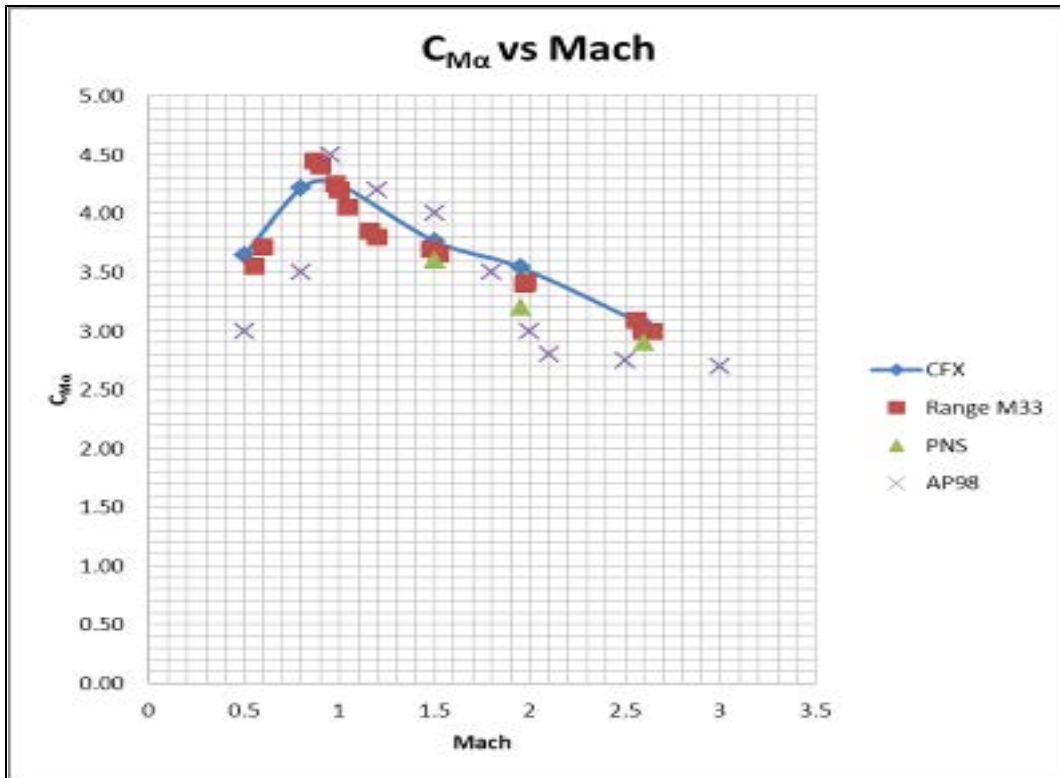


Figure 21. C<sub>Mα</sub> vs Mach Number\_k- ε Model (CFX).

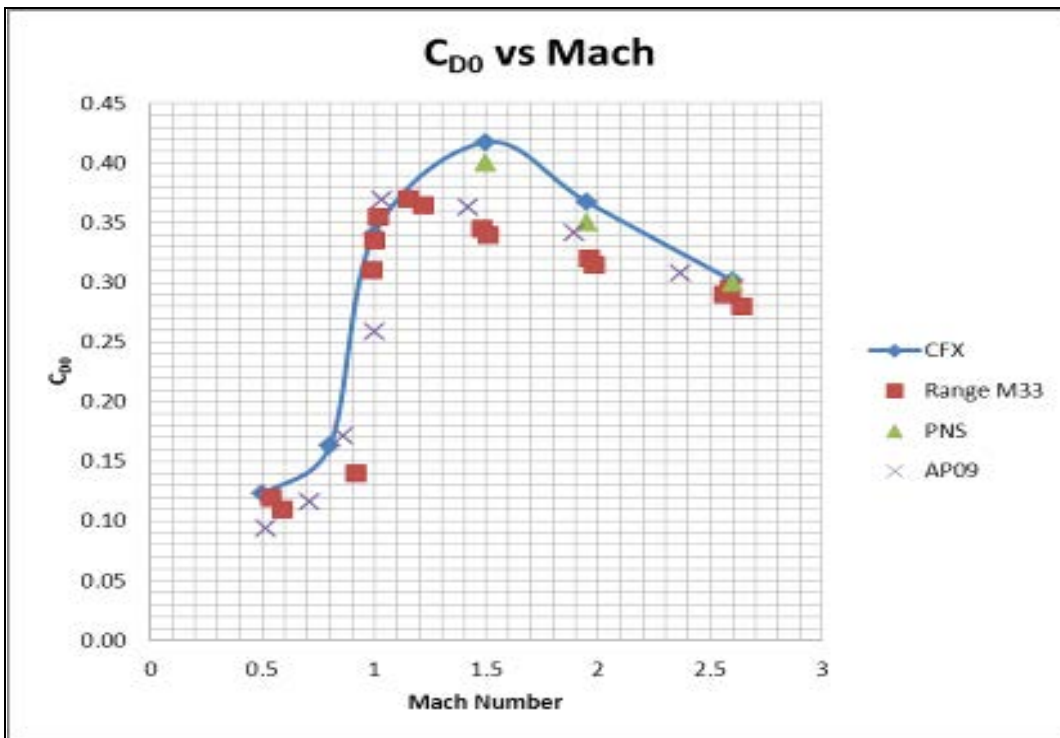


Figure 22. C<sub>D0</sub> vs Mach Number\_k- ε Model (CFX).

## 2. Shear Stress Transport Model

The SST model on the other hand produces good agreement with experimental data only for supersonic Mach numbers as shown in Figures 24, 25 and 26. Although it tends to over predict  $C_{D0}$  as well, the results for  $M= 1.5$  to  $2.6$  are closer to the experimental data as compared to the  $k-\epsilon$  model. The poor results for the subsonic and transonic Mach numbers especially at  $M=1.0$  could be due to the models tendency to over-predict the turbulence level in regions with large normal strain and acceleration as stated in [12].

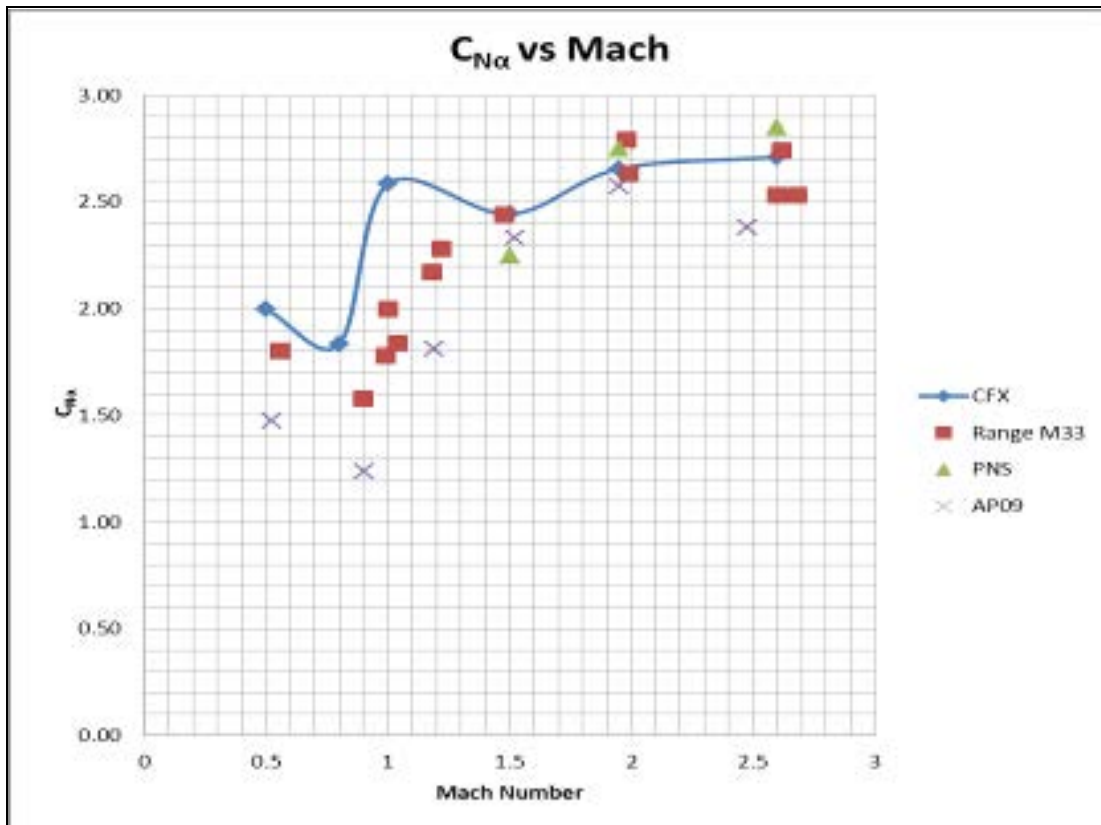


Figure 23.  $C_{N\alpha}$  vs Mach Numbers\_SST Model (CFX).

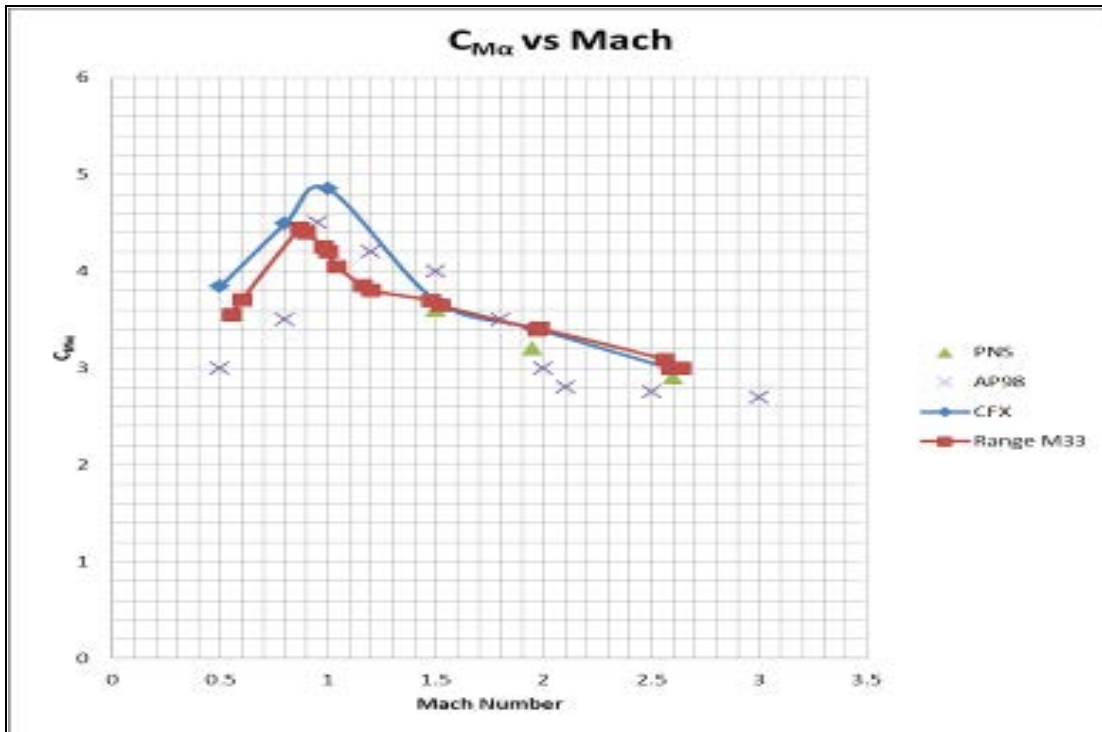


Figure 24.  $C_{M\alpha}$  vs Mach Numbers\_SST Model (CFX).

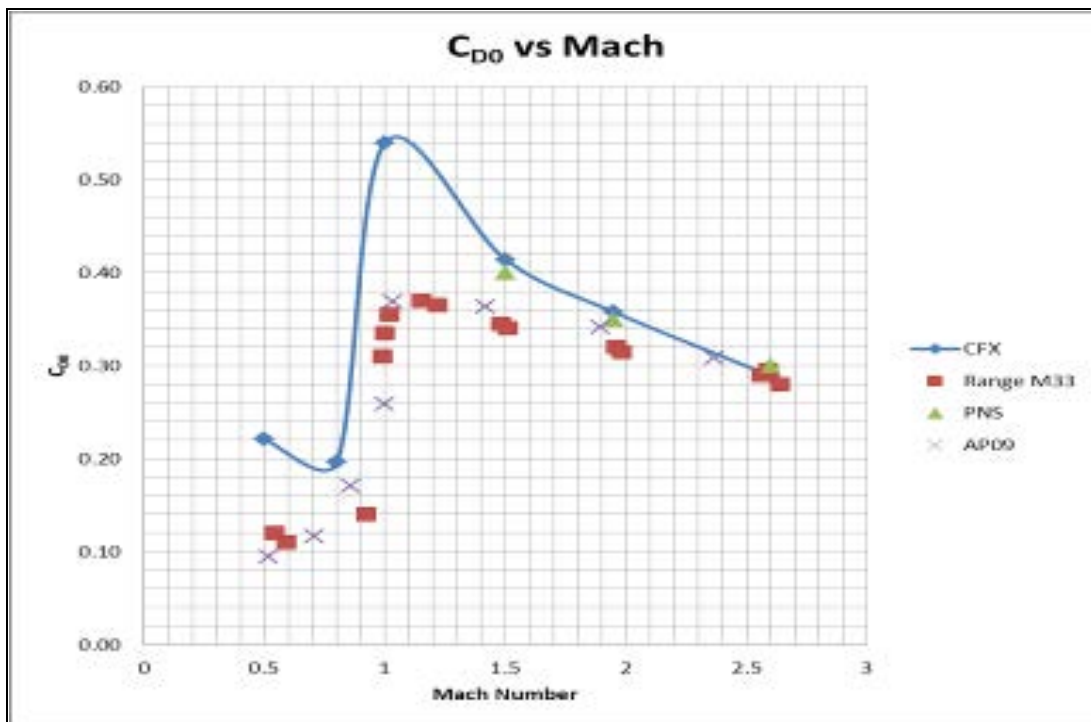


Figure 25.  $C_{D0}$  vs Mach Numbers\_SST Model (CFX).

### 3. Combined k- $\epsilon$ and SST Model

Combining the results from the k-  $\epsilon$  model for  $M= 0.5$  to  $1.0$  and SST model for  $M=1.5$  to  $2.6$  produces good agreement against the experimental range data for  $C_{N\alpha}$  and  $C_{M\alpha}$  as shown in Figures 27 and 28.  $C_{D0}$  tends to be over predicted by an average error of 11.6% with the highest error occurring at  $M= 1.5$  as shown in Figure 29. Detailed data and flow diagrams of the projectile at various Mach numbers can be found in Appendix D.

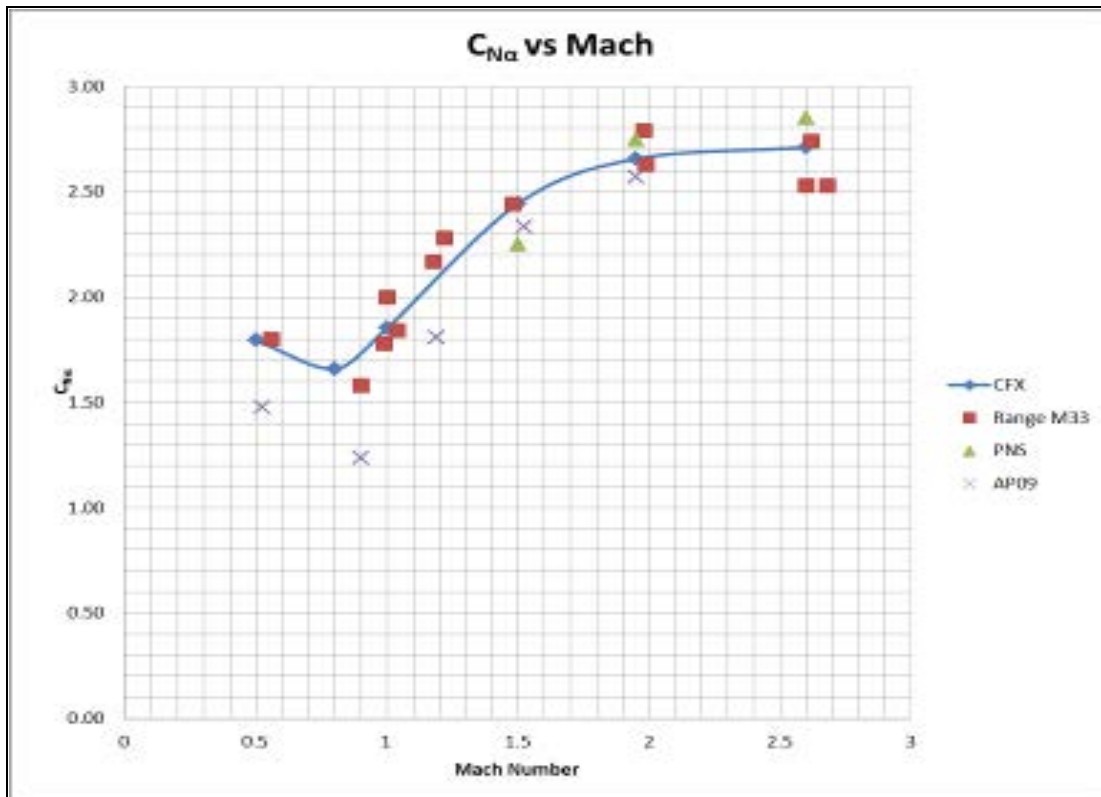


Figure 26.  $C_{N\alpha}$  vs Mach Numbers\_Combined k-  $\epsilon$ / SST Model (CFX).

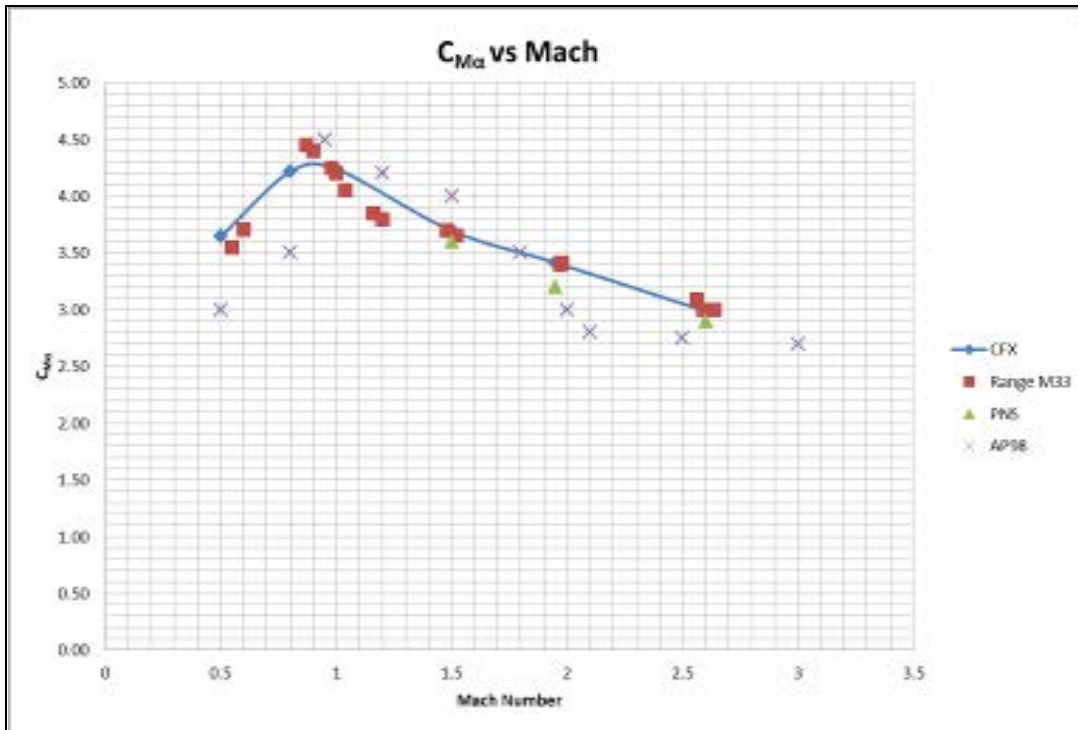


Figure 27.  $C_{M\alpha}$  vs Mach Numbers\_Combined k-  $\epsilon$ / SST Model (CFX).

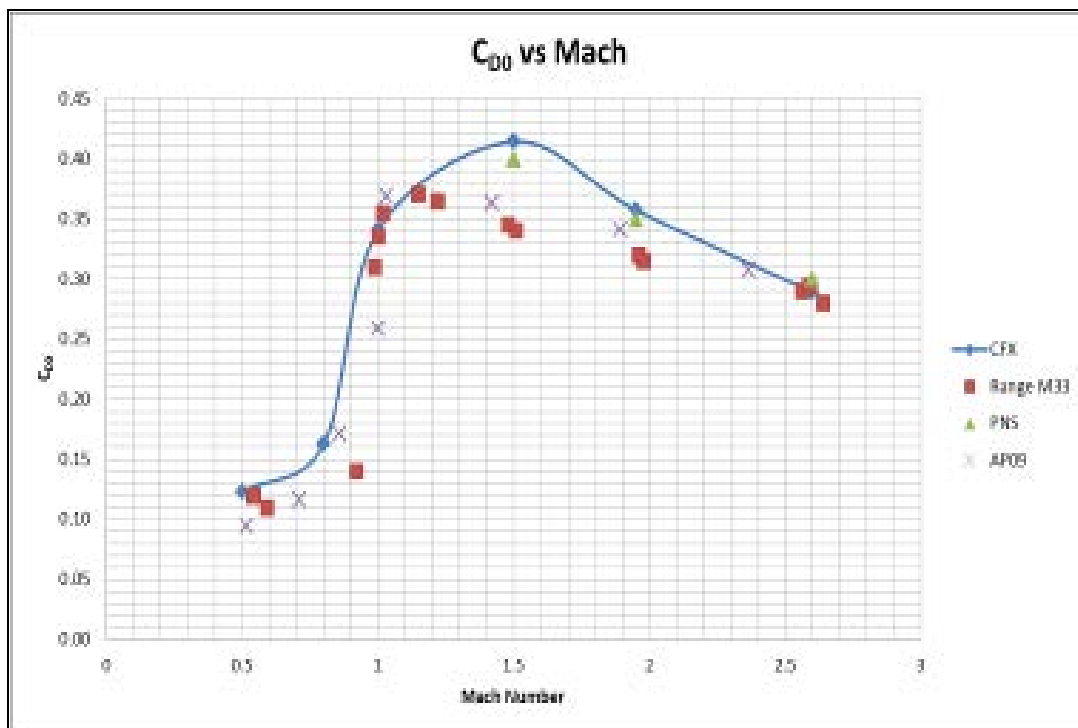


Figure 28.  $C_{D0}$  vs Mach Numbers\_Combined k-  $\epsilon$ / SST Model (CFX).

### C. EFFECTS OF ANGLES OF ATTACK

The model was run for various angles of attack at  $M=0.5$  to predict the stall value for the M33 projectile. The results from the CFX code were compared with the results obtained from AP09 as shown in Figures 30 and 31. Although both codes predicted the stall value to occur at  $60^\circ$  angle of attack, the results differ in magnitudes and agree only up to  $20^\circ$ . Detailed data and flow diagrams of the projectile at various angles of attack can be found in Appendix D.

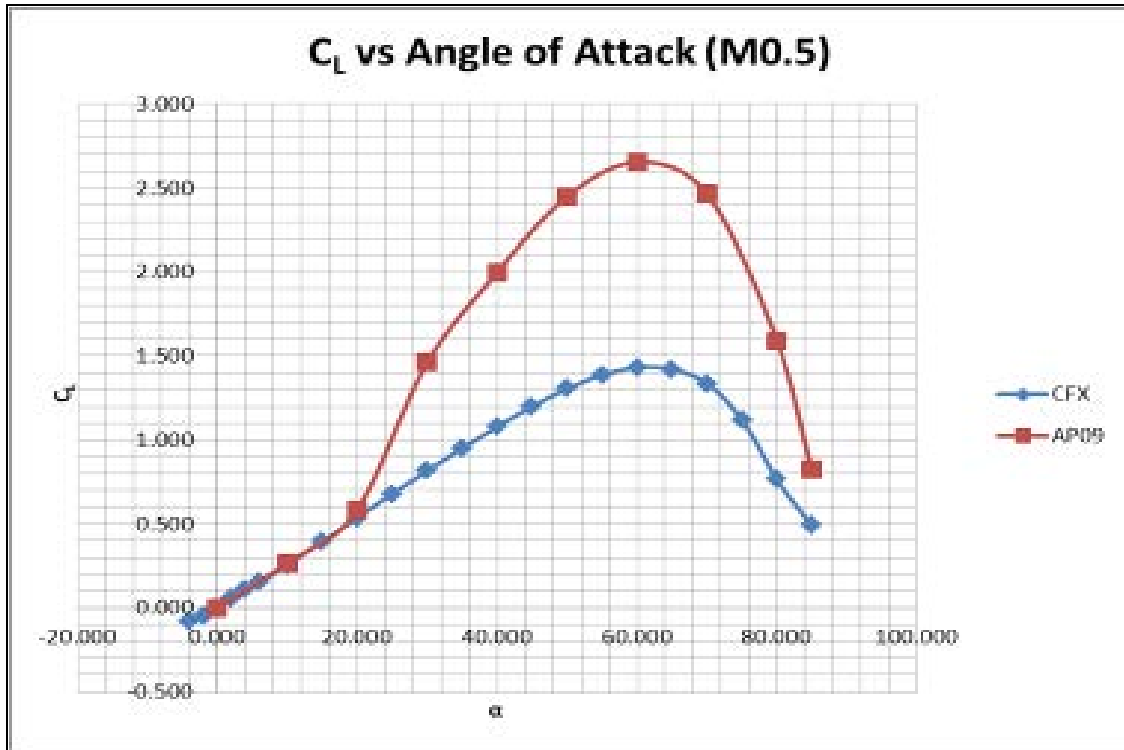


Figure 29.  $C_L$  vs  $\alpha$  (CFX & AP09).

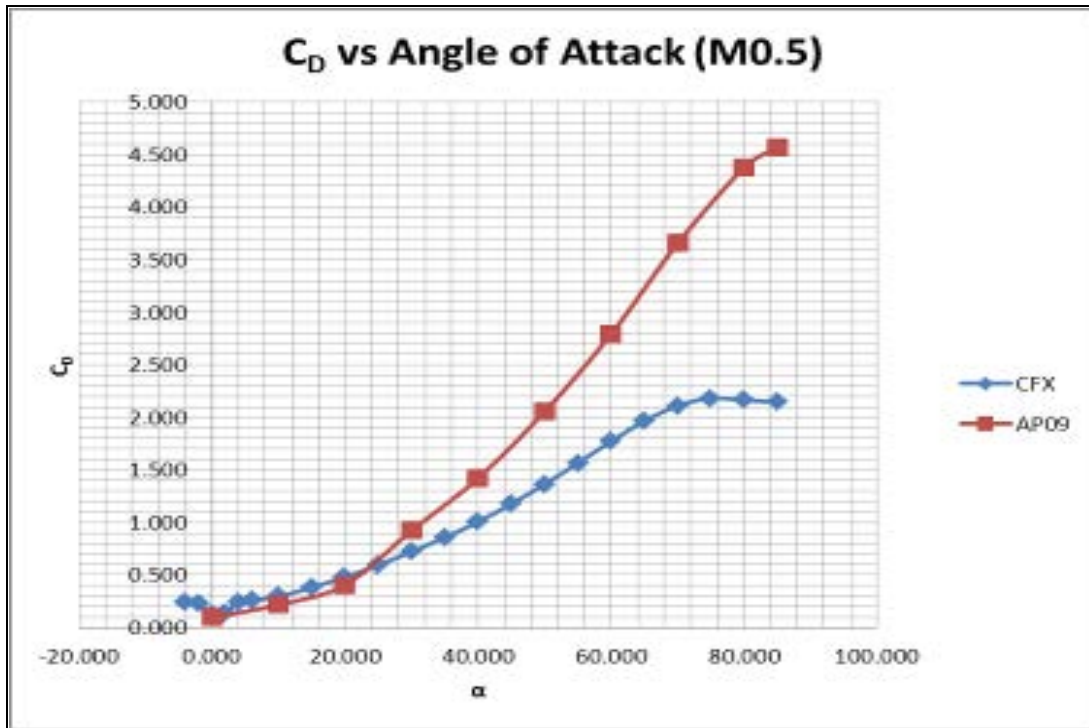


Figure 30.  $C_D$  vs  $\alpha$  (CFX & AP09).

The differences in magnitude sparked off an investigation to study the flow over the cross-section of the projectile body. The model was run at  $M= 0.5$  for  $45^\circ$ ,  $75^\circ$  and  $85^\circ$  angle of attack with the flow diagrams shown in Appendix D. From Figure 31, it was understood that a limitation to the half-bodied symmetry model was its insufficiency to account for the effects across the Y-Z plane. You could see that the flows over the symmetry plane were forced to re-circulate back as if it has encountered a wall. This phenomenon is unnatural as flows may not necessary be symmetrical and could even be shed away. Errors due to this limitation may be magnified at higher angles of attack when the effects of the cross-sectional flow also occur at the nose.

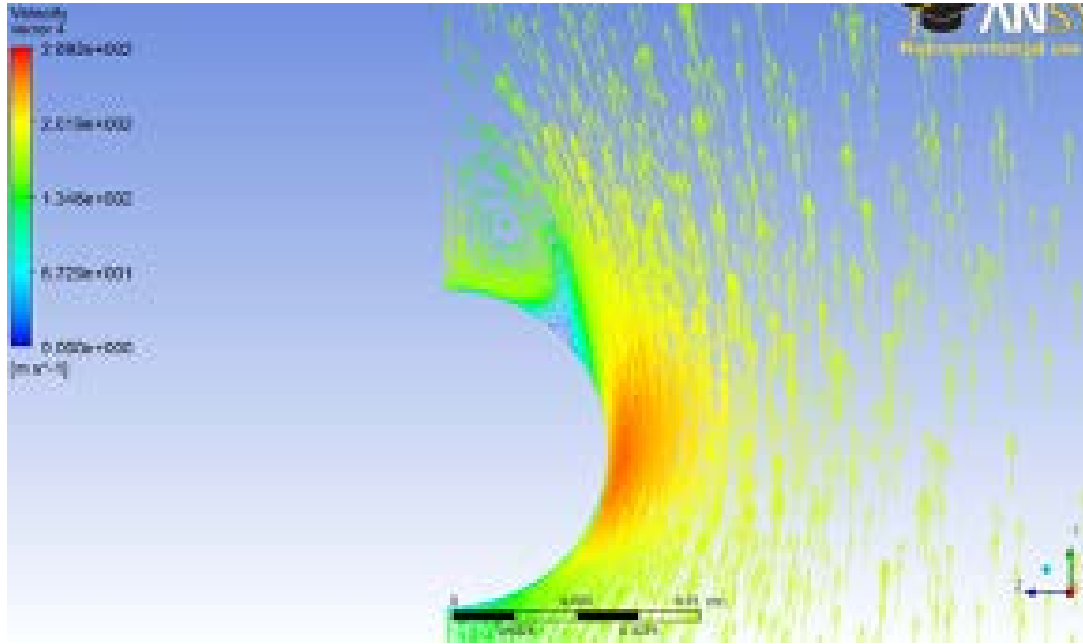


Figure 31. Cross Sectional Flow (CFX)

#### D. SENSITIVITY STUDIES FOR CFX

##### 1. Flow vs Orientation Adjustment Approach

The simulation was run using a half-bodied symmetry model and by adjusting the flow component at various angles of attack. A sensitivity study on adjusting the orientation of the projectile instead of the flow was done to compare the results. The body of the projectile was tilted by  $2^\circ$  and run with the  $k-\epsilon$  model. The results from the simulation as shown in Figure 32 shows fairly good agreement with the results obtained from the flow adjustment approach.

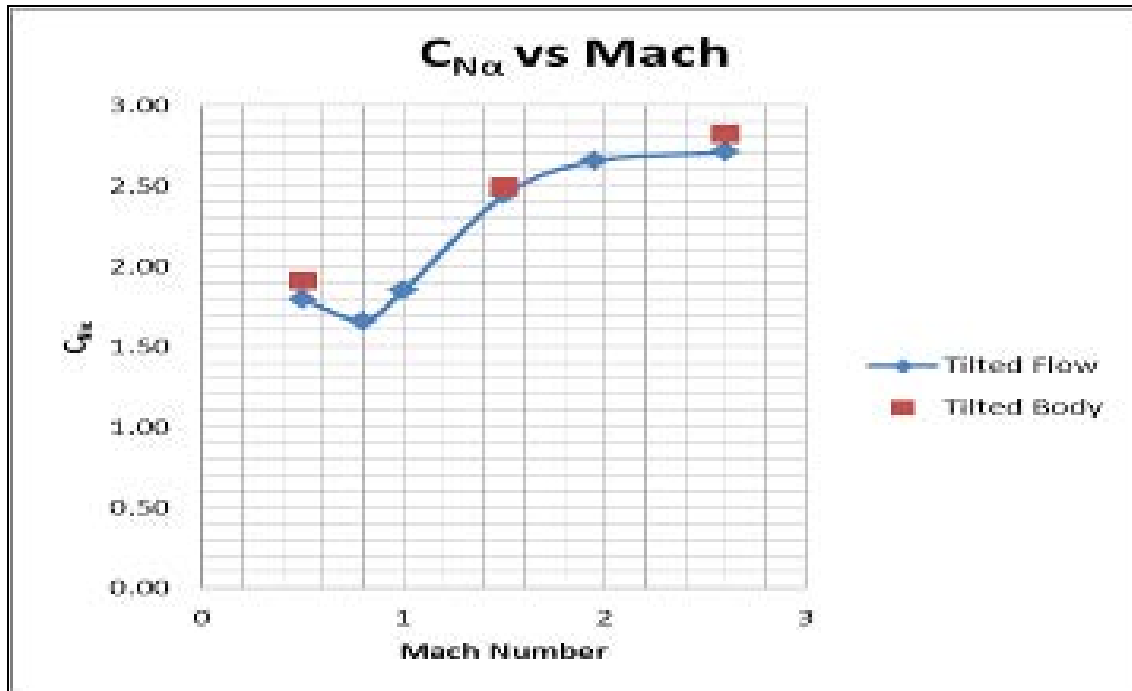


Figure 32. Sensitivity Study on Geometry Adjustment for Angle of Attack (CFX).

## 2. Control Volume

In actual wind tunnel tests, measures need to be taken to minimize the effects of re-circulated flow from the walls to the projectile. This measure was taken into account in the CFX simulation by using a control volume that is 10 times the projectile length. An additional sensitivity study was carried out to verify that this control volume size was sufficient for proper simulation. A control volume of 20 times the projectile length was used with the SST model and the results agree fairly well with the previous control volume as shown in the Figures 33 and 34.

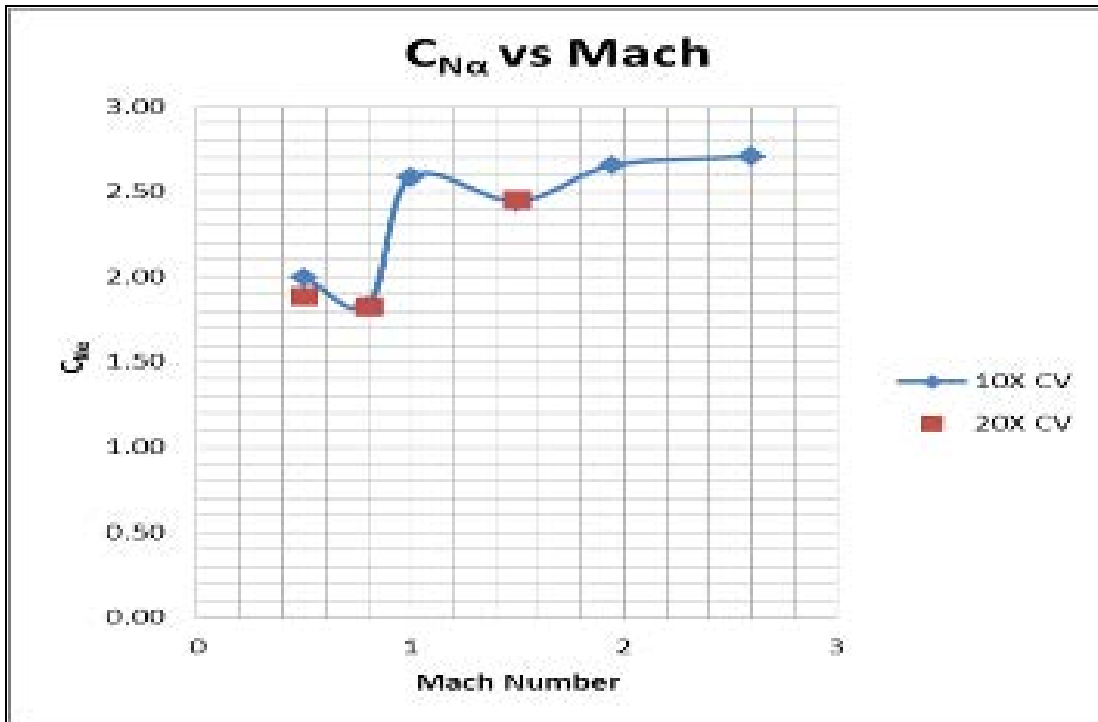


Figure 33. Sensitivity Study on Control Volume for  $C_{N\alpha}$  (CFX).

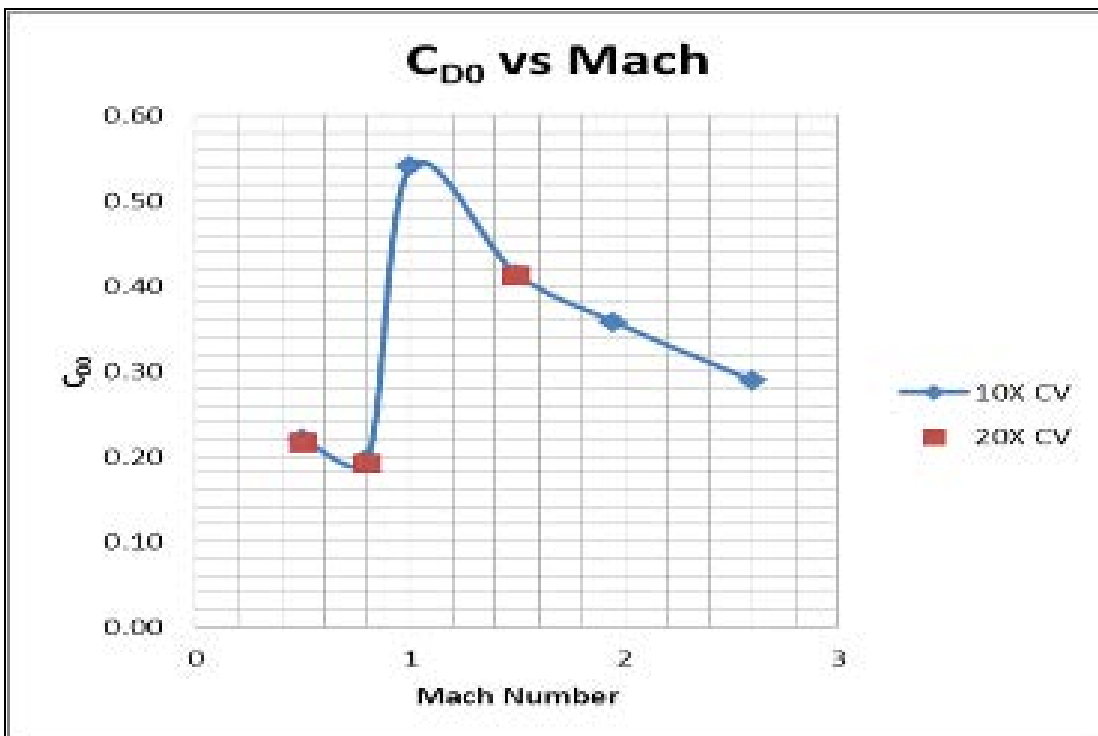


Figure 34. Sensitivity Study on Control Volume for  $C_{D0}$  (CFX).

THIS PAGE INTENTIONALLY LEFT BLANK

## VI. CONCLUSION AND RECOMMENDATIONS

The CFX code, based on the numerical solution of the full Navier-Stokes equations, took about six hours to compute for one data point using a mesh size of over 650,000 nodes and 2 million elements. Mesh refinement using inflation layers and face sizing at critical areas produces better simulation results and higher fidelity.

The combined k-  $\epsilon$  and SST turbulence model produces reasonably good results that showed good agreement with experimental range data for  $C_{N\alpha}$  and  $C_{M\alpha}$ .  $C_{D0}$  tends to be over predicted by an average error of 11.6% with the highest error occurring at  $M=1.5$ . As the simulation was run using the free flight motion of the M33 projectile, a large source of error may be contributed due to the rotational effects of the spin-stabilized round during range testing. For simulation, it is recommended to use the k-  $\epsilon$  model for subsonic Mach numbers that are  $M \leq 1.0$  and the SST model for supersonic Mach numbers that are  $M > 1.0$ .

Stall value of the M33 projectile was predicted at 60° angle of attack. Limitations to the cross flow analysis of the half-bodied symmetry model require further studies on a full-bodied model for better fidelity.

Sensitivity studies showed that a control volume of 10 times the projectile length is sufficient to avoid errors due to re-circulation of flows from the walls. Computational approach of adjusting the flow at various angles of attack also shows good agreement with the results from adjusting the projectile orientation for various angles of attack.

In conclusion, this report serves as a further study from previous report [4] in using the CFX code for the prediction of aerodynamic properties of projectiles at various angles of attack. This report also serves as a foundation for further studies into the cross flow analysis and rotational effects of the spin-stabilized M33 projectile.

THIS PAGE INTENTIONALLY LEFT BLANK

## LIST OF REFERENCES

- [1] J. Sahu, "Drag Prediction for Projectiles at Transonic and Supersonic Speeds," Army Research Laboratory, Aberdeen Proving Ground, MD., BRL-MR-3523, June 1986.
- [2] P. Weinacht, "Prediction of Projectile Performance, Stability, and Free-Flight Motion Using Computational Fluid Dynamics," Army Research Laboratory, Aberdeen Proving Ground, MD., ARL-TR-3015, January 2003.
- [3] F. G. Moore and L. Y. Moore, "The 2009 version of the Aeroprediction Code: The AP09," API Report 3, January 2008.
- [4] W. C. Tan, "Aerodynamic Validation of Emerging Projectile and Missile Configurations", M.S. thesis, Naval Postgraduate School, OMB No. 07040188, December 2010.
- [5] R. L. McCoy, "The Aerodynamic Characteristics of .50 Ball, M33, API, M8 and APIT, M20 Ammunition," Ballistic Research Laboratory, Aberdeen Proving ground, MD., BRL-MR-3810, December 1989.
- [6] B. J. Guidos and S. K. Chung, "Computational Flight Design of 0.5 Caliber Limited Range Training Ammunition," Army Research Laboratory, Aberdeen Proving Ground, MD., ARL-TR-662, January 1995.
- [7] F.G. Moore, R.M. McInville and T.C. Hymer, "The 1998 Version of the NSWC Aeroprediction Code: Part 1- Summary of New Theoretical Methodology," NSWCDD/ TR-98/ 1, April 1998.
- [8] "Missile aerodynamics," class notes for ME3205, Department of Mechanical and Aeronautical Engineering, Naval Postgraduate School, Winter 2011.
- [9] D. Jones, "Numerical Solutions of the Flow Field for Conical Bodies in a Supersonic Stream," AD686646.
- [10] Z. Kopal, "Table of Supersonic Flow Around Cones," Massachusetts Institute of Technology, Dept. of Electrical Engineering , Cambridge, MA., Tech. Report No. 1, 1947.
- [11] J. L. Sims, "Tables for Supersonic Flow around Right Circular Cones at Zero Angle of Attack," National Aeronautics and Space Administration, Washington, DC., NASA SP-3004, 1964.
- [12] F. R. Menter, "Zonal Two Equation  $k-\omega$  Turbulence Models for Aerodynamic Flows," AIAA Paper 93-2906, 1993.

- [13] Computational Fluid Dynamic Discussion Forum. Available: [www.cfdonline.com](http://www.cfdonline.com).
- [14] F. G. Moore, T. C. Hymer *et al.*, “The 2005 Version of the Aeroprediction Code: Part II- Users Guide,” API Report no. 2, June 2004.
- [15] “Flow over NACA2415 airfoil at Reynolds no. of 3 million,” laboratory notes for ME3450, Department of Mechanical and Aeronautical Engineering, Naval Postgraduate School, Winter 2011.

## APPENDIX A. SOLIDWORKS PROCESSES AND PROCEDURES

### A. INTRODUCTION

Gouge material for SolidWorks processes and procedures can be taken from the laboratory work in [15].

### B. 2D MODEL

Select the front plane (XY plane) as the reference plane. Plot the individual points of the projectile on the XY axis at coordinates (0,0), (0, 4.875E-3), (10.101E-3, 6.475E-3), (24.605E-3, 6.475E-3), (55.426E-3, 2.331E-3) and (57.757E-3, 0).

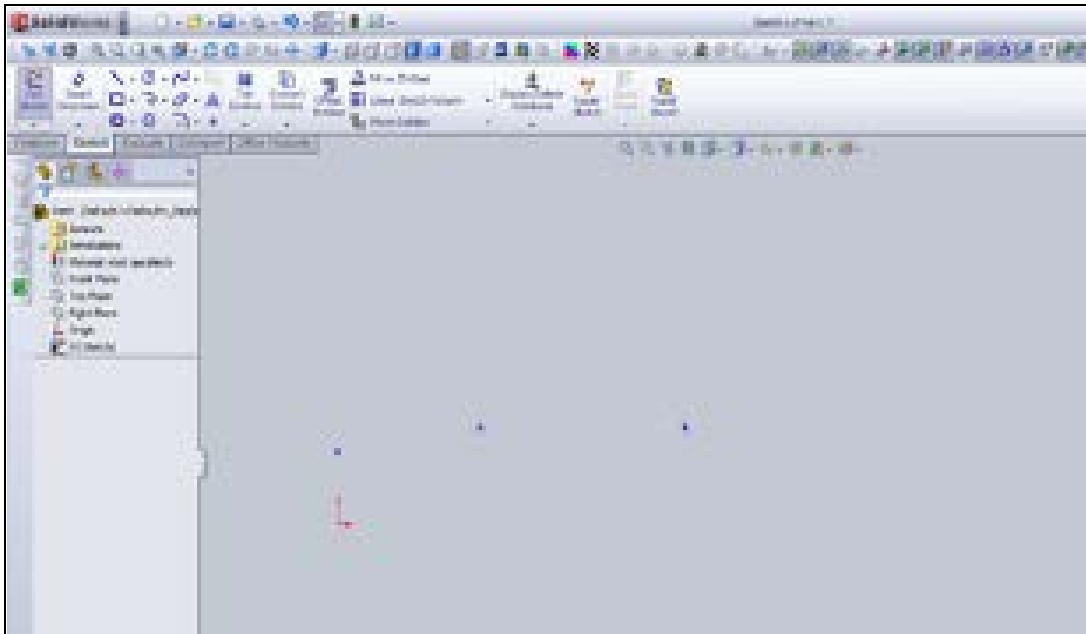


Figure 35. Plotting Individual Points (SolidWorks).

Connect the individual points using straight lines for the afterbody and tangent arcs for the nose cone and nose tip. Set the radius for the nose cone and nose tip to be 113.5715E-3 and 2.331E-3 respectively.

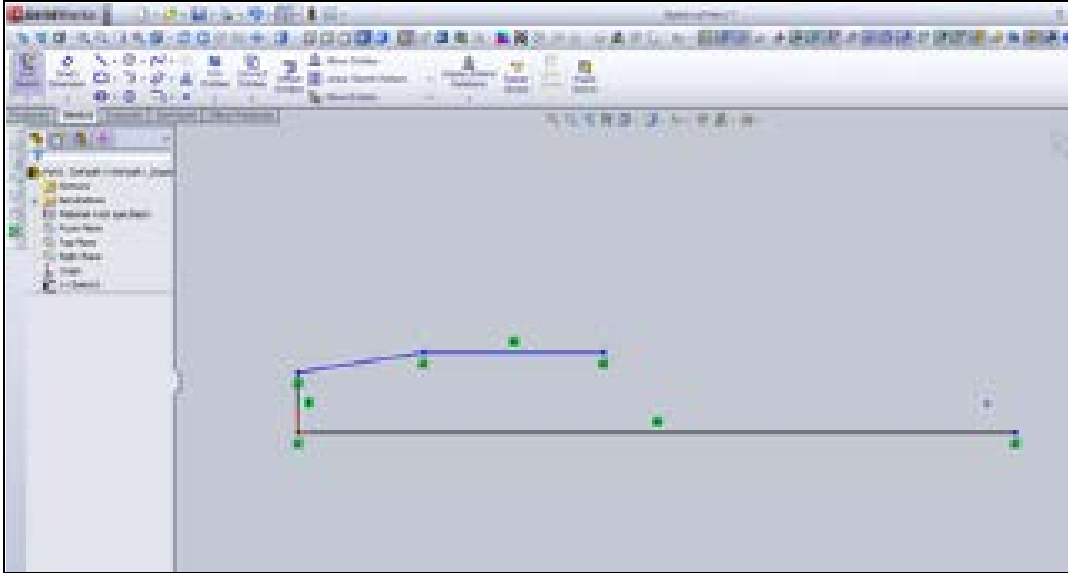


Figure 36. Straight Lines for Afterbody (SolidWorks).

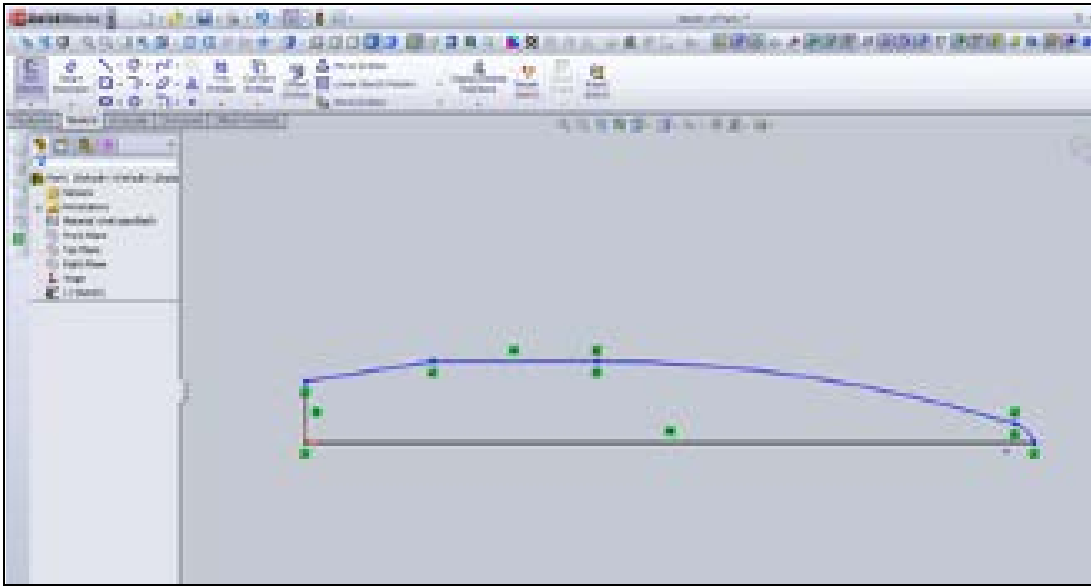


Figure 37. Tangent Arcs for nose (SolidWorks).

The control volume that is 10 times the size of the reference projectile is drawn using a rectangular box on the XY axis with coordinates  $(-570E-3, 570E-3)$ ,  $(-570E-3, -570E-3)$ ,  $(600E-3, 570E-3)$  and  $(600E-3, -570E-3)$ .

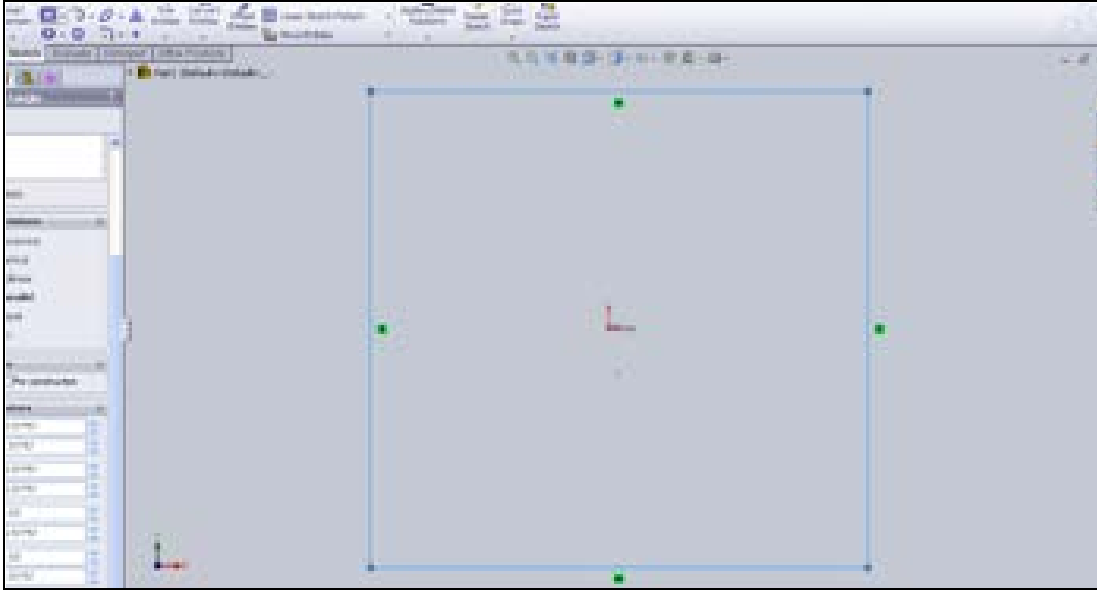


Figure 38. 2D Control Volume (SolidWorks).

### C. 3D MODEL

The 3D model of the control volume is generated by extruding the 2D control volume in the Z axis by  $-570E-3$ .

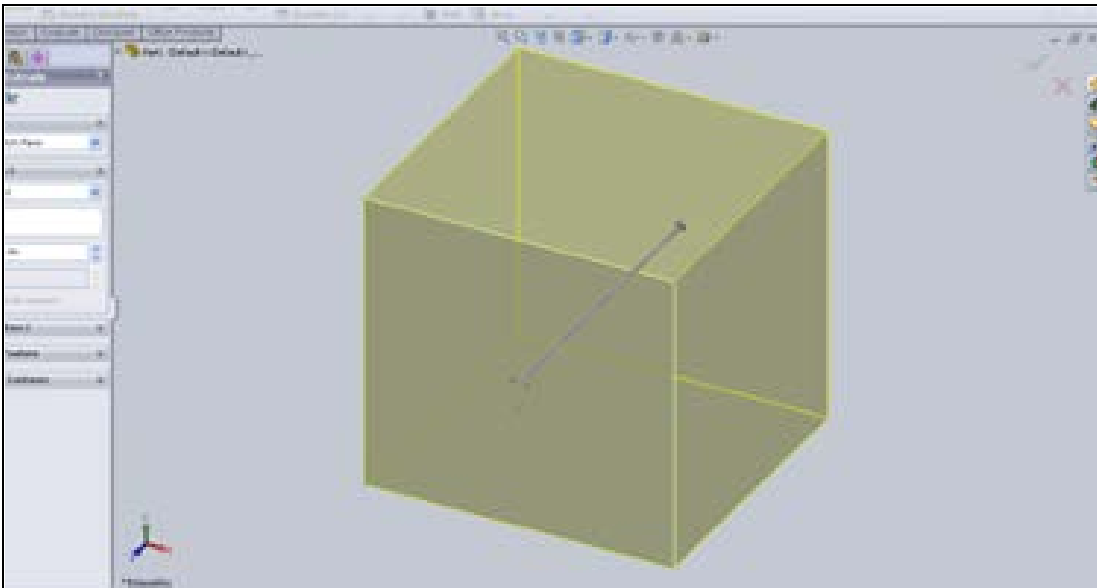


Figure 39. 3D Control Volume (SolidWorks).

Perform a revolved cut for  $360^\circ$  with the 2D sketch of the projectile and it will leave a cavity of the half-bodied projectile in the control volume for simulation purposes.

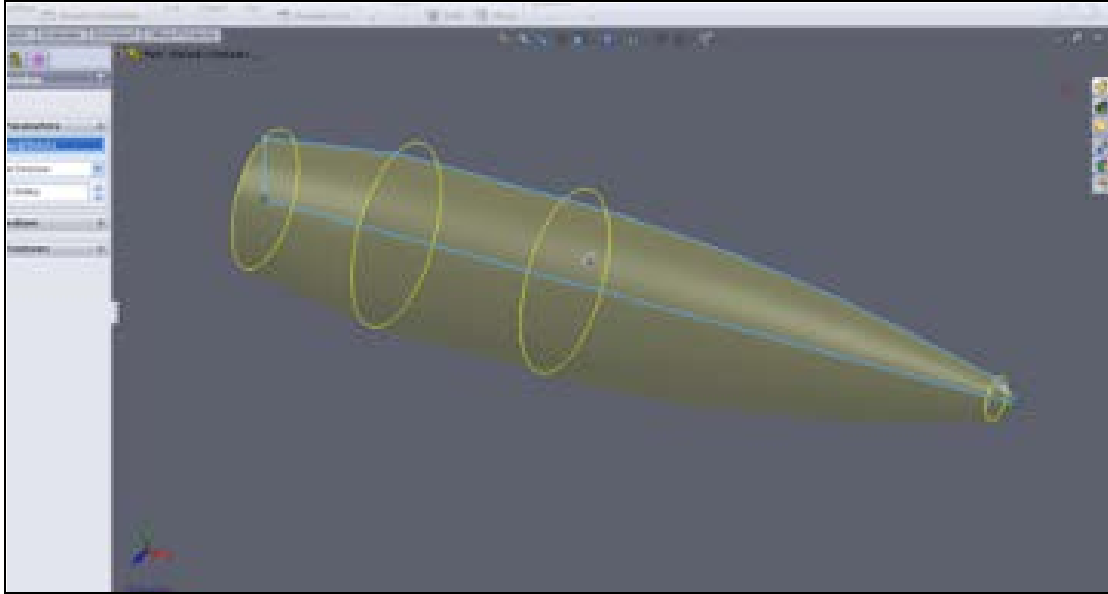


Figure 40. Revolved Cut for 2D Projectile Sketch (SolidWorks).

## APPENDIX B. CFX PROCESSES AND PROCEDURES

### A. INTRODUCTION

Gouge material for CFX processes and procedures can be taken from the laboratory work in [15].

### B. GEOMETRY

After starting up the ANSYS-CFX, import the M33 geometry file from SolidWorks that was saved as a parasolid file.

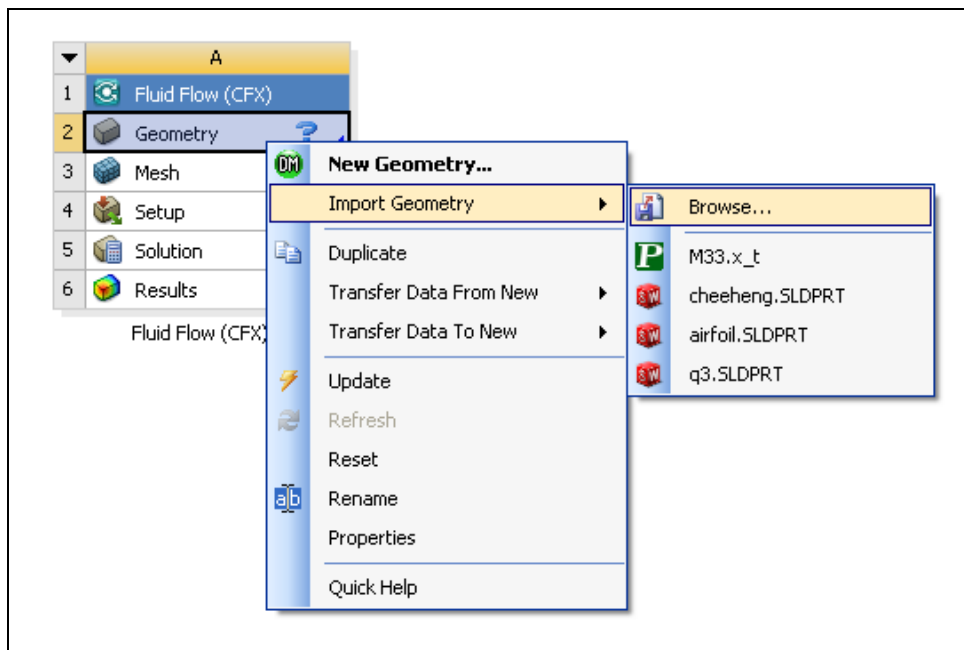


Figure 41. Geometry Interface (CFX).

### C. MESH

#### 1. Named Selections

Inside the mesh interface, insert and define named selections under geometry. Define the projectile surfaces as “body” and the rest of the control volume surfaces as shown in Figure 42.

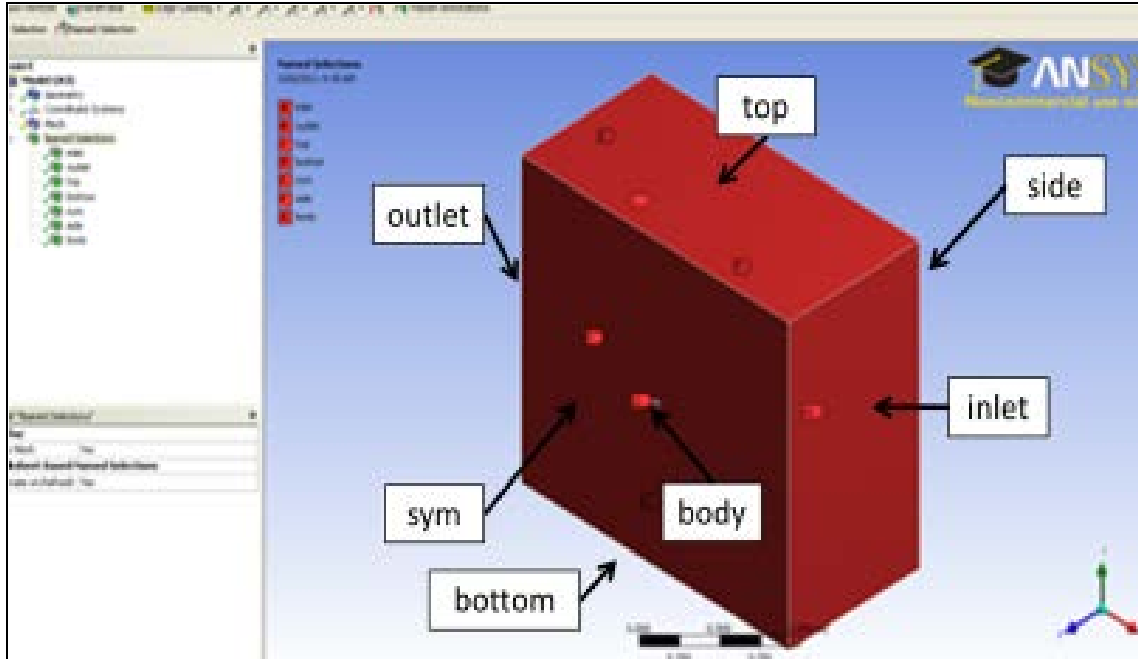


Figure 42. Named Selections (CFX).

## 2. Mesh Sizing

Table 2 shows the input parameters that were set for the mesh.

Sizing	Relevance Center	Fine
	Curvature Angle	2°
	Min Size	$1 \times 10^{-4}$ m
	Max Size	0.1m
	Max Face Size	0.1m
Inflation	Use Automatic Inflation	All faces in chosen selection
	Named Selection	Body
	Inflation Option	Total Thickness
	Number of Layers	12
	Growth Rate	0.8
	Max Thickness	$1 \times 10^{-5}$ m

Table 2. Mesh Sizing Input Parameters (CFX).

## 3. Face Sizing

Insert face sizing under mesh and select the base and nose tip surface. Select type to be element size of  $1 \times 10^{-6}$  m.

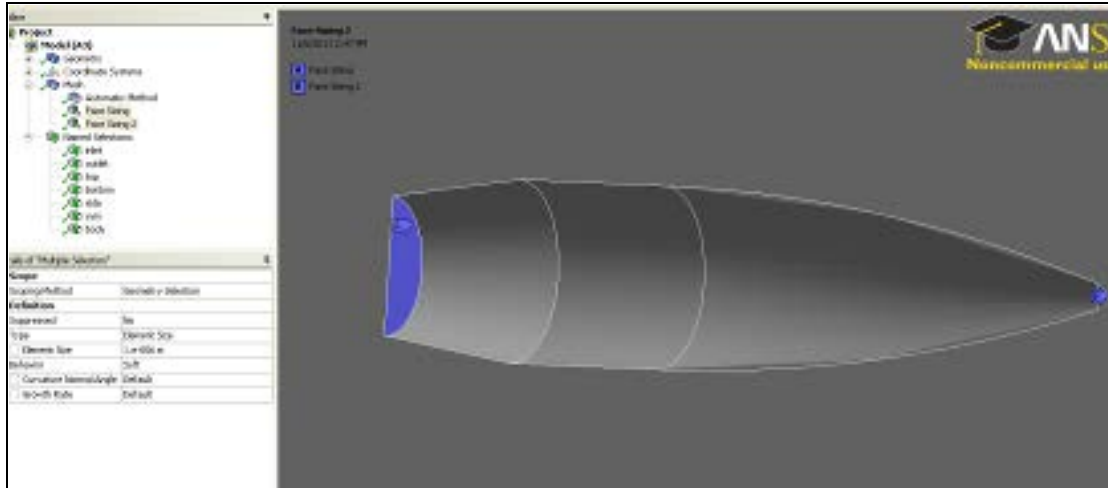


Figure 43. Face Sizing (CFX).

Insert method under mesh to be automatic and the program should generate a mesh with over 650,000 nodes and 2 million elements.

## D. PRE-PROCESSOR

### 1. Domain Conditions

Set the analysis type to steady-state. Inside the default domain, define material for fluid and particle under basic setting to be air-ideal gas. Set the fluid model for heat transfer to be for total energy and the turbulence model to be either SST or k- $\epsilon$  model. For SST model, insert additional parameter under transitional turbulence for Gamma Theta Model. Check the option for high speed (compressible) wall heat transfer model. Initialize the default domain condition as the free-stream condition with Cartesian velocity values set for the u and v component depending on the Mach number and angle of attack.

### 2. Boundary Conditions

Define and insert boundary conditions under the default domain as the following parameters.

Boundary	Basic Setting	Boundary Details
body	Boundary Type – Wall Location - body	Mass and Momentum – No Slip Wall
		Wall Roughness – Smooth Wall
		Heat Transfer - Adiabatic

Boundary	Basic Setting	Boundary Details
inlet	Boundary Type – Inlet Location - inlet	Flow Regime – Mixed Flow (M0.5 to M1.0)/ Supersonic Flow (M1.5 to M2.6)
		Turbulence – Medium (Intensity = 5%)
		Heat Transfer – Static Temperature (288.15K)
outlet	Boundary Type – Outlet Location - outlet	Flow Regime – Subsonic
		Mass and Momentum – Static Pressure (0Pa)
top	Boundary Type – Opening ( $\alpha=0^\circ$ )/ Outlet ( $\alpha=2^\circ$ ) Location - top	For Opening:
		Flow Regime – Subsonic
		Mass and Momentum – Entrainment (0Pa)
		Turbulence – Zero Gradient
		Heat Transfer – Static Temperature (288.15K)
		For Outlet: Same as outlet
bottom	Boundary Type – Opening ( $\alpha=0^\circ$ )/ Inlet ( $\alpha=2^\circ$ ) Location - bottom	For Opening:
		Flow Regime – Subsonic
		Mass and Momentum – Entrainment (0Pa)
		Turbulence – Zero Gradient
		Heat Transfer – Static Temperature (288.15K)
		For Inlet: Same as inlet
side	Boundary Type – Opening Location - side	Flow Regime – Subsonic
		Mass and Momentum – Entrainment (0Pa)
		Turbulence – Zero Gradient
		Heat Transfer – Static Temperature (288.15K)
sym	Boundary Type – Symmetry Location - side	

Table 3. Boundary Condition Input Parameters (CFX).

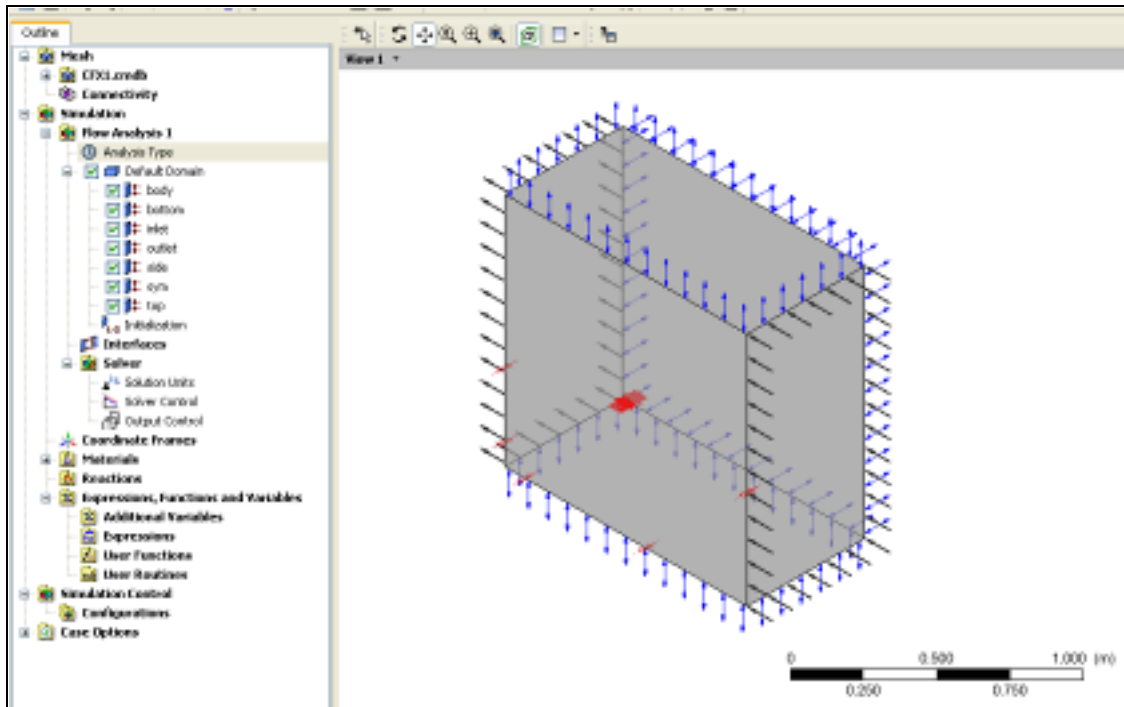


Figure 44. Boundary Conditions at 0° (CFX).

### 3. Solver

Insert expert parameters under solver and set convergence control in high speed models for three continuity loops. For solver control, set the turbulence numeric to high resolution. Set maximum number of iterations to be 100 with a residual target of  $1 \times 10^{-9}$ . In the advance options, set high speed numeric for compressibility control.

## E. POST-PROCESSOR

### 1. Flow Field

Insert Plane on the XY-axis and set the Z-axis distance to be  $-0.05 \times 10^{-3}$  m. Insert vector on plane with variable set as velocity to obtain the velocity field vector. Insert contour on plane and set variable as local Mach number or pressure to obtain the Mach number and pressure contours.

### 2. Forces

Use the function calculator to obtain the values for the forces acting on the projectile. Table 4 shows the input parameters to obtain the results.

Y-Plus	Function – Ave
	Location – Default Domain
	Variable – Y-plus
Forces	Function – Force
	Location – Body
	Direction – X/ Y/ Z
Torque	Function – Torque
	Location – Body
	Axis – X/ Y/ Z

Table 4. Post-Processor Input Parameters (CFX).

## APPENDIX C. AP09 PROCESSES AND PROCEDURES

### A. M33 PROJECTILE CONFIGURATION AND INPUT PARAMETERS

To input the geometry and aerodynamic parameters for the M33, create a new “body-alone” configuration and configure the geometry input units to millimeters.

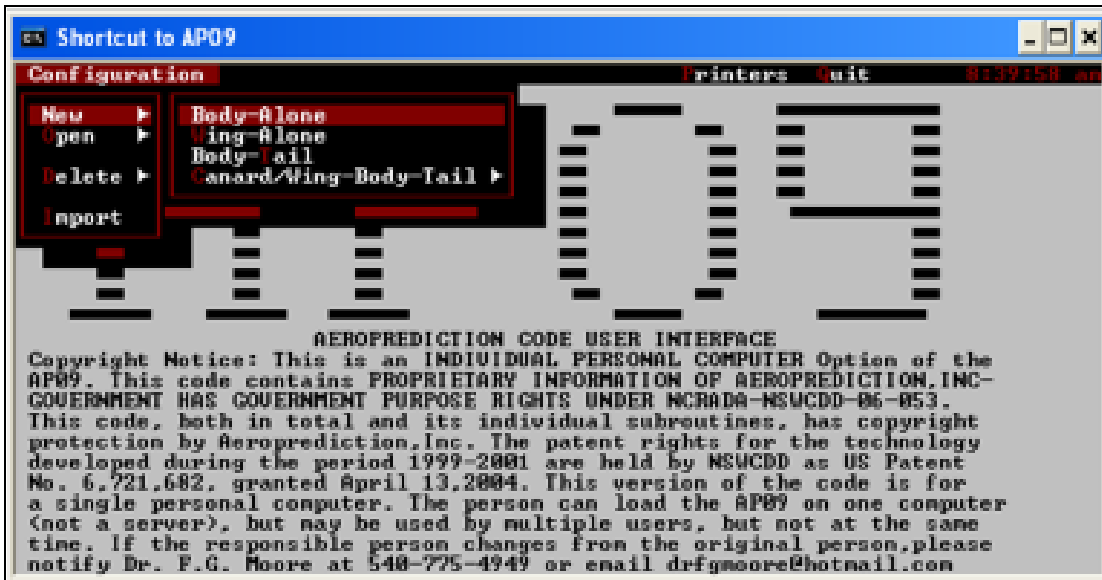


Figure 45. Configuration-New-Body-Alone (AP09).

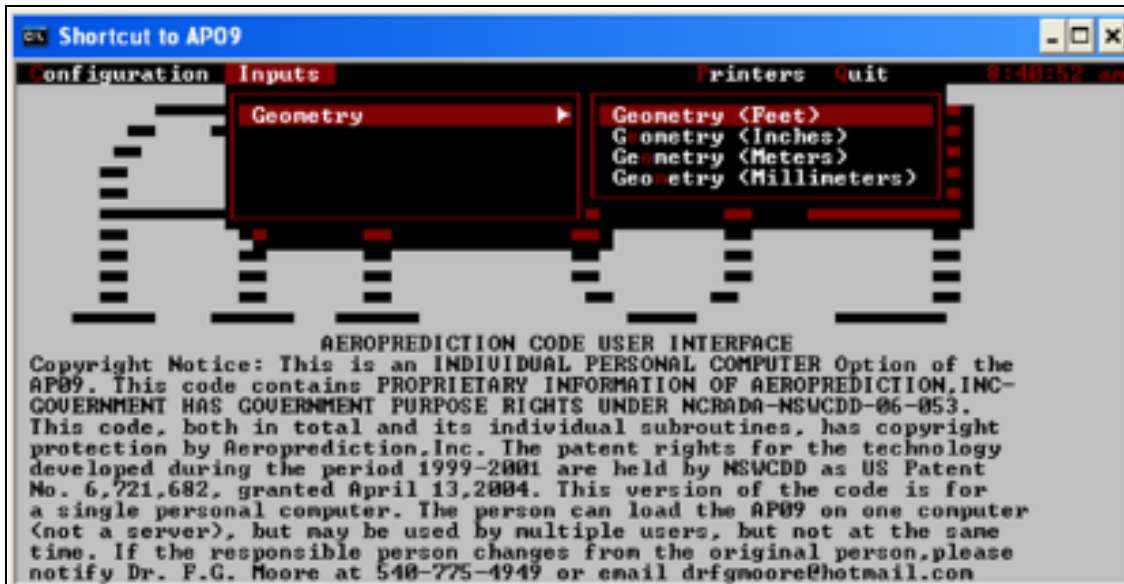


Figure 46. Inputs-Geometry-Geometry (AP09).

## B. GEOMETRY INPUTS

Inside the geometry data entry interface, set the following body roughness for typical flight configuration, reference diameter or width of the body to be 12.95mm and distance of moment reference from nose tip to be 33.15mm.

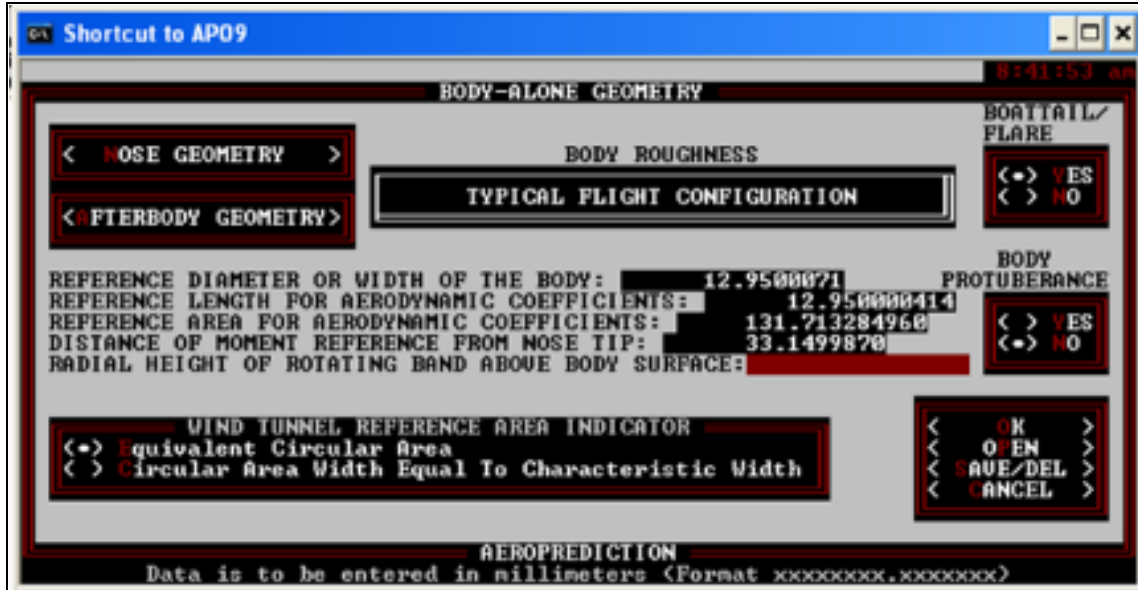


Figure 47. Geometry Data Entry Interface (AP09).

To configure nose profile, select “Nose Geometry” under the geometry data entry interface. Select nose cross sectional shape to be circular and set circular radius to 6.475mm. Next, select “Secant Ogive Blunt” for nose profile and set radius of curvature to be 113.57mm, spherical cap radius to be 2.33mm and length of nose tip to shoulder to be 33.15mm.

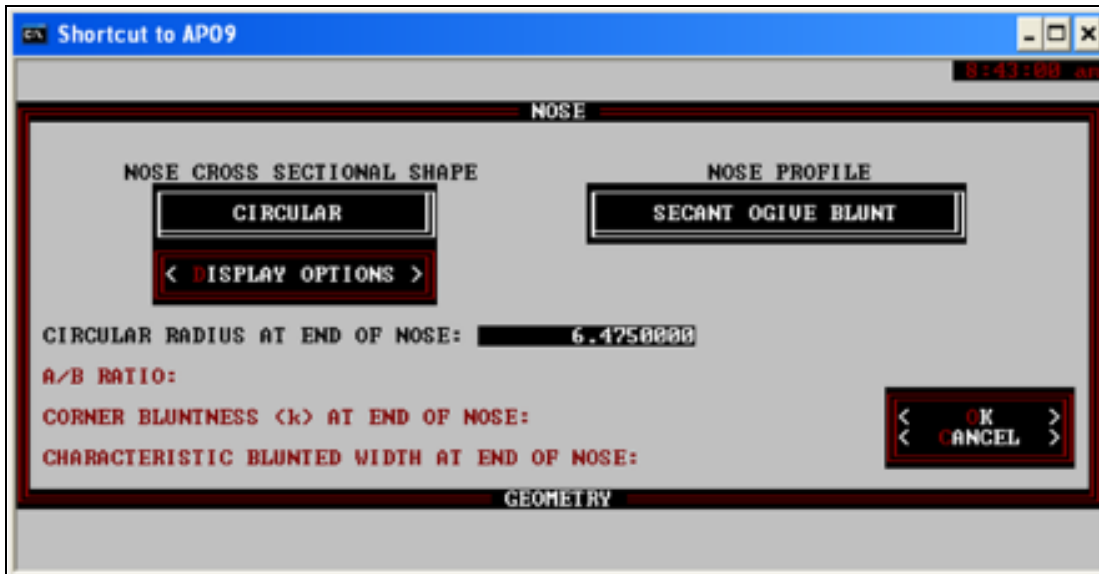


Figure 48. Nose Geometry Data Entry Interface (AP09).

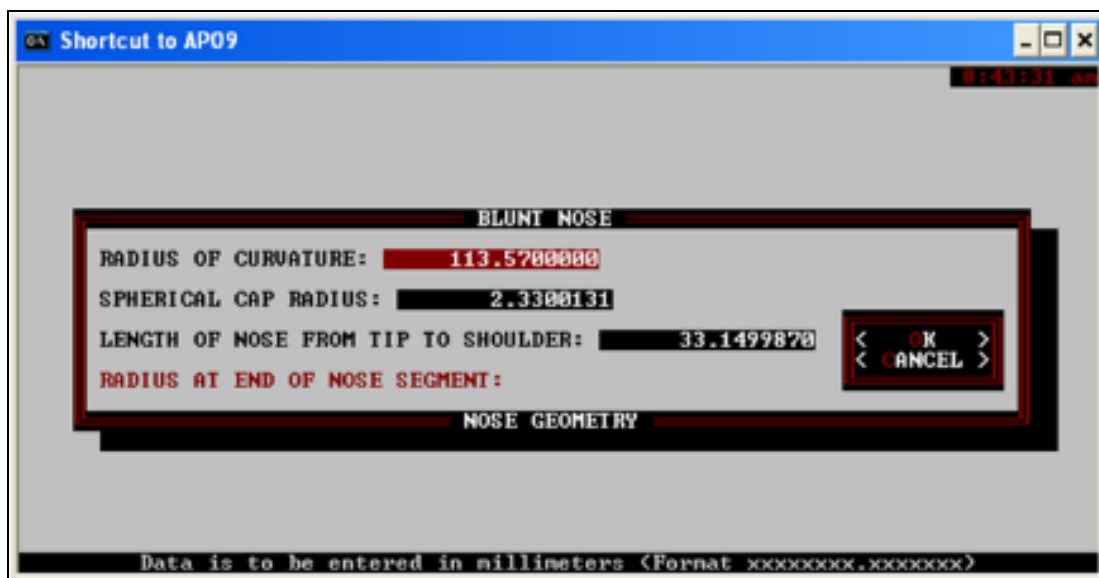


Figure 49. Nose Profile Data Entry Interface (AP09).

To configure the body geometry of the M33, select “Afterbody Geometry” under the geometry data entry interface and set longitudinal afterbody coordinate from nose tip to be 47.66mm.

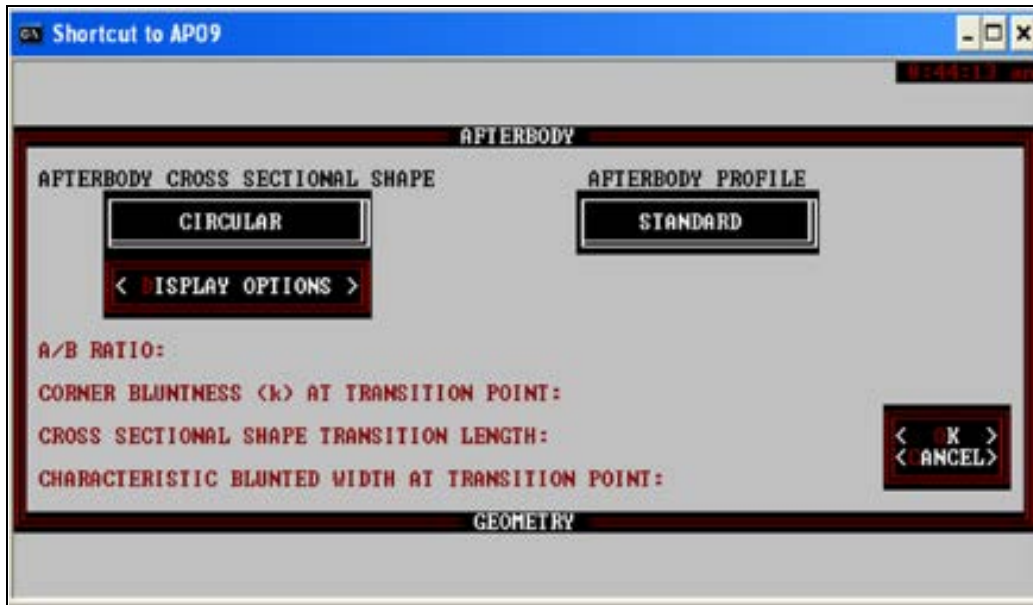


Figure 50. Afterbody Geometry Data Entry Interface (AP09).

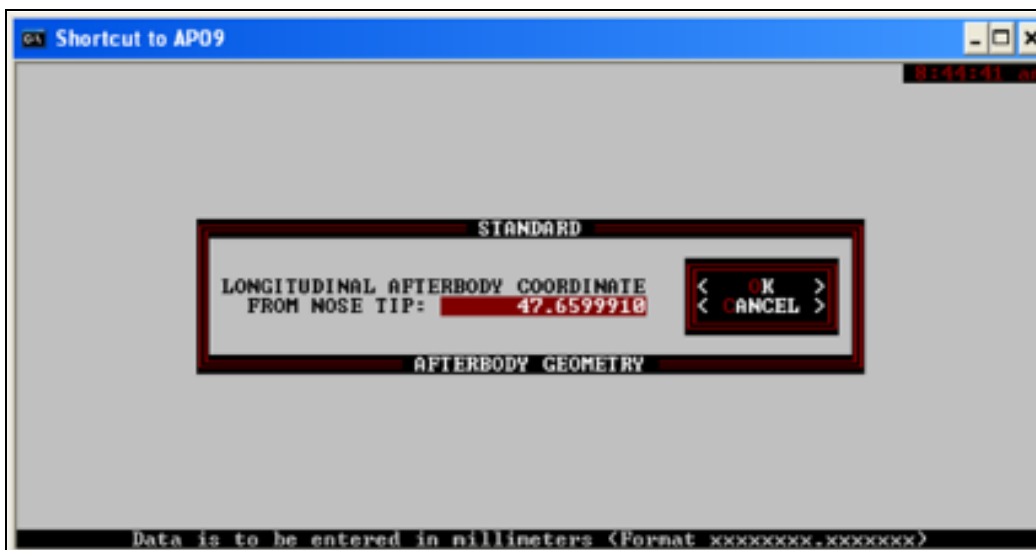


Figure 51. Afterbody Profile Data Entry Interface (AP09).

Lastly for geometry inputs, check “yes” for “Boattail/ Flare” under the geometry data entry interface and set longitudinal boattail/ flare coordinate from nose tip to be 57.76mm and corresponding boattail/ flare characteristic half width to be 4.875mm.

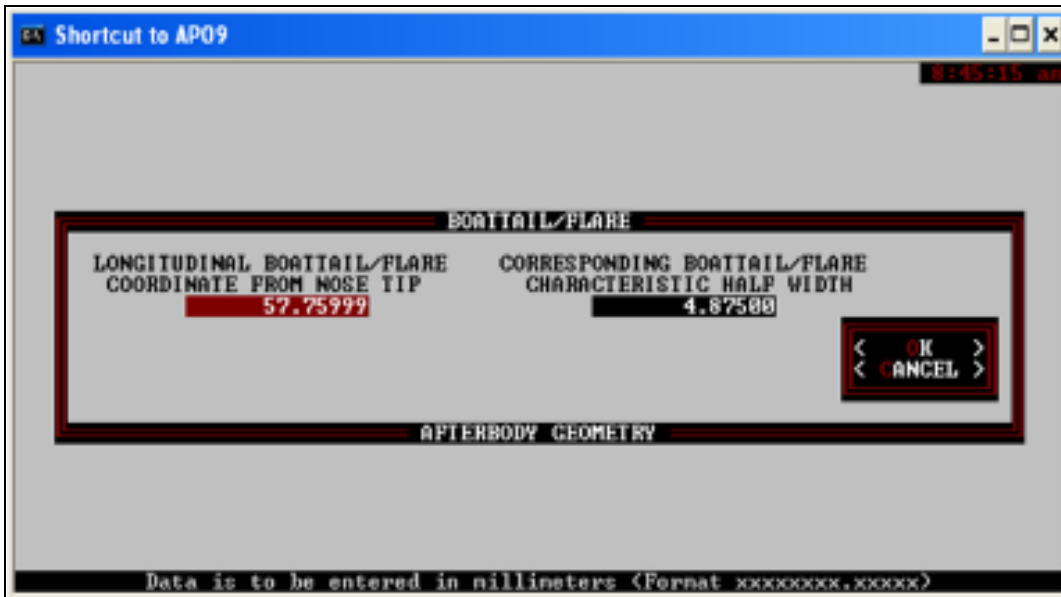


Figure 52. Boattail/ Flare Data Entry Interface (AP09).

### C. AERODYNAMIC INPUTS

To enter aerodynamic parameters, select “Aerodynamics” under “Inputs” and set the free-stream conditions for Mach sweep.



Figure 53. Inputs-Aerodynamics (AP09).

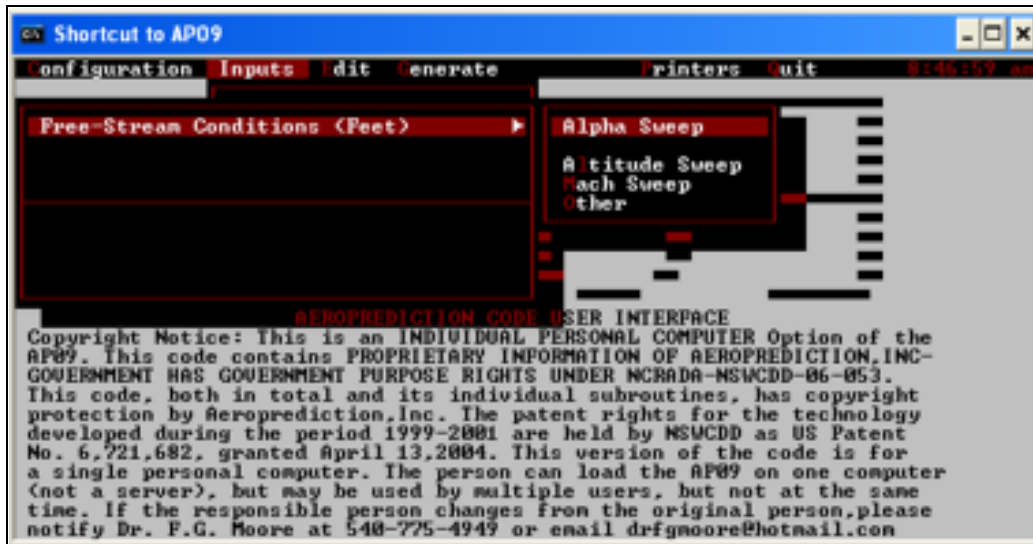


Figure 54. Aerodynamics Data Entry Interface-Free-Stream Conditions (AP09).

Inside the Mach sweep data entry interface, set initial Mach number to be  $M=0.5$ , final Mach number to be  $M=3$ , interval size to be 0.15, constant angle of attack to be  $0^\circ$  or  $2^\circ$  and altitude to be 1 feet (sea level).

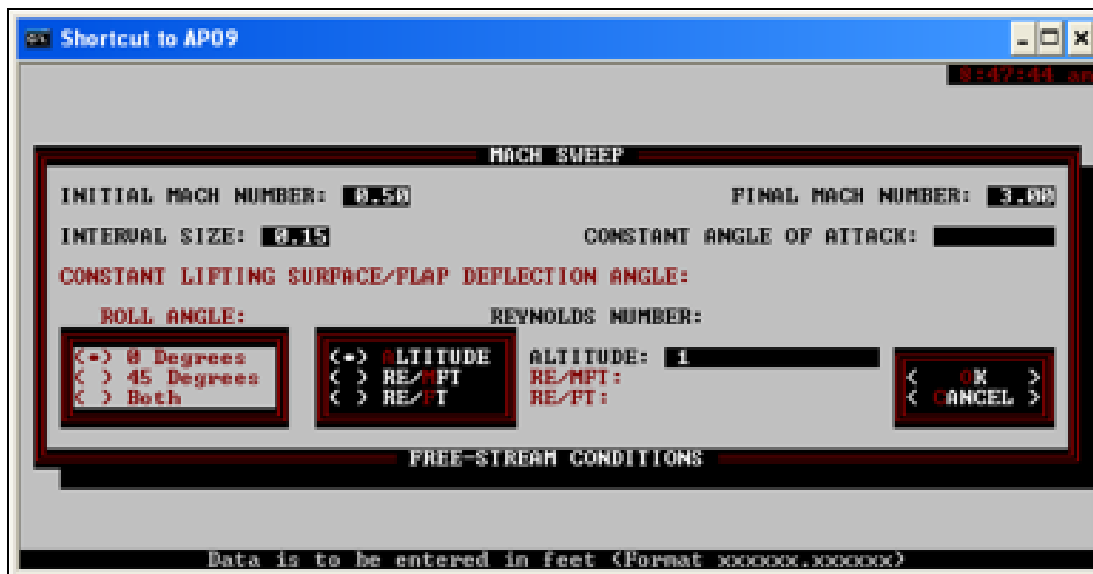


Figure 55. Mach Sweep Data Entry Interface (AP09).

After keying in the aerodynamic parameters, select “Options” under the aerodynamic data entry interface. Check “yes” for dynamic derivatives, spin stabilized

and set aerodynamic smoother to “on”. A title is required in order to proceed. Simply enter CASE1 or anything of preference.

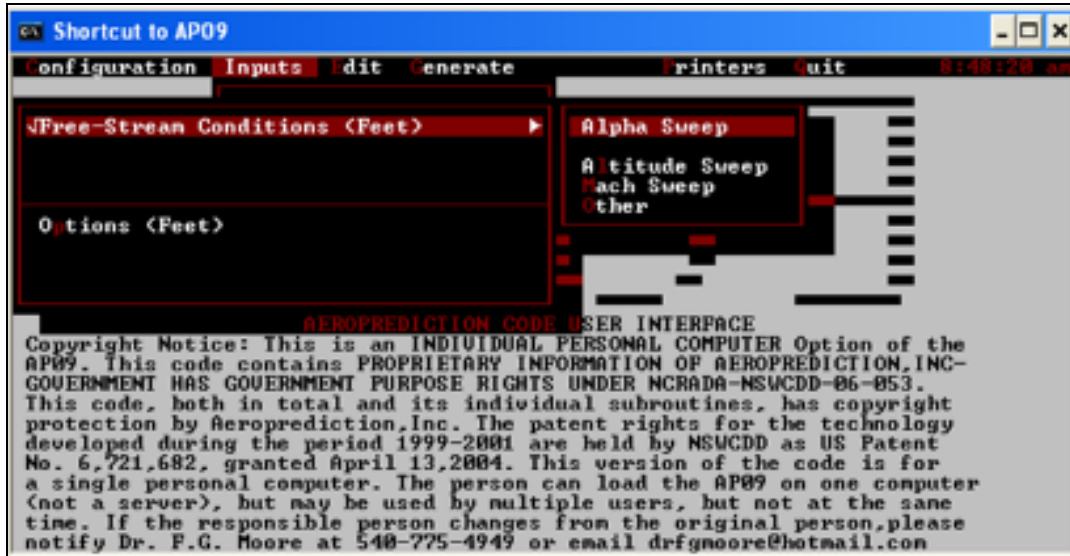


Figure 56. Aerodynamics Data Entry Interface-Options (AP09).



Figure 57. Aerodynamic Options Data Entry Interface (AP09).

## D. RESULTS

The geometry sketch from the geometry inputs can be previewed under “Generate”. After confirming the geometry, generate the aerodynamic output file. This process will take a few seconds.

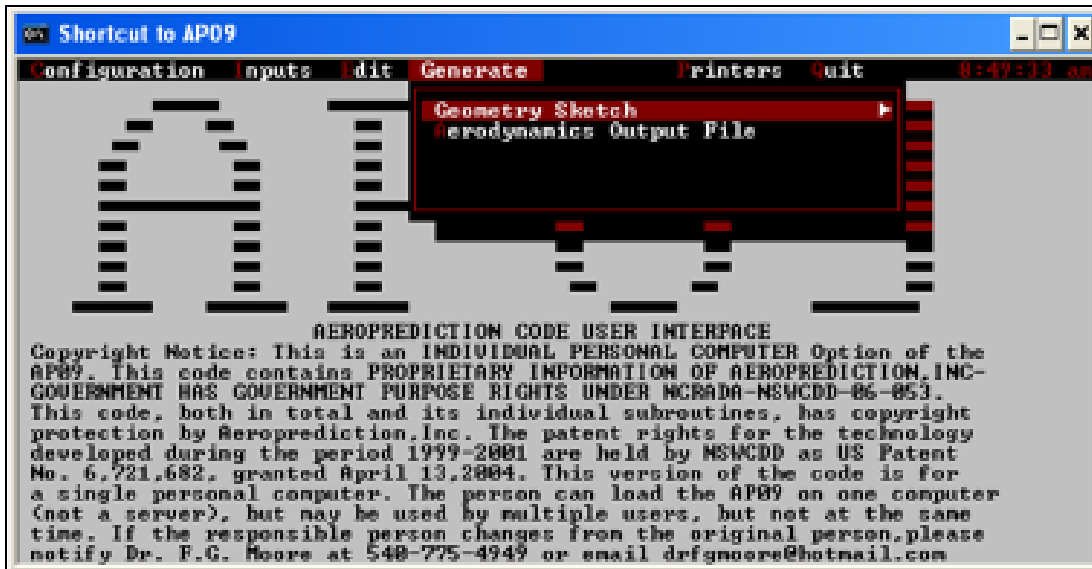


Figure 58. Generate – Aerodynamic Output File (AP09).

Select “Plots” under “Output” to retrieve the generated results for the M33 projectiles. Tabulated results from the output files can be saved as text documents and expressed using excel spreadsheet.

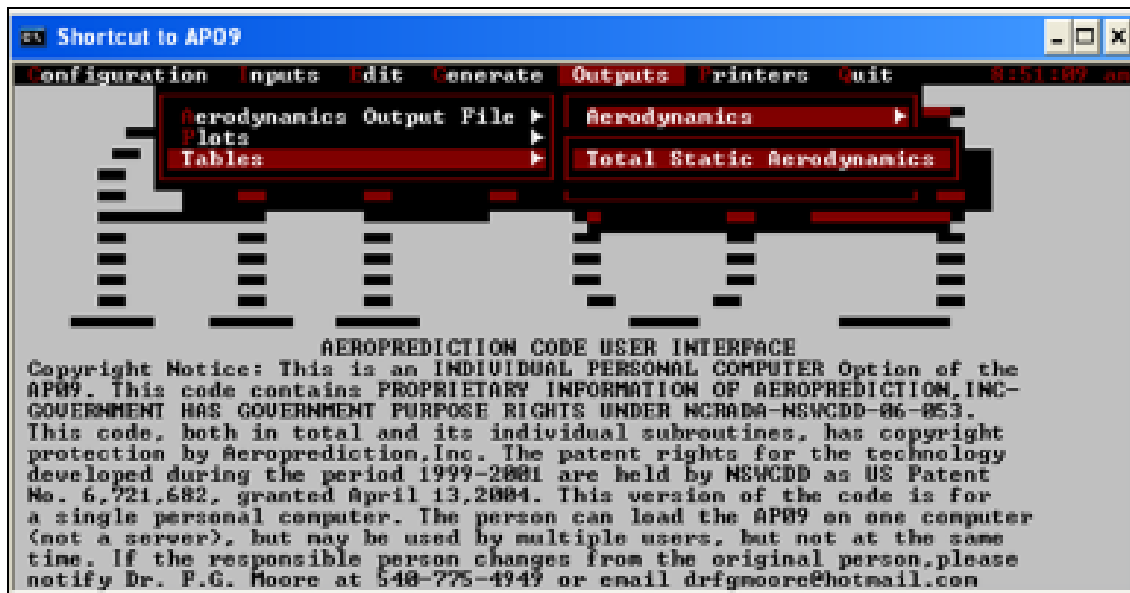


Figure 59. Outputs-Aerodynamics-Plots/ Tables (AP09).

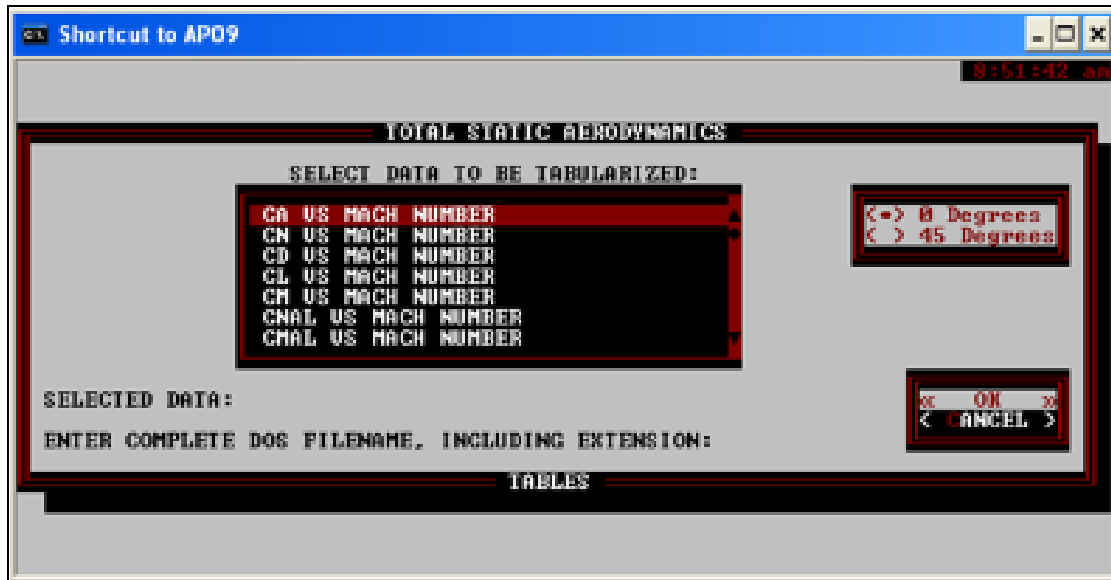


Figure 60. Output Interface (AP09).

THIS PAGE INTENTIONALLY LEFT BLANK

## APPENDIX D. DETAILED RESULTS

### A. CFX

#### 1. Simulation Data

Simulation Data for $C_N$ vs AOA (M0.5)						
Drag Ref Area (m <sup>2</sup> )	0.00013					
Density (kg/m <sup>3</sup> )	1.180					
Mach Number	0.500					
Velocity (m/s)	170.150					
$\alpha$ (°)	<b>-4.000</b>	<b>-2.000</b>	<b>0.000</b>	<b>2.000</b>	<b>4.000</b>	<b>6.000</b>
$\alpha$ (rad)	-0.070	-0.035	0.000	0.035	0.070	0.105
<b>u</b> (m/s)	169.735	170.046	170.150	170.046	169.735	169.218
<b>v</b> (m/s)	-11.871	-5.939	0.000	5.939	11.871	17.788
<b>F<sub>y</sub></b> (N)	-0.107	-0.060	-0.001	0.069	0.137	0.198
<b>F<sub>x</sub></b> (N)	0.259	0.253	0.138	0.155	0.261	0.265
<b>F<sub>L</sub></b> (N)	-0.089	-0.051	-0.001	0.064	0.118	0.169
<b>F<sub>D</sub></b> (N)	0.265	0.255	0.138	0.158	0.269	0.285
<b>C<sub>L</sub></b>	-0.080	-0.046	-0.001	0.057	0.106	0.152
<b>C<sub>D</sub></b>	0.239	0.230	0.125	0.142	0.243	0.256
<b>C<sub>N</sub></b>	<b>-0.097</b>	<b>-0.054</b>	<b>-0.001</b>	<b>0.062</b>	<b>0.123</b>	<b>0.178</b>

Table 5. Simulation Results for  $C_N$  vs  $\alpha$  Subsonic (CFX).

Simulation Data for $C_N$ vs AOA (M0.8)						
Drag Ref Area (m <sup>2</sup> )	0.00013					
Density (kg/m <sup>3</sup> )	1.180					
Mach Number	0.800					
Velocity (m/s)	272.240					
$\alpha$ (°)	<b>-4.000</b>	<b>-2.000</b>	<b>0.000</b>	<b>2.000</b>	<b>4.000</b>	<b>6.000</b>
$\alpha$ (rad)	-0.070	-0.035	0.000	0.035	0.070	0.105
<b>u</b> (m/s)	271.577	272.074	272.240	272.074	271.577	270.748
<b>v</b> (m/s)	-18.993	-9.502	0.000	9.502	18.993	28.461
<b>F<sub>y</sub></b> (N)	-0.177	-0.093	0.000	0.166	0.340	0.393
<b>F<sub>x</sub></b> (N)	0.580	0.572	0.469	0.475	0.600	0.624
<b>F<sub>L</sub></b> (N)	-0.136	-0.073	0.000	0.150	0.298	0.326

Simulation Data for $C_N$ vs AOA (M0.8)						
$F_D$ (N)	0.591	0.575	0.469	0.481	0.622	0.662
$C_L$	-0.048	-0.026	0.000	0.053	0.105	0.115
$C_D$	0.208	0.202	0.165	0.169	0.219	0.233
$C_N$	-0.062	-0.033	0.000	0.059	0.120	0.138

Table 6. Simulation Results for  $C_N$  vs  $\alpha_{\text{Transonic}}$  (CFX).

Simulation Data for $C_N$ vs AOA (M1.5)						
Drag Ref Area (m <sup>2</sup> )	0.00013					
Density (kg/m <sup>3</sup> )	1.180					
Mach Number	1.500					
Velocity (m/s)	510.450					
$\alpha$ (°)	-4.000	-2.000	0.000	2.000	4.000	6.000
$\alpha$ (rad)	-0.070	-0.035	0.000	0.035	0.070	0.105
$u$ (m/s)	509.206	510.139	510.450	510.139	509.206	507.653
$v$ (m/s)	-35.612	-17.817	0.000	17.817	35.612	53.363
$F_y$ (N)	-1.247	-0.626	0.000	0.863	1.756	2.706
$F_x$ (N)	4.316	4.242	4.194	4.240	4.346	4.468
$F_L$ (N)	-0.942	-0.478	0.000	0.715	1.449	2.224
$F_D$ (N)	4.393	4.262	4.194	4.267	4.458	4.727
$C_L$	-0.094	-0.048	0.000	0.072	0.145	0.223
$C_D$	0.440	0.426	0.420	0.427	0.446	0.473
$C_N$	-0.125	-0.063	0.000	0.086	0.176	0.271

Table 7. Simulation Results for  $C_N$  vs  $\alpha_{\text{Supersonic}}$  (CFX).

Simulation Data (k-e Model)												
Diameter (m)	0.01295											
Drag Ref Area (m <sup>2</sup> )	0.00013											
Air Density (kg/m <sup>3</sup> )	1.180											
length (m)	0.058											
$X_{CG}$ from Base (m)	0.023											
Mach Number	0.500	0.800	1.000	1.500	1.950	2.600						
Velocity (m/s)	170.150	272.240	340.300	510.450	663.585	884.780						
$\alpha$ (°)	0.000	2.000	0.000	2.000	0.000	2.000	0.000	2.000	0.000	2.000	0.000	2.000

Simulation Data (k-e Model)												
$\alpha$ (rad)	0.000	0.035	0.000	0.035	0.000	0.035	0.000	0.035	0.000	0.035	0.000	0.035
$u$ (m/s)	170.1 50	170.0 46	272.2 40	272.0 74	340.3 00	340.0 93	510.4 50	510.1 39	663.5 85	663.1 81	884.7 80	884.2 41
$v$ (m/s)	0.000	5.939	0.000	9.502	0.000	11.87 8	0.000	17.81 7	0.000	23.16 2	0.000	30.88 2
$Y_+$	0.926		1.650		2.030		2.800		3.250		3.700	
$F_y$ (N)	-0.001	0.069	0.000	0.166	-0.001	0.290	0.001	0.865	0.005	1.597	-0.005	2.893
$F_x$ (N)	0.138	0.155	0.469	0.475	1.534	1.549	4.228	4.285	6.287	6.341	9.168	9.212
$F_L$ (N)	-0.001	0.064	0.000	0.150	-0.001	0.235	0.001	0.715	0.005	1.374	-0.005	2.569
$F_D$ (N)	0.138	0.158	0.469	0.481	1.534	1.558	4.228	4.313	6.287	6.393	9.168	9.307
$T_z$ (Nm)	0.000	0.003	0.000	0.010	0.000	0.015	0.000	0.031	0.000	0.049	0.000	0.075
$C_L$	-0.001	0.057	0.000	0.052	0.000	0.052	0.000	0.071	0.000	0.080	0.000	0.084
$C_D$	0.123	0.140	0.163	0.167	0.341	0.346	0.418	0.426	0.367	0.374	0.301	0.306
$C_N$	-0.001	0.062	0.000	0.058	0.000	0.064	0.000	0.085	0.000	0.093	0.000	0.095
$C_M$	-0.001	0.127	0.000	0.147	0.000	0.148	0.000	0.131	0.000	0.124	0.000	0.107
$C_{Nu}$	1.794		1.660		1.852		2.445		2.664		2.729	
$C_{Ma}$	3.646		4.217		4.241		3.762		3.539		3.053	

Table 8. Simulation Results for k-  $\epsilon$  model (CFX).

Simulation Data (SST Model)												
Diameter (m)	0.01295											
Drag Ref Area (m <sup>2</sup> )	0.00013											
Air Density (kg/m <sup>3</sup> )	1.180											
length (m)	0.058											
$X_{CG}$ from Base (m)	0.023											
Mach Number	0.500		0.800		1.000		1.500		1.950		2.600	
Velocity (m/s)	170.150		272.240		340.300		510.450		663.585		884.780	
$\alpha$ (°)	0.000	2.000	0.000	2.000	0.000	2.000	0.000	2.000	0.000	2.000	0.000	2.000
$\alpha$ (rad)	0.000	0.035	0.000	0.035	0.000	0.035	0.000	0.035	0.000	0.035	0.000	0.035
$u$ (m/s)	170.1 50	170.0 46	272.2 40	272.0 74	340.3 00	340.0 93	510.4 50	510.1 39	663.5 85	663.1 81	884.7 80	884.2 41
$v$ (m/s)	0.000	5.939	0.000	9.502	0.000	11.87 8	0.000	17.81 7	0.000	23.16 2	0.000	30.88 2
$Y_+$	1.500		2.030		2.430		2.800		3.050		3.280	
$F_y$ (N)	-0.002	0.076	-0.004	0.180	0.000	0.406	0.000	0.863	0.006	1.593	-0.007	2.872
$F_x$ (N)	0.249	0.257	0.566	0.583	2.430	2.453	4.194	4.240	6.119	6.173	8.790	8.838
$F_L$ (N)	-0.002	0.067	-0.004	0.160	0.000	0.320	0.000	0.715	0.006	1.376	-0.007	2.562

Simulation Data (SST Model)												
<b>F<sub>D</sub> (N)</b>	0.249	0.259	0.566	0.589	2.430	2.466	4.194	4.267	6.119	6.224	8.790	8.933
<b>T<sub>z</sub> (Nm)</b>	0.000	0.003	0.000	0.010	0.000	0.018	0.000	0.030	0.000	0.047	0.000	0.073
<b>C<sub>L</sub></b>	-0.002	0.060	-0.001	0.056	0.000	0.071	0.000	0.071	0.000	0.080	0.000	0.084
<b>C<sub>D</sub></b>	0.221	0.230	0.197	0.204	0.540	0.548	0.414	0.421	0.358	0.364	0.289	0.294
<b>C<sub>N</sub></b>	-0.002	0.068	-0.001	0.063	0.000	0.090	0.000	0.085	0.000	0.093	0.000	0.094
<b>C<sub>M</sub></b>	-0.002	0.132	-0.001	0.156	0.000	0.169	0.000	0.129	0.000	0.119	0.000	0.104
<b>C<sub>Nα</sub></b>	1.997		1.835		2.585		2.443		2.656		2.711	
<b>C<sub>Mα</sub></b>	3.844		4.493		4.850		3.696		3.414		2.988	

Table 9. Simulation Results for SST Model (CFX).

Simulation Data for Various $\alpha$												
<b>Area (m<sup>2</sup>)</b>	0.00013											
<b>Density (kg/m<sup>3</sup>)</b>	1.180											
<b>Mach Number</b>	0.500											
<b>Velocity (m/s)</b>	170.150											
<b><math>\alpha</math> (°)</b>	<b>-4.000</b>	<b>-2.000</b>	<b>0.000</b>	<b>2.000</b>	<b>4.000</b>	<b>6.000</b>	<b>10.000</b>	<b>15.000</b>	<b>20.000</b>	<b>25.000</b>	<b>30.000</b>	
<b><math>\alpha</math> (rad)</b>	-0.070	-0.035	0.000	0.035	0.070	0.105	0.175	0.262	0.349	0.436	0.524	
<b>u (m/s)</b>	169.73 5	170.04 6	170.15 0	170.04 6	169.73 5	169.21 8	167.56 4	164.35 1	159.88 6	154.20 4	147.34 8	
<b>v (m/s)</b>	-11.871	-5.939	0.000	5.939	11.871	17.788	29.550	44.044	58.202	71.917	85.085	
<b>F<sub>y</sub> (N)</b>	-0.107	-0.060	-0.001	0.069	0.137	0.198	0.337	0.536	0.742	0.961	1.185	
<b>F<sub>x</sub> (N)</b>	0.259	0.253	0.138	0.155	0.261	0.265	0.275	0.293	0.300	0.279	0.238	
<b>F<sub>L</sub> (N)</b>	-0.089	-0.051	-0.001	0.064	0.118	0.169	0.284	0.442	0.595	0.753	0.908	
<b>F<sub>D</sub> (N)</b>	0.265	0.255	0.138	0.158	0.269	0.285	0.329	0.422	0.535	0.659	0.799	
<b>C<sub>L</sub></b>	-0.080	-0.046	-0.001	0.057	0.106	0.152	0.255	0.398	0.536	0.678	0.817	
<b>C<sub>D</sub></b>	0.239	0.230	0.125	0.142	0.243	0.256	0.297	0.380	0.482	0.594	0.720	
<b><math>\alpha</math> (°)</b>	<b>35.000</b>	<b>40.000</b>	<b>45.000</b>	<b>50.000</b>	<b>55.000</b>	<b>60.000</b>	<b>65.000</b>	<b>70.000</b>	<b>75.000</b>	<b>80.000</b>	<b>85.000</b>	
<b><math>\alpha</math> (rad)</b>	0.611	0.698	0.786	0.873	0.960	1.047	1.135	1.222	1.309	1.396	1.484	
<b>u (m/s)</b>	139.37 1	130.33 3	120.30 2	109.35 6	97.577	85.055	71.886	58.169	44.010	29.516	14.797	
<b>v (m/s)</b>	97.605	109.38 2	120.32 6	130.35 5	139.39 1	147.36 6	154.21 9	159.89 8	164.36 0	167.57 0	169.50 5	
<b>F<sub>y</sub> (N)</b>	1.410	1.636	1.864	2.091	2.307	2.500	2.644	2.709	2.661	2.513	2.419	
<b>F<sub>x</sub> (N)</b>	0.173	0.086	-0.017	-0.137	-0.264	-0.392	-0.508	-0.594	-0.572	-0.419	-0.339	

Simulation Data for Various $\alpha$											
<b>F<sub>L</sub> (N)</b>	1.056	1.197	1.330	1.449	1.540	1.590	1.577	1.485	1.240	0.849	0.548
<b>F<sub>D</sub> (N)</b>	0.951	1.118	1.306	1.514	1.738	1.969	2.181	2.342	2.422	2.402	2.381
<b>C<sub>L</sub></b>	0.951	1.078	1.198	1.305	1.387	1.432	1.421	1.337	1.117	0.764	0.493
<b>C<sub>D</sub></b>	0.856	1.007	1.176	1.364	1.566	1.774	1.965	2.110	2.182	2.163	2.144

Table 10. Simulation Results for C<sub>L</sub> and C<sub>D</sub> at High AOA (CFX).

Sensitivity Study on Tilted Model for 2° AOA						
<b>Diameter (m)</b>	0.013					
<b>Drag Ref Area (m<sup>2</sup>)</b>	0.000					
<b>Air Density (kg/m<sup>3</sup>)</b>	1.180					
<b>Mach Number</b>	<b>0.500</b>		<b>1.500</b>		<b>2.600</b>	
<b>Velocity (m/s)</b>	170.150		510.450		884.780	
<b><math>\alpha</math> (°)</b>	0.000	2.000	0.000	2.000	0.000	2.000
<b><math>\alpha</math> (rad)</b>	0.000	0.035	0.000	0.035	0.000	0.035
<b>u (m/s)</b>	170.150	170.046	510.450	510.139	884.780	884.241
<b>v (m/s)</b>	0.000	5.939	0.000	17.817	0.000	30.882
<b>F<sub>y</sub> (N)</b>	-0.001	0.069	0.000	0.732	-0.007	2.695
<b>F<sub>x</sub> (N)</b>	0.138	0.155	4.194	4.271	8.790	8.599
<b>C<sub>L</sub></b>	-0.001	0.061	0.000	0.072	0.000	0.089
<b>C<sub>D</sub></b>	0.123	0.138	0.414	0.422	0.289	0.283
<b>C<sub>N</sub></b>	-0.001	0.066	0.000	0.087	0.000	0.098
<b>C<sub>N<math>\alpha</math></sub></b>	1.914		2.492		2.825	

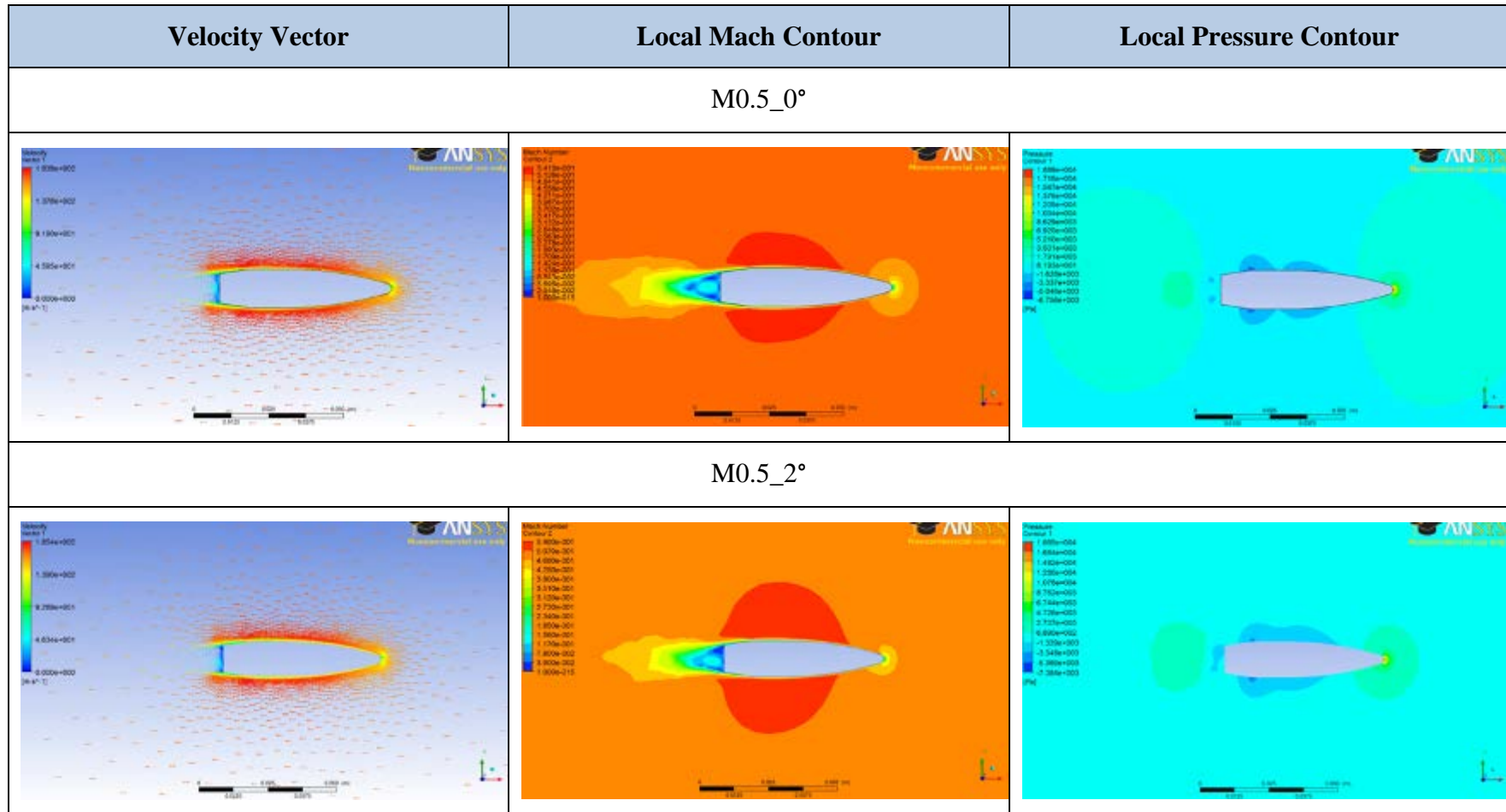
Table 11. Sensitivity Study on Tilted Body vs Tilted Flow (CFX).

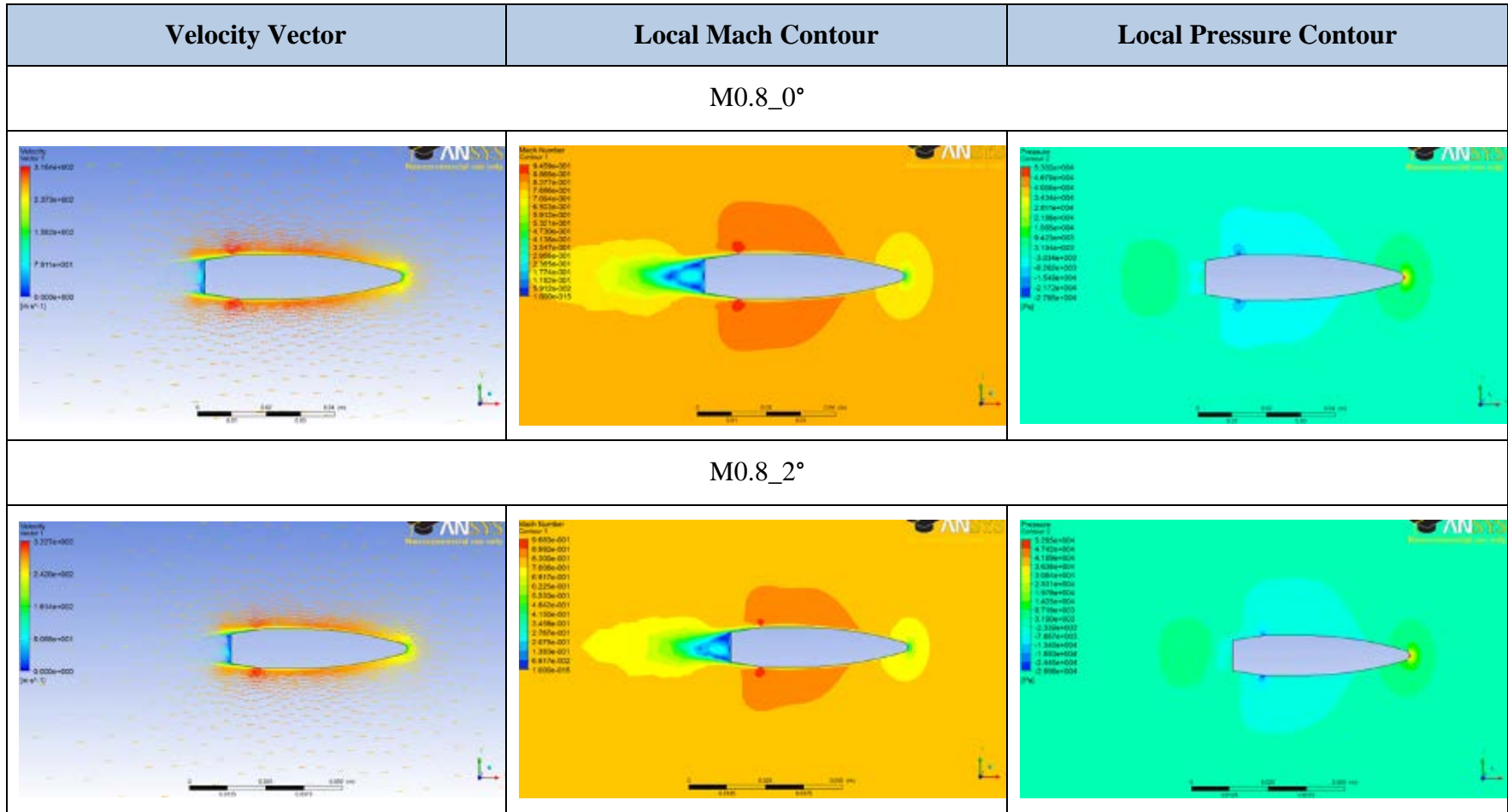
Sensitivity Study on 20X Control Volume (SST)						
<b>Diameter (m)</b>	0.013					
<b>Drag Ref Area (m<sup>2</sup>)</b>	0.000					
<b>Air Density (kg/m<sup>3</sup>)</b>	1.180					
<b>Mach Number</b>	<b>0.500</b>		<b>0.800</b>		<b>1.500</b>	
<b>Velocity (m/s)</b>	170.150		272.240		510.450	
<b><math>\alpha</math> (°)</b>	0.000	2.000	0.000	2.000	0.000	2.000
<b><math>\alpha</math> (rad)</b>	0.000	0.035	0.000	0.035	0.000	0.035
<b>u (m/s)</b>	170.150	170.046	272.240	272.074	510.450	510.139
<b>v (m/s)</b>	0.000	5.939	0.000	9.502	0.000	17.817
<b>F<sub>y</sub> (N)</b>	0.001	0.075	0.002	0.185	0.000	0.867

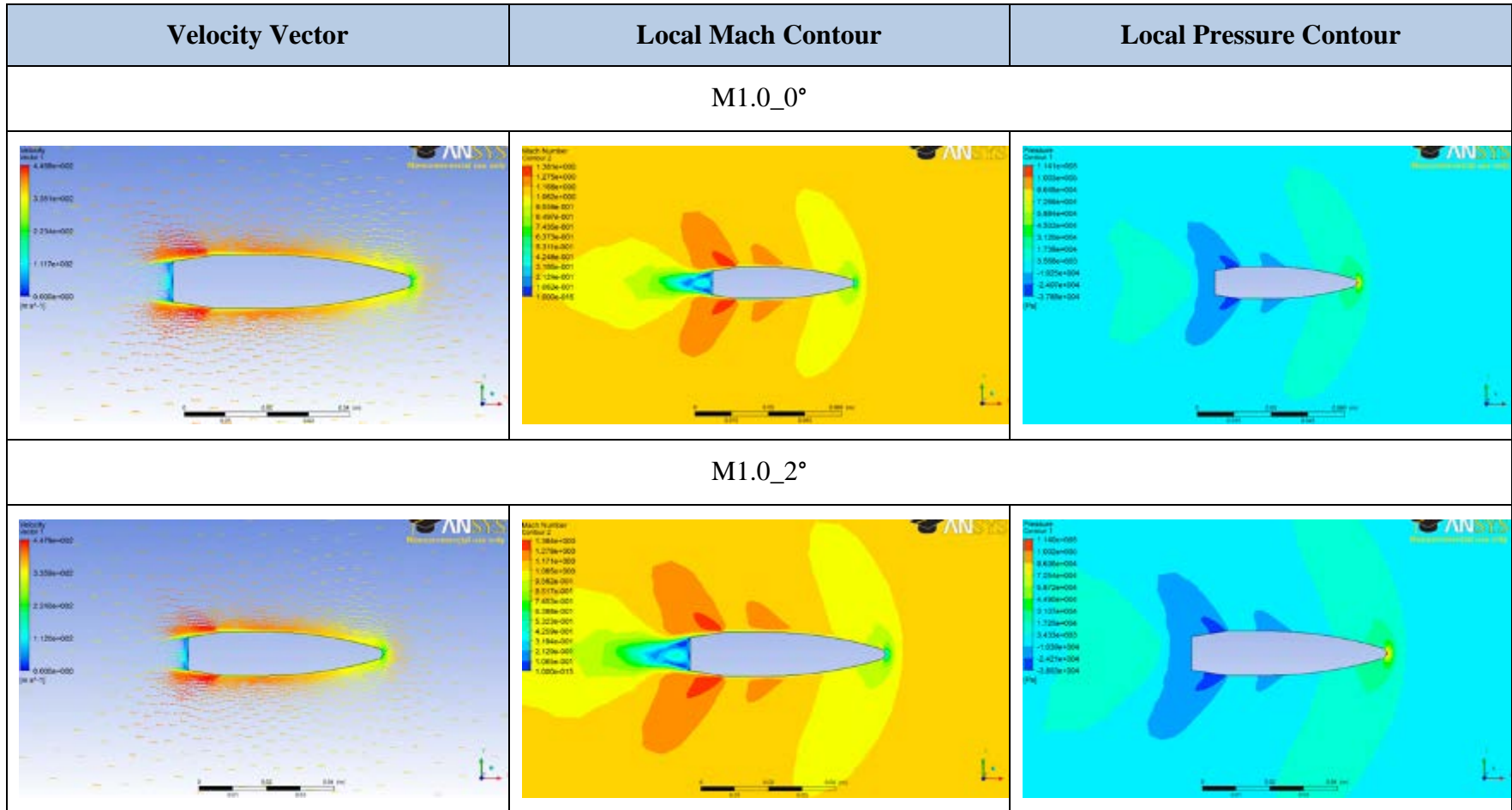
Sensitivity Study on 20X Control Volume (SST)						
$F_x(N)$	0.243	0.250	0.552	0.568	4.173	4.222
$F_L(N)$	0.001	0.066	0.002	0.165	0.000	0.719
$F_D(N)$	0.243	0.252	0.552	0.574	4.173	4.250
$C_L$	0.001	0.059	0.001	0.057	0.000	0.071
$C_D$	0.216	0.224	0.192	0.199	0.412	0.420
$C_N$	0.001	0.067	0.001	0.064	0.000	0.086
$C_{Na}$	1.885		1.824		2.451	

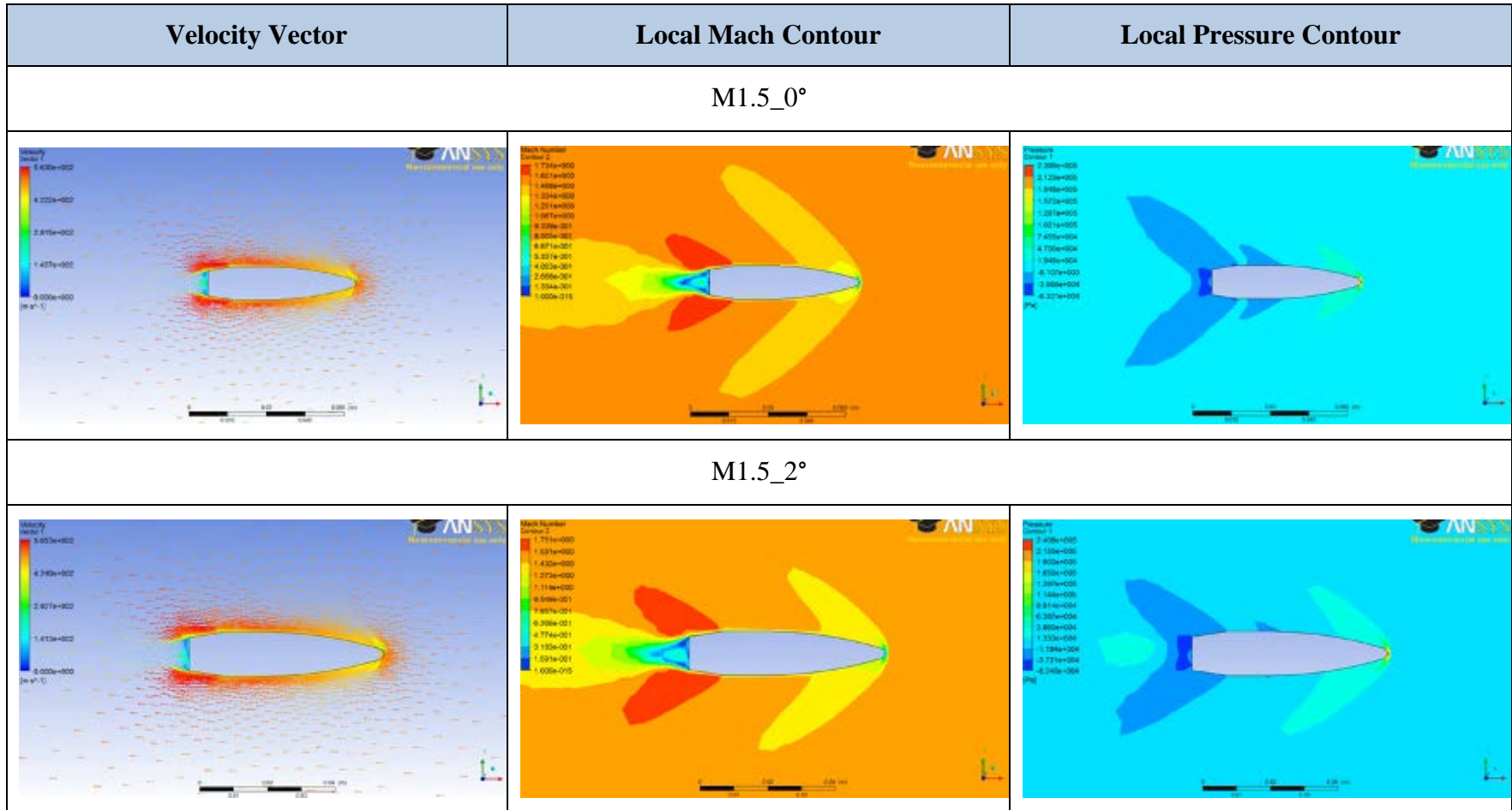
Table 12. Sensitivity Study on 20X Control Volume (CFX).

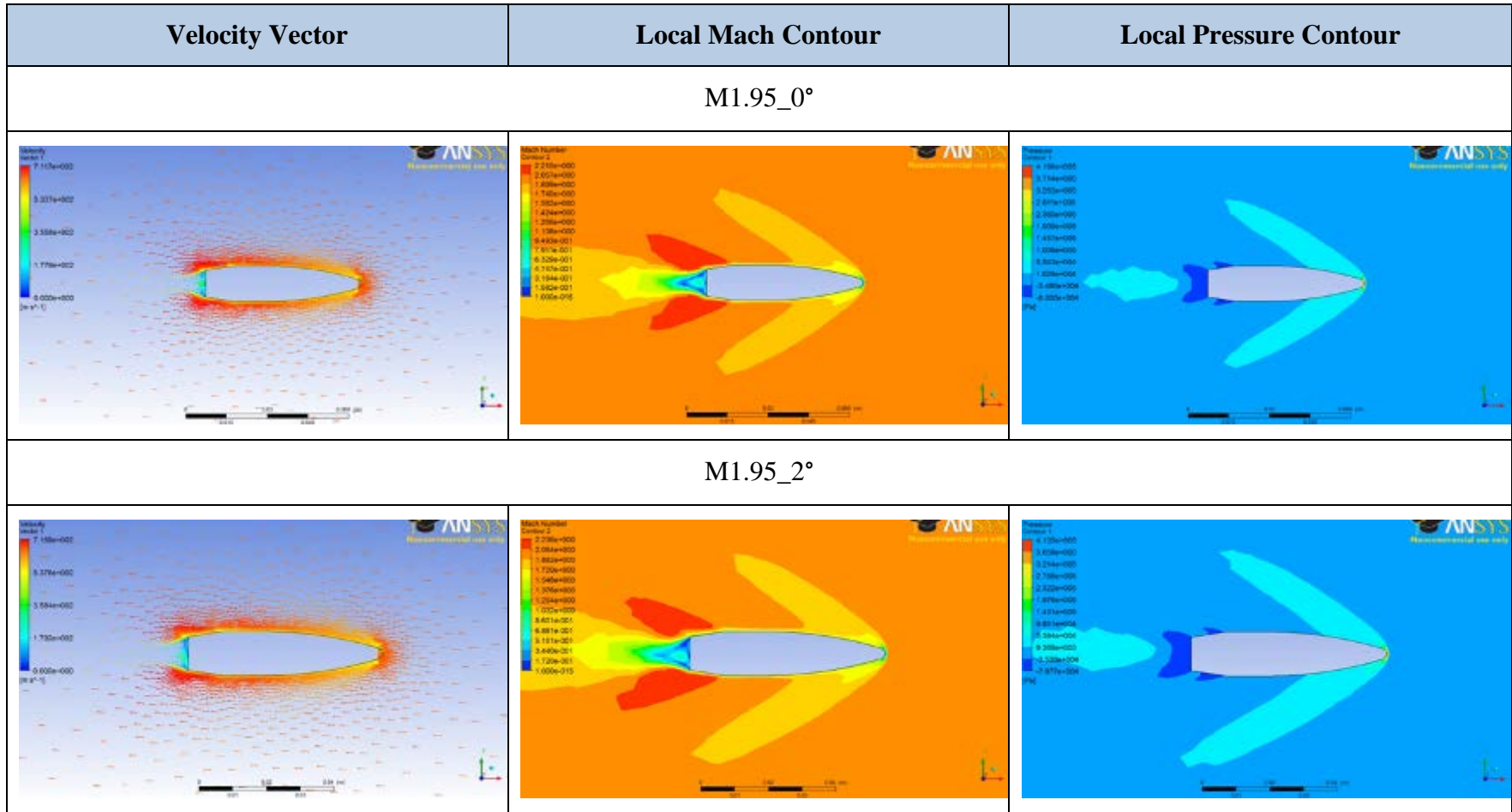
## 2. Flow Diagrams at Various Mach Numbers











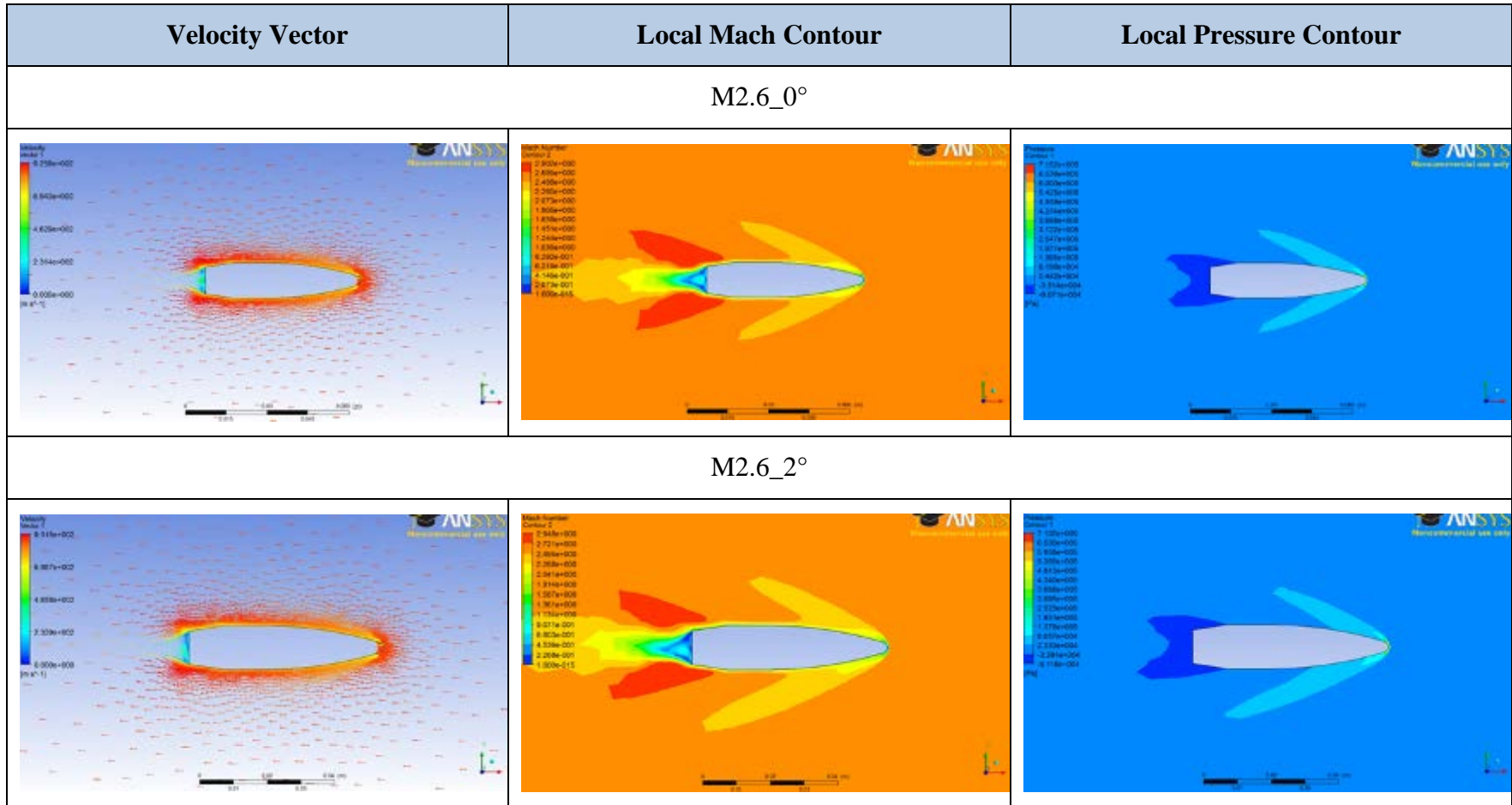
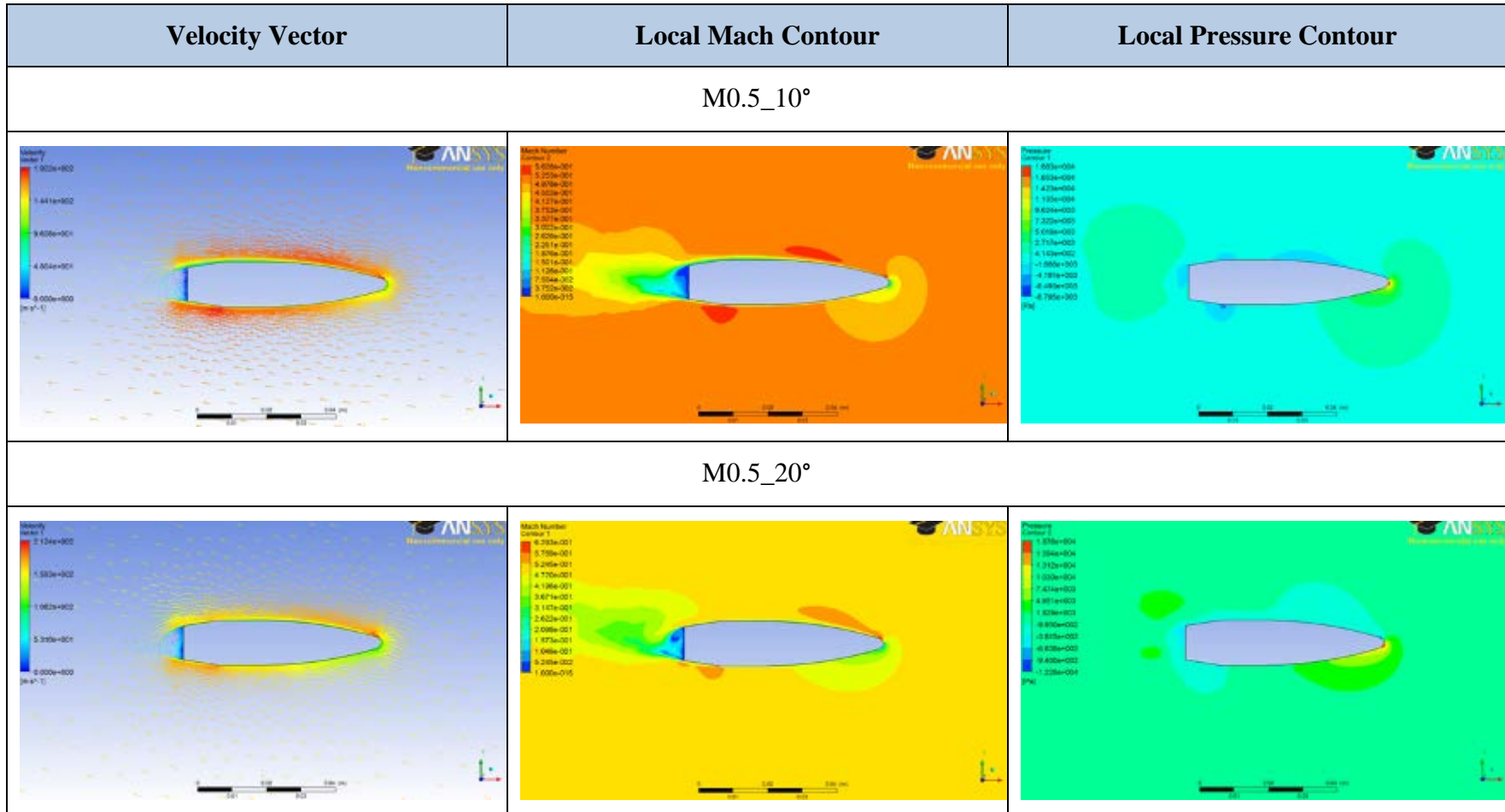
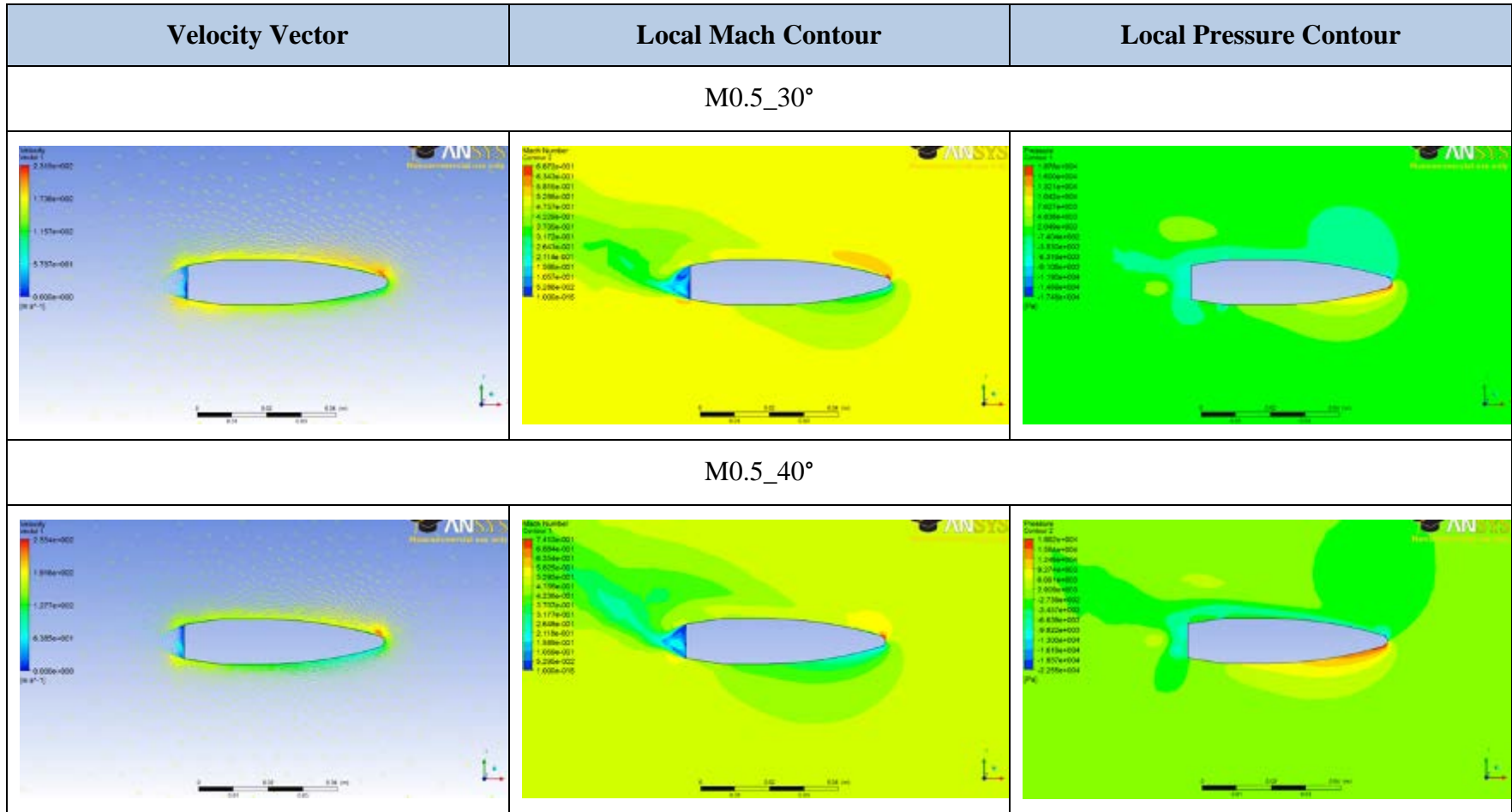
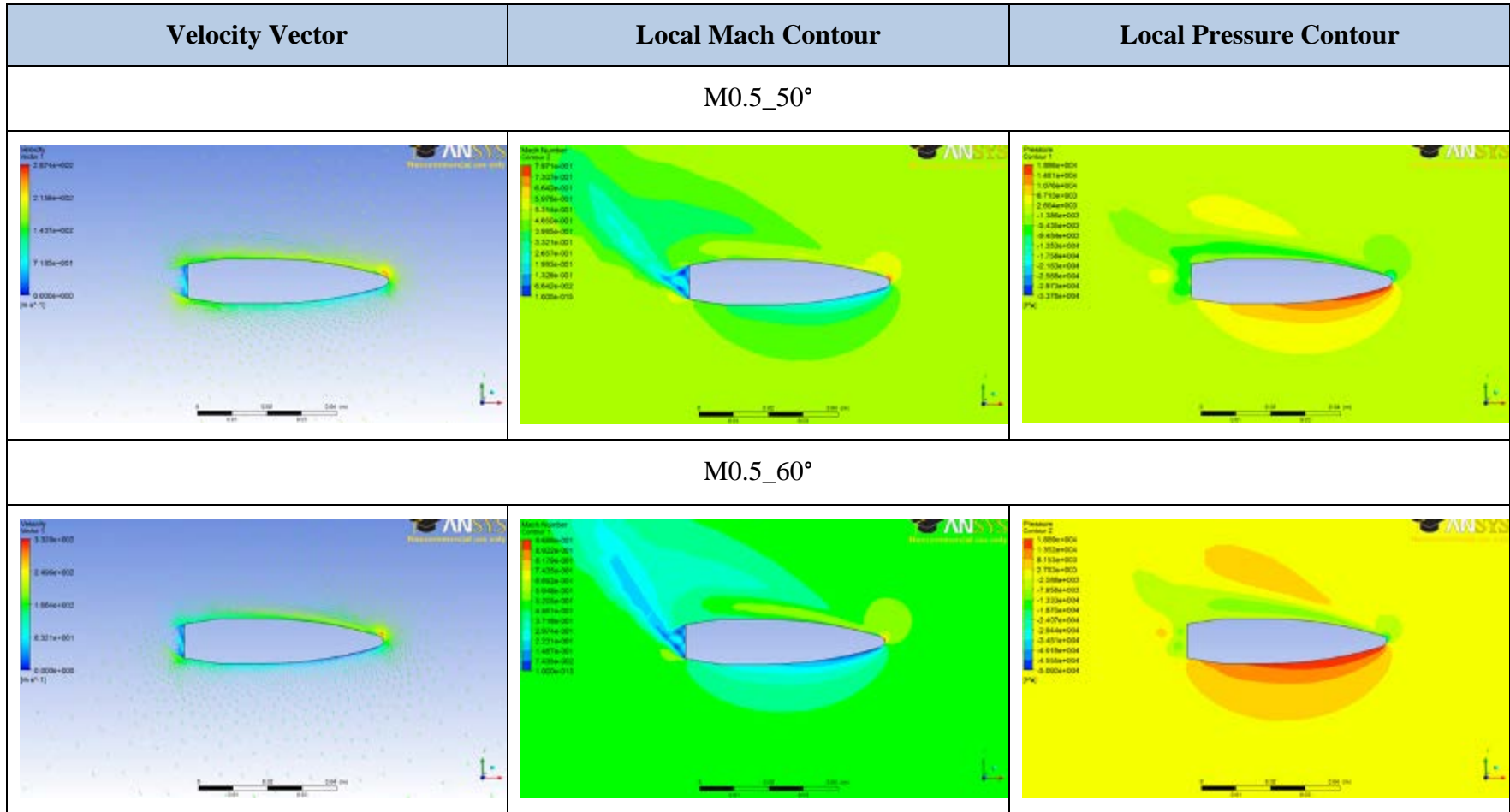


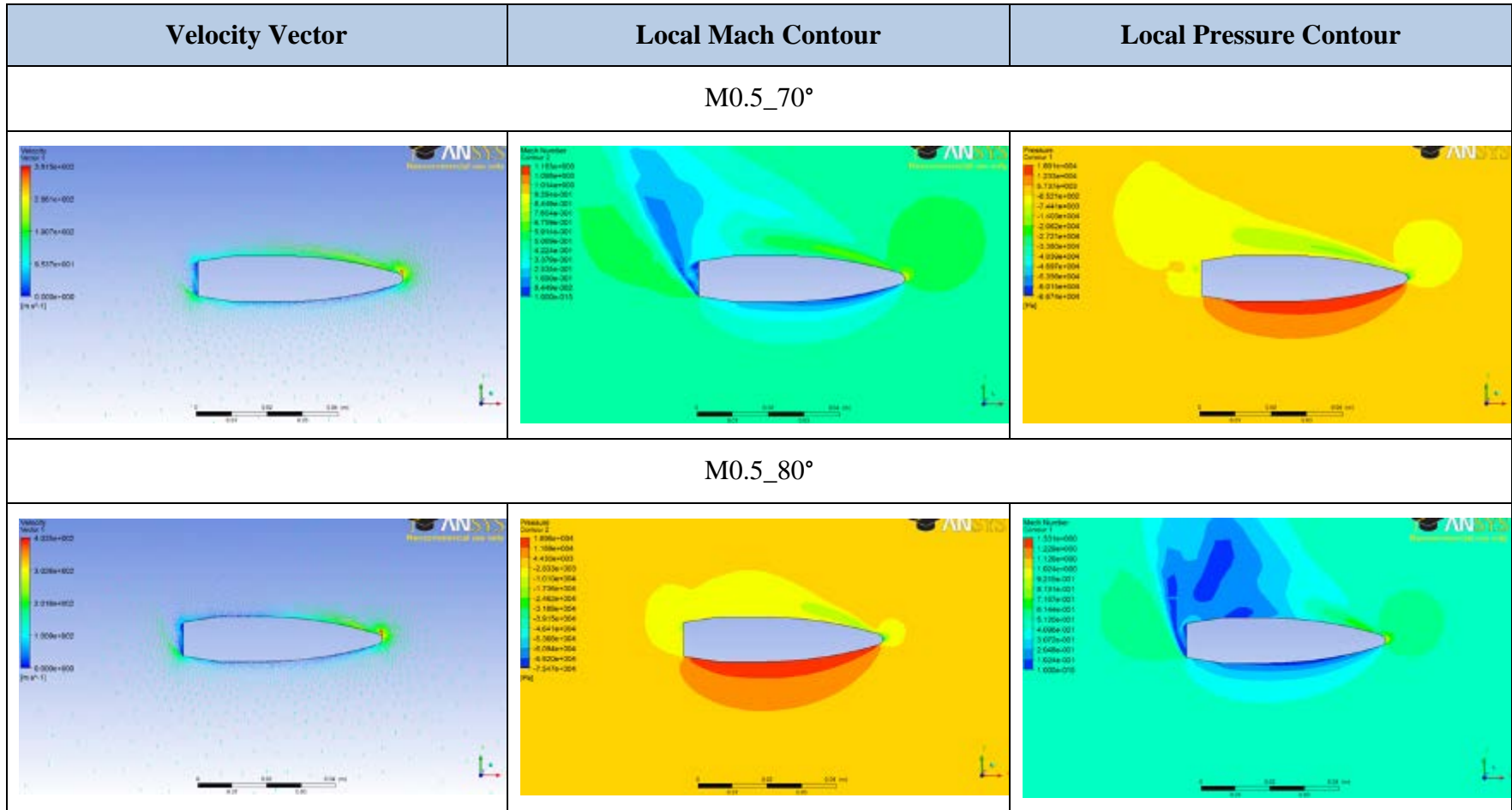
Figure 61. Flow Diagrams at Various Mach Numbers for 0° and 2° (CFX).

### 3. Flow Diagrams at Various Angles of Attack









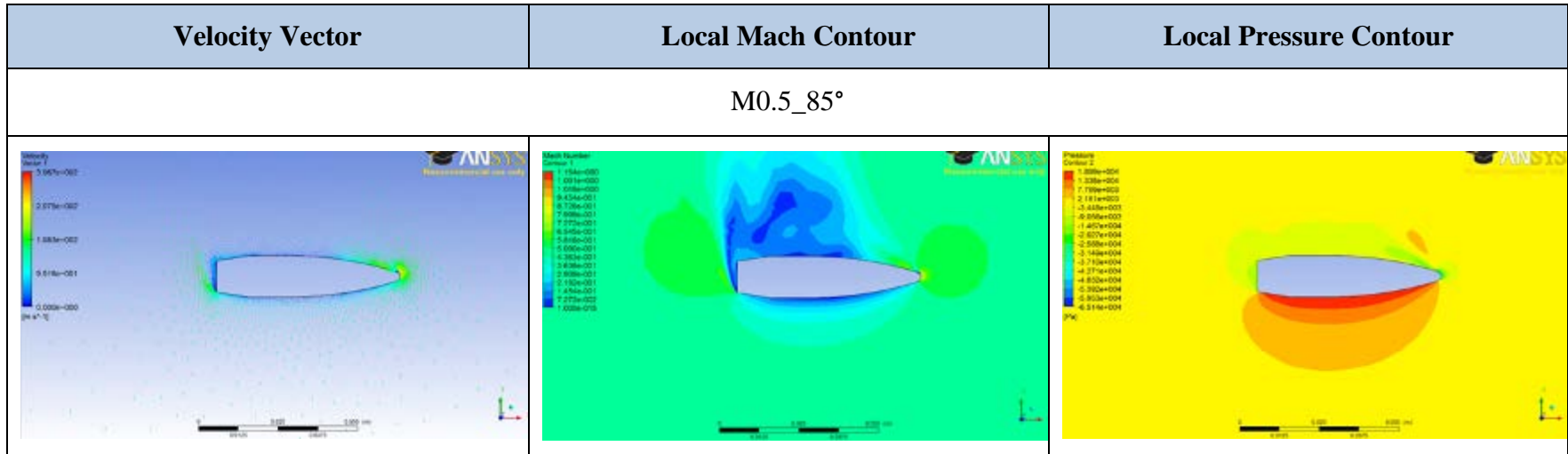
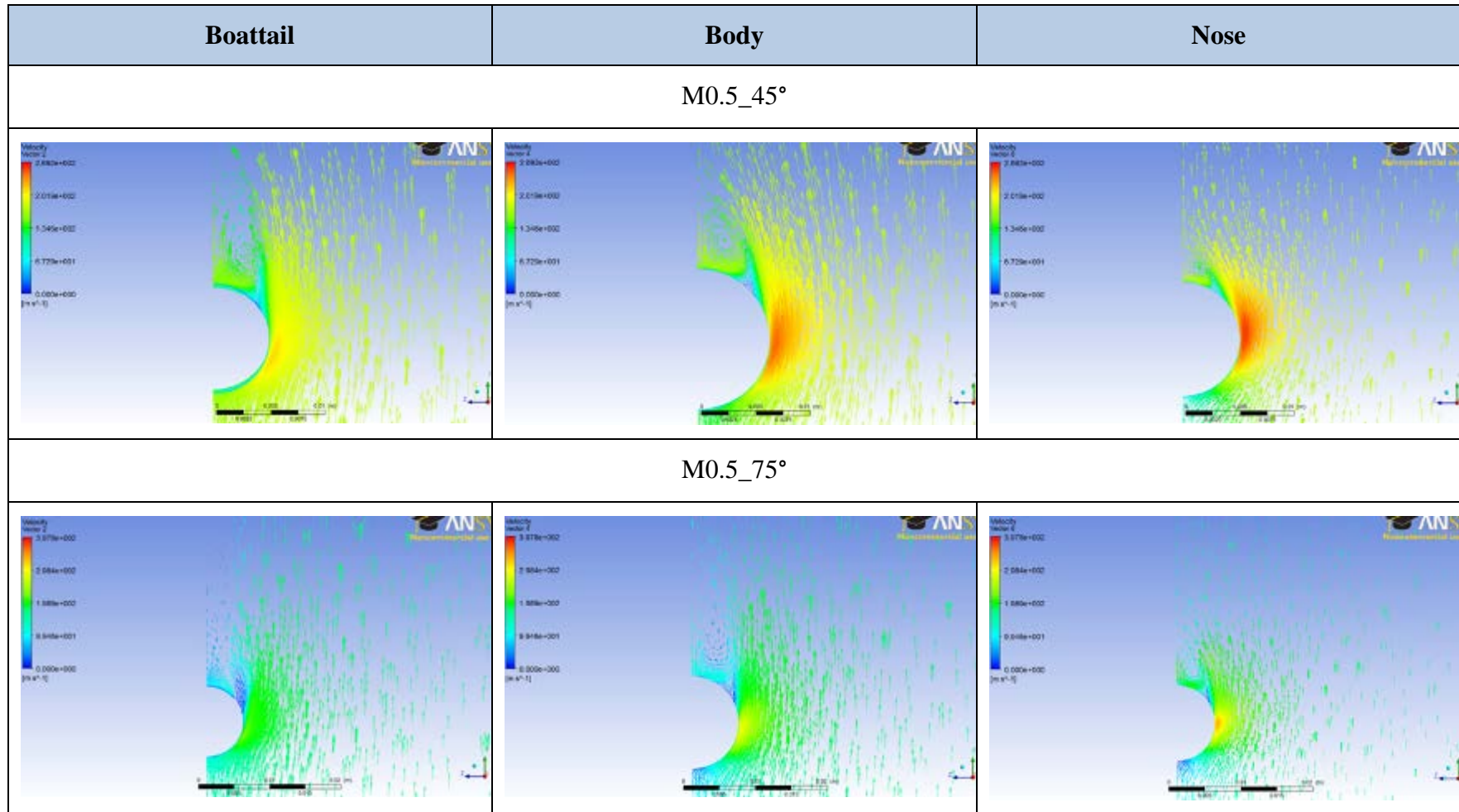


Figure 62. Flow Diagram at Various Angles of Attack (CFX).

#### 4. Cross-Sectional Flow



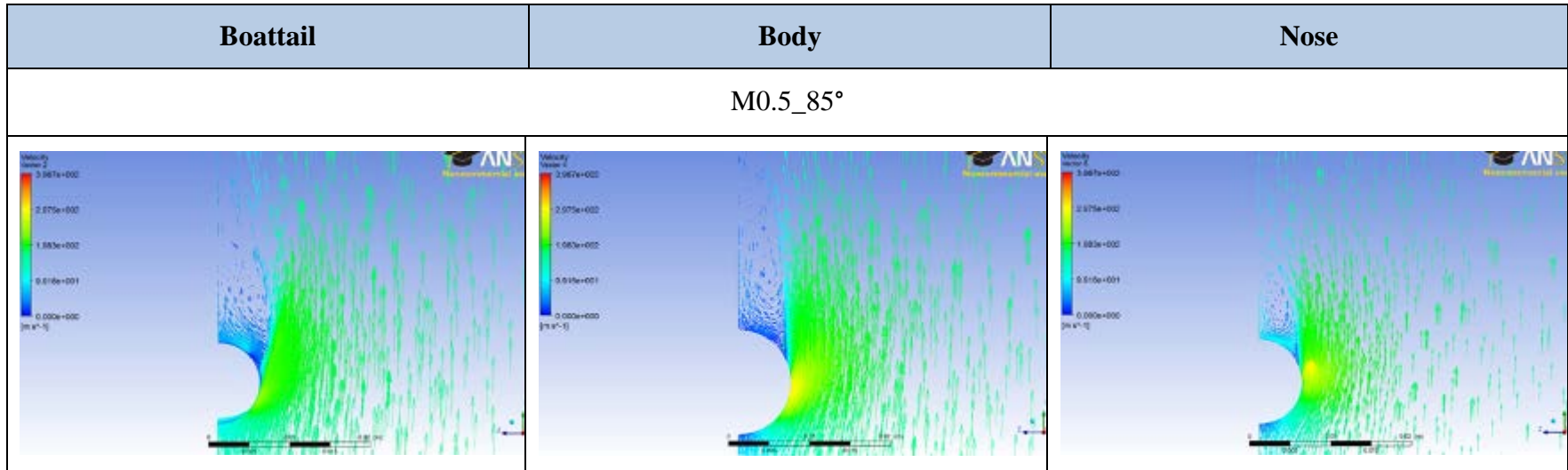


Figure 63. Cross-Sectional Flow across Symmetry Plane (CFX).

## B. AP09

Simulation Data (AP09)												
Mach Number	0.5		0.65		0.8		0.95		1.1		1.25	
$\alpha$ (°)	0.000	2.000	0.000	2.000	0.000	2.000	0.000	2.000	0.000	2.000	0.000	2.000
$\alpha$ (rad)	0.000	0.035	0.000	0.035	0.000	0.035	0.000	0.035	0.000	0.035	0.000	0.035
$C_L$	0.000	0.050	0.000	0.047	0.000	0.044	0.000	0.042	0.000	0.040	0.000	0.055
$C_D$	0.097	0.111	0.098	0.112	0.116	0.129	0.194	0.208	0.337	0.358	0.350	0.374
$C_N$	0.000	0.054	0.000	0.051	0.000	0.048	0.000	0.049	0.000	0.052	0.000	0.068
$C_{N\alpha}$	1.542		1.457		1.389		1.410		1.503		1.948	
Mach Number	1.4		1.55		1.7		1.85		2		2.15	
$\alpha$ (°)	0.000	2.000	0.000	2.000	0.000	2.000	0.000	2.000	0.000	2.000	0.000	2.000
$\alpha$ (rad)	0.000	0.035	0.000	0.035	0.000	0.035	0.000	0.035	0.000	0.035	0.000	0.035
$C_L$	0.000	0.063	0.000	0.070	0.000	0.076	0.000	0.072	0.000	0.073	0.000	0.073
$C_D$	0.345	0.369	0.336	0.359	0.330	0.352	0.311	0.331	0.310	0.329	0.309	0.326
$C_N$	0.000	0.076	0.000	0.082	0.000	0.088	0.000	0.084	0.000	0.084	0.000	0.084
$C_{N\alpha}$	2.172		2.363		2.528		2.392		2.419		2.416	
Mach Number	2.3		2.45		2.6		2.75		2.9		3	
$\alpha$ (°)	0.000	2.000	0.000	2.000	0.000	2.000	0.000	2.000	0.000	2.000	0.000	2.000
$\alpha$ (rad)	0.000	0.035	0.000	0.035	0.000	0.035	0.000	0.035	0.000	0.035	0.000	0.035
$C_L$	0.000	0.073	0.000	0.072	0.000	0.071	0.000	0.070	0.000	0.069	0.000	0.068
$C_D$	0.306	0.321	0.302	0.316	0.299	0.311	0.296	0.307	0.292	0.302	0.289	0.299
$C_N$	0.000	0.084	0.000	0.083	0.000	0.082	0.000	0.081	0.000	0.079	0.000	0.078
$C_{N\alpha}$	2.411		2.377		2.343		2.311		2.277		2.246	

Table 13. Simulation Results for  $C_{N\alpha}$  and  $C_{D0}$  (AP09).

Simulation Data (AP09)										
Mach	0.5									
$\alpha$ (°)	0	10	20	30	40	50	60	70	80	85
$C_L$	0.000	0.268	0.584	1.462	1.997	2.449	2.655	2.464	1.590	0.828
$C_D$	0.097	0.216	0.406	0.922	1.421	2.056	2.793	3.656	4.377	4.569

Table 14. Simulation Results for  $C_L$  and  $C_D$  at High AOA (AP09).

## INITIAL DISTRIBUTION LIST

1. Defense Technical Information Center  
Ft. Belvoir, Virginia
2. Dudley Knox Library  
Naval Postgraduate School  
Monterey, California
3. Professor and Chairman Knox Millsaps  
Department of Mechanical and Aeronautical Engineering  
Naval Postgraduate School  
Monterey, California
4. Professor Maximilian F. Platzler  
Department of Mechanical and Aeronautical Engineering  
Naval Postgraduate School  
Monterey, California
5. Professor Anthony Gannon  
Department of Mechanical and Aeronautical Engineering  
Naval Postgraduate School  
Monterey, California
6. Professor Joshua Gordis  
Department of Mechanical and Aeronautical Engineering  
Naval Postgraduate School  
Monterey, California
7. Professor Yeo Tat Soon  
Temasek Defense Systems Institute  
National University of Singapore  
Singapore
8. Ms. Tan Lai Poh  
Temasek Defense Systems Institute  
National University of Singapore  
Singapore